Validation of a Commercial Three-Dimensional Whole-Body Laser Scanner for the Collection of Obesity-Related Measurements

by

Ian Andrew Stanley Westhaver

Submitted in partial fulfilment of the requirements
for the degree of Master of Applied Science

at

Dalhousie University
Halifax, Nova Scotia
August 2014

Dedication Page

First of all, I would like to thank my funding agencies NSERC and Encana for allowing me the financial ability to pursue this research while also meeting my personal financial obligations.

With fervor I thank my thesis advisor Dr John Kozey, not only for his wisdom, guidance, and knowledge as he led me through this process, but also for his mentorship in helping me to build a solid career, and become accurate *and* precise in my pursuit of science.

I would further like to thank the members of my thesis committee, Dr Janie Astephen-Wilson, Dr Rob Adamson, and Dr James Ellsmere, as well as my external reader Dr Michel Ladouceur, for their time, perspective, and knowledge as they challenged me to refine my approach to scientific methodology.

My burden was constantly ameliorated by fantastic group of lab mates, who were not only there to provide insight and support in my research, but also there to commiserate in failures and celebrate success: Audrey Prayal-Brown, Colleen Dews, Joshua Goreham, Cynthia Ly, Fiona Fan, and Jinyu Li, Warren Hefford, and Colin Wicks.

To my friends and family who bore my gripes, and shared my victories: I am grateful for each and every one of you.

I would be remiss not to specifically thank my incredible sister, Bridget Westhaver, who has been my constant champion with enthusiasm.

Finally, I would like to thank my fiancé and partner, David St. Laurent, who through this entire process has provided steadfast support, realistic perspective, and has gingerly cradled my often fragile ego.

Table of Contents

List of Tables

List of Figures

Abstract

This study aimed to develop a systematic method of comparing manual and digital anthropometric measurements and validate a commercial three-dimensional laser scanner, for measurements related to obesity. Firstly, novel manual volumetry methodologies were developed. 20 participants were measured for a variety of linear, circumferential, and segmental volumetric measurements. Error between manual and scan-extracted measurements was compared based on ISO20685, and clinical standards. Regression analysis improved the quality of the measurements and residuals were again compared to the standards. After regression, 18 of 23 of the measurements were within, or close to (two times standard), standards. Error was caused by a combination of image quality issues associated with the laser scanner, as well as algorithmic issues associated with larger participants. Overall, the results are promising, and given the indicated population, a small number of minor improvements may very quickly allow the scanner to collect measurements on a clinical population.

Chapter 1. Introduction

The overarching objectives of this research are twofold. Firstly, the document outlines the justification for the body of research proposed based on an analysis of current and past research activities performed in the Occupational Ergonomics and Biomechanics Lab at Dalhousie, as well as documented research in the relevant literature related to human anthropometry and health. Secondly, a description of processes and methods undertaken are presented that tested the technical and logical issues associated with the area of research in human anthropometry and health.

1.1. Anthropometry

Anthropometry is the scientific field associated with measuring the human form, motion, and the forces and working capacity associated with motion. (Pheasant, 1996) The word anthropometry is a derivative of the Greek *anthropo-*, meaning man, and *-metry*, meaning measurement; thus, anthropometry is literally the measurement of man.(Oxford english dictionary.2011) Anthropometry has served an important role in the quantification of human interaction with working environments since the industrial revolution of the 19th century; however, evidence of the study of anthropometry existed long before the modern scientific perspective was adopted.

The Occupational Ergonomics and Biomechanics Laboratory (OEAB Lab) at Dalhousie University investigates three research foci relating to the study of anthropometry (see Figure 1). Engineering ergonomics division is involved in using measurements collected on human subjects to design workspaces, personal protective equipment, and other products. Biomechanics and body composition uses body measurements as a means of predicting relative composition of various body tissues, and to calculate the kinetics related to body motion. Finally, the focus of this proposal which deals primarily with research performed in the *Health*

Research, which deals fundamentally with issues related to obesity and other health risk factors.

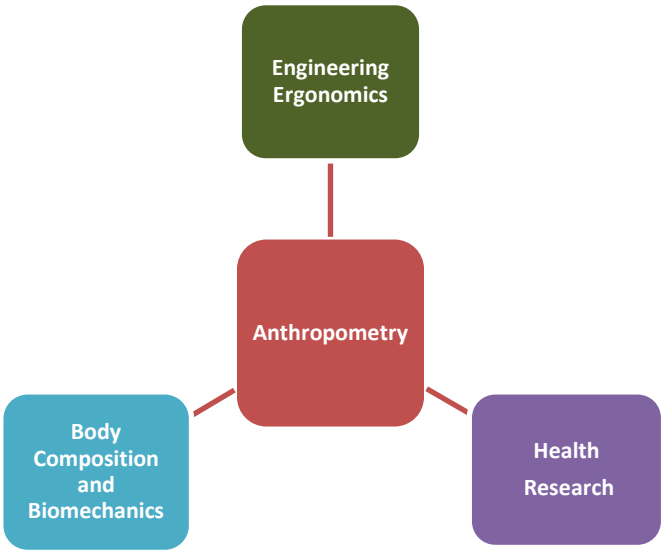

Figure 1: Divisions of the Occupational Ergonomics and Biomechanics Laboratory

Previous literature has demonstrated that a relationship exists between non-invasive, surface measurements and the relative composition of body tissues, especially body fat (Brozek, Grande, Anderson, & Keys, 1963). With this understanding, researchers have been able to relate the presence of adipose (fat) tissue with disease risk factors (Kissebah & Krakower, 1994). Currently, the most commonly used, albeit crude, predictor of adiposity is the body mass index (BMI), which has been related to the presence of disease in obese subjects. Further work has demonstrated that regional measurements of adiposity, such as waist circumference (WC) (Janssen, Katzmarzyk, & Ross, 2004) or waist-to-hip ratio (WHR) (J. Lin, Chiou, Weng, Tsai, & Liu, 2002), better predict the presence of disease than do such whole-body measurements as BMI.

Early means of collecting anthropometric measurements involved the use of manual measuring apparatus and methodologies, including measuring tapes, anthropometers and specialized calipers for skinfold thickness measurement, as well as the measurement of linear distances and girths. The skin folds methods were constructed by regressions of selective skin folds measures against body density and the resulting predictions of percent body fat using underwater weighing or whole body immersion. Recent technological improvements in anthropometric measurement and data acquisition technology have culminated in the design of whole-body laser scanners capable of collecting measurements relevant to health research. Furthermore, the literature has shown that with the use of three-dimensional laser imaging, new indices of health can be developed which more positively correlate to risk for disease than currently used standards of BMI and WHR (J. Lin et al., 2002). These improved measures require measurements beyond one-dimensional scalar measures.

1.2. Statement of Problem

The overriding objective of this research was to validate the ability of a commercial laser scanner and associated software to identify anthropometric landmark markers, identify body segments, and measure the whole and segmental volumes in normal weight and obese populations. In addition, a validation procedure for selected length, circumferential, and girth measurements was developed and tested; specifically, this study established the following three processes:

1. Three dimensional laser scanning apparatus was evaluated. This consisted of a comparison of directly measured manual linear, circumferential, and volumetric measurements to scan extracted measurements. Where appropriate and available, previously defined measurement tolerances from the literature were applied.

2. To accurately compare the volume measurements of the various body segments and the whole body, customized limb volumetry equipment and methods were designed and validated

3. As required based on objective 1, customized software was designed, refined, and validated for effectiveness

This study will form the foundation of a further investigations focussed on developing relationships between metabolic changes – i.e. the remission of metabolic diseases – and changes in body shape following weight loss surgery. The measurements investigated in this study will be used to validate clinically relevant methods of assessing adiposity (WHR, WC, BMI) and explore other shape factors that may demonstrate better relationships to adiposity and indicators of metabolic disorders than those measurements currently used. Eventually, a database of metabolic disease and anthropometric relationships may be used as a method of predicting disease risk factors as a function of body shape.

Chapter 2. Review of Literature

2.1. Historical Perspective

The importance of the study of man-machine interactions arose as a result of industrialization and the growing demand for products and systems that that required worker efficiency and mass production to lower production costs. Increases in population allowed a young, unskilled labour force to become available for large-scale production plants. As a result, complex manufacturing processes were broken down into simpler, repetitive tasks requiring well-defined workstations. In order to increase the efficiency of these processes, the relationship between machines and their operators had to be analysed. Through an understanding of the geometric and functional constraints of machine operators, as well as an in-depth analysis of workplace conditions, workspace designers were able to maximize the efficiency of the positions and increase output, while decreasing physical burden on the employee (Bridger, 2009).

2.1.1. Anthropometric Surveys

Typically, the outcome of a large-scale anthropometric survey is a database or a statistical summary of predetermined anthropometric characteristics over a defined population. The objective of collecting such a survey is to accumulate sufficient quantitative information such that the representative measurements of the population can be defined. These measures can be used in a variety of design and research based applications, including individual or group workspaces and personal protective equipment design. In either case, constraints of man-machine interactions must be defined in order to increase employee efficiency and workplace safety. Health research also benefits from anthropometric surveys as many disease states can be related to static and functional anthropometric measurements (Schneider et al., 2010). Furthermore, medical devices must be designed with consideration for the user populations, as well as for the patients for whom the devices are developed.

2.1.2. Measurement Standardization - ANSUR

Military organizations have been the primary generators of many of the early studies of anthropometry. The diversity of enlistees drives the militaries' interest in anthropometry, as does the requirement to accommodate as wide a variety of people as possible in uniform, equipment, and workspace as is reasonably and economically possible. For example, the earlier studies of forward reach were developed in order to optimize fighter aircraft designs (Dempster, 1955).

In recent times, the largest anthropometric survey performed using manual measurement methods, before the modernization of collection methods, was the ANSUR (Anthropometric Survey) survey (Gordon, Churchill, Clauser, Bradtmiller, & McConville, 1989). Collected in 1988, ANSUR comprised the benchmark survey that defined mean absolute differences (MAD) within and between measurers when collecting multiple measurements that became the standard for the precision error of future, modernized measurement techniques (Robinette, 2006) .

2.2. Mid-Century Developments

The sophistication of the equipment used to perform anthropometric surveys has increased almost as quickly as the need for the surveys themselves. Early measurements were taken almost exclusively with linear mechanical measurement devices. Later, specialized calipers were developed to aid in the identification of palpable landmarks, resulting in the anthropometer (Hrdlicka, 1972). As image capturing technology was developing, so were methods of photogrammetric analysis for anthropometry. The early methods of capturing anthropometric measurements involved the scaling of linear measurements in 2-D. When a second view was incorporated into the image, either by means of a mirror reflection, or by the use of a second camera, a three-dimensional image was able to be approximated as a contour map comprised of cross-sectional slices. These three-dimensional approximations allowed for such anthropometric measurements as surface area and total body volume to be approximated (Hertzberg, Dupertuis, & Emanuel, 1957). Although there are some reports of the use of photogrammetric measures for

functional reach (Dempster, Gabel, & Felts, 1959), little else happened until the mid-1970's when Jensen (Jensen, 1978) used photogrammetry to analyse biomechanical properties in body shapes of children.

2.3. Modern Imaging Techniques

Similar to the stereophotogrammetric methods discussed prior, 3-D body scanners rely on the interpretation of image data from multiple view positions for each scanned portion to create a data file of three dimensional data points. Several technologies, such as laser imaging, and millimetre wave imaging, exist for the collection of image data.

2.3.1. Laser Imaging

In most laser scanners, one scanning head uses two image capture devices to view a single or series of points of illumination on the scanned subject. Based on known calibration standards, image processing software triangulates the location of points identified by laser illumination, with reference to an origin position. These systems require the subject to be clad in pre-defined clothing; typically, highly reflective and tight-fitting garments are chosen. The participant is also asked to assume and remain in a standardized position for the duration of the scan, usually less than one minute.

2.3.1.1. Data Point Triangulation

A scanner head is calibrated based on an object with known dimensions. When the calibration object is photographed from two directions, a transformation matrix can be developed that converts a local coordinate system interpreted by the scanner head to the global coordinate system defining the object. This transformation matrix can then be used to convert data points interpreted by a scan head into a point cloud of 3-dimensional in a global coordinate system for any scanned object (Zhengyou Zhang, 2000).

2.3.1.2. Data Processing

Built into scanner data processing software is a filtering algorithm that removes points that do not indicate a location on the surface of the subject. By combining the point clouds from each of the scanner heads into one point cloud file, an acceptance envelope can be defined that allows all points outside a volume of expected dimensions to be rejected. These points can be indicative of scanner walls, floors, or optical anomalies.

After the Cartesian point cloud has been filtered, a three-dimensional spline algorithm (J. C. K. Wells, 2007), or in some cases a straight-line linear interpolation (Allen, 2003), fits a mesh to the data points so that calculations (such as volumetric approximations) can be made. While some algorithms utilize a template of expected topography to fit the surface spline to the acquired data points, others fit only points that are acquired, without a preconceived template of the expected human form (J. Wells, Douros, Fuller, Elia, & Dekker, 2000).

Much of the literature related to photonic imaging involves demonstrating that scanning devices more efficiently measure the human form than standard classical methods, within a reasonable margin of error. To achieve the efficiency that justifies the utility of many of the currently researched scanners, landmark identification and measurement processes have been either fully or semi-automated (Robinette, 2006). The key motivation has been to extend the number of measurements possible in the least amount of time for set-up, subject preparation and data collection and reduction time.

2.3.2. Millimeter Wave Imaging

A second technology investigated is the millimeter wave scanning technology. This device uses microwave-range electromagnetic radiation that is reflected off of the surface of the skin and received by a linear array of antennae. These antennae transmit and receive the signals and through the interference and phase changes of reflected waves, calculate the distance to the surface of the subject.

Several benefits are apparent with the use of the millimeter wave scanner, when compared the laser scanner. Firstly, the millimeter wave scanner completes a single scan in approximately five to ten seconds as compared to the nearly one minute scan performed by the laser imaging device. Furthermore, privacy concerns of the subjects can be alleviated as the millimeter wave scanner does not require the wearing of specific garments during the scan. Rather the participant is free to his or her "normal" attire. However, if specific anatomical landmarks are required from the scanned image, additional considerations are necessary.

The millimeter wave scanner output "fog" file contains approximately 14.75 million voxels arranged in a three dimensional grid. The transverse plane is divided into a 256 by 256 voxel grid, and 225 of these grids are stacked along the vertical axis of the erect subject. After scanning, each voxel is assigned an intensity value corresponding to the strength of signal indicating that point in space. In general, reflective metallic objects and the water in the human skin provide high intensity values of reflectance that differentiate these surfaces from the surroundings, and the subjects' garments.

In our case, using proprietary software supplied by Unique Solutions, these fog files can be converted to the three dimensional "point cloud" data type for which software has been developed in-house to extract anthropometric data.

2.4. **Automatic Measurement Collection**

While the three-dimensional images rendered in the data processing procedures discussed prior are a novel rendering of human topography, they have little value if the data points cannot be converted into measurements for practical use. In order for the anthropometric measurement data to be collected from the three-dimensional image captured and processed by a scanner, the landmarks identifying these measurements must first be located. Manually identifying these landmarks, and measuring between them on the digital image would be a time consuming process, and would need to be completed within one study session. Photonic

imaging allows the subject to be dismissed and the image from which measurements are collected to be retained (J. Lin et al., 2002).

2.4.1. Landmark Identification and Linear Measurement Calculation

Currently, there are several automatic methods of identifying anthropometric landmarks in three-dimensional imaging, usually applied to laser scanning methods. The first method involves manual identification of palpable landmarks using the classical methods, and the placement of removable targets on these landmarks. After the subject is scanned, a computer algorithm recognizes these targets and uses them as proximal and distal measurement points for anthropometric measurements (Robinette, 2006).

The second and less common method of identifying anthropometric landmarks consists of an automatic landmark recognition algorithm that automatically locates the locations on the topography of the scan, without the need for pre-placed targets. The benefit of this method is that less time is required to prepare a subject for a scan; however, the cost of this efficiency is that errors can be introduced due to variability of subjects (Burnsides, Boehmer, & Robinette, 2001).

Once landmarks have been identified, and assigned 3D coordinates, distances between landmarks can be easily calculated using a three dimensional distance formula based on Euclidian geometry.

2.4.2. Circumferential and Volumetric Measurements

The measurement of circumferential and volumetric dimensions is more complicated that the simple straight-line lengths discussed previous. After the point cloud has been collected and converted to a three dimensional mesh, the resulting model of the subject is sliced horizontally and the circumference (girth) and the area of that slice calculated. The calculated areas are multiplied by the slice thicknesses and summed over body regions or totalled over the whole subject model. This yields body segment volumes, or total body volume, which can be used in percent fat calculations (Siri, 1956). The circumferential measures are obtained via one of

two different methods; either the circumferential shape is represented as a simple geometric shape – usually an ellipse – or a detailed method of following the concavity-convexity of the object is developed (Jensen, 1978b).

2.5. Measurement Validation

In order to ensure that the methods of collecting scan-extracted measurements are valid, they must be compared to standard methods that have been previously validated and accepted by the scientific community. Validation schemes vary depending on the specific measurements collected.

As the act of measuring fleshy landmarks can result in compression of tissue, affecting the result, initial validation should be performed on standardized inflexible phantoms (Robinette, 2006). This will minimize some of the potential direct measurer error, and errors associated with human variation; however, as the objective of designing a laser imaging system is the eventual use on human populations, paired testing on subjects against a known measurement standard must also be performed.

2.5.1. Linear and Circumferential Measurements

The most obvious means of validating any new measurement methodology is to compare to the existing "gold standard" which in this case is manual methods of collecting the measurements. Classically, linear straight-line measurements are collected using a pair of calipers, known as an anthropometer, which measures distances between palpable bony landmarks. Circumferential measurements are generally collected using a flexible cloth or steel measuring tape (Hrdlicka, 1972).

The results of the CAESAR study, a large-scale anthropometric survey jointly conducted jointly in the Netherlands, North America, and Italy, using laser scanning technologies, were compared to results collected using the methods developed in the ANSUR survey a decade prior for the American military. The study compared the mean absolute differences (MAD values) within linear measures of subsequent scans to ensure the repeatability of the measurement process, as compared to

expected MAD values presented in the ANSUR survey. The MAD values determined in the ANSUR work ranged from 2 to 11 mm and are reported with respect to the true length of the measure recorded. The laser scanning technology performed sufficiently according to these standards. (Robinette, 2006).

In 2010, the International Standards Organization (ISO) building upon the ANSUR work, published standards governing the collection of anthropometric measurements for the creation of large-scale databases. Amongst other things, this document outlined maximum allowable error between scan-extracted values and manually measured one dimension scalar values, shown in Table 1. Furthermore ISO 20685 described the means of performing validation studies of anthropometric hardware (STANDARD & ISO, 2010). Interestingly, there have been very few reports in the literature that truly compare manual measures to scan extracted measures on the same sample of participants. For the most part the emphasis has been on documenting the repeatability of the measures within on measurement system.

Table 1: Maximum allowable error between extracted value and traditionally measured value

Measurement type	Maximum mean difference (mm, Standard, ISO 2010)
Segment lengths	5
Body heights	4
Large circumferences	9
Small circumferences	4
Body breadths	4
Body depths	5
Head dimensions without hair	1
Head dimensions with hair	2
Hand dimensions	1
Foot dimensions	2

2.5.2. Volumetric and Body Fat Measurements

Direct measurement of body volume is a more difficult process and until the development of modern imaging technologies, could only be performed using indirect calculation, or approximation. The earliest direct measurement work

calculated body and segmental volumes using direct volumetric immersion from which the segmental and whole body density could be determined (Dempster. (1956?) These body volume measurements are critical in the determination of percent body fat, an indicator of a patient's adiposity. Standards against which imaging units compare volume measurements vary depending on the application of the volume measurement. In 2006, Wang published a paper wherein he described an experiment where a laser scanning apparatus collecting segmental volumes on a mannequin, and comparing to manual volume measures using the displacement of water (Wang et al., April 2006). The results can be seen in Table 2.

Table 2: Body volumes of a mannequin measured 9 times by a 3-dimensional laser scanner and water displacement techniques (Wang et al., April 2006)

Volumes (L)	3DPS – Scan (L)	Water Displacement (L)	Difference (L)	p	Relative Error (%)
Total body	23.87 ± 0.03	23.62 ± 0.03	-0.25 ± 0.04	0.0001	-1.1
Head (top)	1.88 ± 0.02	1.82 ± 0.01	-0.06 ± 0.02	0.0149	-3.3
Left arm	0.51 ± 0.00	0.53 ± 0.00	0.01 ± 0.00	0.0016	1.9
Right arm	0.42 ± 0.00	0.40 ± 0.00	-0.02 ± 0.00	0.0001	-5.0
Left leg	2.33 ± 0.02	2.37 ± 0.01	0.04 ± 0.03	0.1256	1.7
Right leg	2.08 ± 0.02	2.08 ± 0.00	0.00 ± 0.02	0.9564	<0.0

Two important points are evident from this paper. Firstly, there are small but statistically significant differences in the values and secondly, the total body volume of the manikin is approximately 23.62 L which substantially less than the total body volumes of typical adults.

The simplest and least time consuming approximations of total body volume are performed using underwater weighing where the buoyant force of a submerged subject is measured. According to Archimedes' Principle, the buoyant force is equal to the weight of the water displaced by the volume of the immersed object. The weight of the displaced fluid is equal to the product of the density of the water and the volume. By taking the difference between the subject's dry-land weight and the in-water weight of the submerged subject as shown by a load cell attached to the submerging apparatus, and dividing by the density of water, the volume of a subject can be determined. Segmental techniques use variations of this technique by

directly capturing the volume of displaced water and from this, determine the volume of the immersed segment.

Finally, photonic scanners can compare the quickly-extracted volume measurements to the more time consuming volume measurements collected using medical imaging apparatus such as dual-energy x-ray absorptiometry (DEXA), computed tomography (CT), or magnetic resonance imaging (MRI). While DEXA, CT, and MRI are purported to precisely identify body composition and volumes, these methods are time consuming and costly, and require specialized environments and technical staff for their operation (J. C. K. Wells, 2007). Several research institutions have validated laser imaging units against these medical imaging technologies and have demonstrated that laser scanners provide reasonable approximations of body volume at a much lower cost point (J. C. K. Wells, 2007). All of these measures must deal with the small changes in body volume associated with normal breathing, and movement of the subject during the measurement process as well as subsequent image related measurement errors.

2.5.3. **Definition of Axes**

For this document, all axes will be defined according to Figure 2.

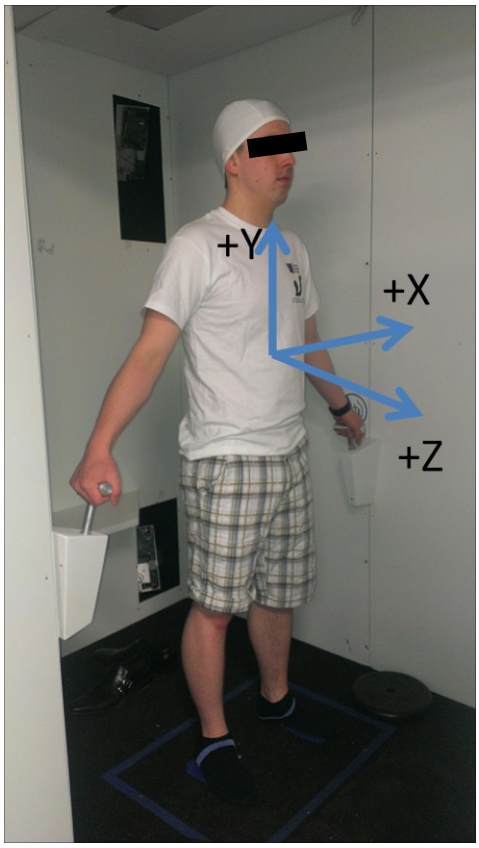

Figure 2: Axis definitions

In this definition, the X-axis is the medial-lateral axis, the Y-axis is the inferior-superior axis, and the Z-axis is the anterior-posterior axis.

2.6. Obesity, Classical Adiposity Indication, and Metabolic Disease

The literature demonstrates that many disease states develop secondary to obesity, resulting in strong correlations between obesity and hypertension, diabetes mellitus, and many other metabolic disorders. Waist circumference and waist to hip ratio, discussed later, serve as a metric in many studies investigations the relationships between obesity and such diseases as ischemic heart disease and diabetes, because these diseases have been shown to be best predicted by the quantification of central obesity. The World Health Organization defines overweight and obesity as *abnormal or excessive fat accumulation that presents a risk to health*. The WHO has classified obesity as a global epidemic (World Health Organization, 2014).

2.6.1. **Metabolic Syndrome**

Several cardiovascular and metabolic risk factors can be grouped under a single term, known as metabolic syndrome, as these risk factors often coincide. Such symptoms as hypertension, obesity, dysglycemia, and elevated triglyceride levels can be attributed to metabolic syndrome, or Syndrome X, where obesity has been established to be an important cause of the disease state (Alberti et al., 2009).

Lin, Chiou et. Al. (2002), utilized a 3D laser imaging device to perform a cross-sectional study of metabolic diseases as correlated to a variety of anthropometric characteristics. Included in their study were correlations of metabolic disorders to WHR, BMI, and a custom health index involving anthropometric data including two-dimensional area measurements (J. Lin et al., 2002).

2.6.2. **Classical Adiposity Indication**

Metrics for obesity have been developed using external anthropometric characteristics as greater emphasis is placed on obesity as a cause for a variety of metabolic and other diseases and disorders. While some measures utilize single-dimension measurements such as waist circumference, other measurements account for relative body shape through a multidimensional approach (J. D. Lin, Chiou, Weng, Fang, & Liu, 2004).

2.6.3. **Body Mass Index**

The current medical standard determining a patient's adiposity is the body mass index (BMI), calculated using a formula that incorporates the anthropometric measures of height and mass, seen in Eq. 1. While this measure has clinical advantages because it utilizes simple, commonly obtained measures it has been shown to be a poor indicator of actual % body fat. This metric is only a rough guide to determine excess fat, and does not account for body macrostructure or soft tissue composition.

$$BMI = \frac{mass}{height^2} \tag{1}$$

A person with a BMI greater than $25\ \frac{kg}{m^2}$ is considered overweight. A person whose BMI exceeds or is equal to $30\ \frac{kg}{m^2}$ is considered obese. For example, all of the calculations in Table 3 result in a similar BMI value that would be classified as obese.

Table 3: Example mass and stature parameters for a BMI of 30

Stature (m)	Mass (kg)	BMI
1.41	60	30
1.47	65	30
1.53	70	30
1.58	75	30
1.63	80	30

It should be reasonably obvious that physically these are very different people who may or may not actually be at risk for metabolic disorders.

2.6.3.1. Percent Body Fat

A more accurate assessment of soft tissue composition is a percent body fat analysis, which requires greater measurement time, but provides greater insight into adiposity, and accounts for more muscular builds. Several standards exist for the determination of body fat. The first method involves the use of calipers to measure the thicknesses of folds of skin at known positions on the body. These measurement values are operated upon by regression equations that can be used to approximate body density. This density value can be used in another equation yield an approximation of the percentage of fat tissue with respect to the patient's overall mass.

The second method of determining percent body fat involves the use of Siri's equation, except in this case, body density is derived by dividing the participant's mass by their volume – calculated using the differential force method during an underwater submersion discussed prior. Unfortunately, both of these measures would require additional clinical time to obtain the measures and subsequent calculations (Siri, 1956) . Siri's formula that uses the parameter of density to

estimate percent body fat is shown in Equation (2), where f is the desired measure of percent body fat, and d is the measurement of density.

$$f = \frac{4.950}{d} - 4.500 \quad (2)$$

Participants undergoing hydrostatic weighing to determine percent body fat are often asked to exhale forcefully, and the force used to calculate density is taken at the end of a maximal expiration to correct for air volume in the lungs. Further adjustments are made for residual lung volume (Biaggi et al., 1999). Waist Circumference and Waist-to-Hip Ratio

Waist circumference has been demonstrated as another means of predicting health risks associated with obesity. Like BMI, waist circumference does not account for the frame of the participant, nor does it account for the body composition. Both measurements have demonstrated relationships to indicators of metabolic syndrome, yet it is inconclusive from the literature which measure is better correlated. Both have been found to be superior to BMI as a predictor of cardiovascular disease (Schneider et al., 2010). Waist to hip ratio has been found to be significantly correlated to total cholesterol – an indicator of metabolic syndrome – ($r = 0.384$, $p = 0.0001$). Other studies have suggested that waist to hip ratio (WHR), while correlated to disease, is a poor indicator of fat distribution (Chan, Watts, Barrett, & Burke, 2003). Nevertheless, waist circumference and WHR continue to be clinical standards in the evaluation of adiposity and have led to the development of health indices, discussed in the next section.

2.6.3.2. Chang Gung Research and Health Index

Several large-scale studies were performed at the Chang Gung Medical Centre in Taiwan that sought to demonstrate a correlation between the prevalence of metabolic syndrome and certain pre-determined anthropometric factors, measured using a full-body laser scanner.

Waist circumference has been shown to be an indicator of obesity; however, further correlations exist for measurements that are referenced to another body measurement, such as the waist to hip ratio. The ratio of the waist width to the hip width was researched in the Chang Gung studies discussed above in order to predict metabolic diseases. In addition, a complicated formula combining anthropometric data and laboratory blood test result values yielded a *Health Index (HI),* shown in Eq. 3 (J. Lin et al., 2002) that was even more strongly correlated to some metabolic diseases.

$$HI = \frac{(body\ weight)\times 2\times(waist\ profile\ area)}{[body\ height^2\times(breast\ profile\ area+hip\ profile\ area)]} \quad (3)$$

The Chinese ethics rules under which the Chang Gung studies operated allowed those conducting the studies in Taiwan access to the clinical files associated with study participants. This allowed for relationships to be built between the acquired data and clinical histories. Such broad content release is more difficult to attain in North America. Furthermore, this study analysed a sample with a broad distribution of adiposity.

2.7. Bariatric Surgical Interventions and Post-Operative Evaluation

The most practical solution to excess adiposity is a lifestyle change, adjusting activity and eating habits. Unfortunately, people who are extremely overweight have been shown also to have a decrease in mobility (Vincent, Vincent, & Lamb, 2010). As a result, it becomes difficult for this population to achieve the required mobility to effect significant weight loss. Furthermore, emotional factors can also result in this population consuming excess food, or types of food conducive to excess adiposity. Candidates like these can benefit from a bariatric surgical program as an option to help to decrease appetite, and aid in the process of weight loss.

2.7.1. Bariatric Surgery Program Requirements

Gastric surgery at Capital District Health Authority is viewed as a tool to aid in the decrease of excess body weight, to be used along with lifestyle changes such as

healthy eating and exercise. After surgery, the gastrointestinal systems of patients will be greatly modified, requiring extreme diet modification for months following surgery. Before patients are allowed to enter the gastric surgery program at Capital District Health Authority in Halifax NS, they must demonstrate that they are going to perform the required lifestyle changes by making these changes prior to surgery. These changes include:

- Quitting smoking
- Improving eating habits
- Becoming knowledgeable on weight loss surgery
- Increasing activity level
- Journaling all lifestyle changes

Weight loss surgery candidates are screened by a panel at CDHA consisting of a nurse practitioner, a surgeon, a dietician, and a psychologist, to determine if the candidates are ready mentally and physically for the changes to their lifestyle that bariatric surgery will entail (Obesity Network, 2010).

2.7.2. **Vertical Sleeve Gastrectomy**

While many different options exist for gastric surgery, including temporary and permanent restrictive surgeries, as well as surgeries that bypass parts of the gastrointestinal tract that absorb nutrients, the singular surgery that is performed at CDHA is called a vertical sleeve gastrectomy (VSG), or gastric sleeve. The VSG is an irreversible surgery that involves the restriction of the stomach by removing over 85% of it and creating a *sleeve* that connects the esophagus to the small intestine.

The vertical sleeve gastrectomy offers several improvements over the alternative surgical options (Obesity Network, 2010), including:

- The portion of stomach removed contains the glands that produce *ghrelin,* the hormone that induces hunger

- The portion of stomach that remains is less stretchy, thus *satiety* is achieved with less food
- The lack of intestinal bypass means that vitamins and nutrients can be absorbed properly

2.7.3. **Laboratory and Anthropometric Evaluation**

In order to evaluate patients pre- and post-operatively, gastric surgery patients are subjected to a battery of tests in clinic before, as well as after the surgery is performed. These tests encompass physical measurements, as well as laboratory investigation. . The only anthropometric investigations currently conducted clinically are a single dimension measure of waist circumference, and BMI, as calculated using height and mass. It is the long term goal of this research to develop the technical and clinical components that would allow for the rapid, accurate measure of body volumes and shapes to explore whether these may be valuable in the clinical component of obesity. Additionally, a more "patient friendly" means of measuring total body volume – in order to compute percent body fat – than hydrostatic weighing, which is mechanically difficult for this population due to mobility requirements such as climbing the ladder into the tank, and limitations in apparatus strength. However, in order to proceed with this work, fundamental biomedical engineering work in imaging and extracted measurements is required which is the focus of this study.

Chapter 3. Methods

3.1. Population Sampling

The first phase of this study comprised a proof of concept validation to ensure proposed technology will adequately measure the linear, circumferential and volumetric measurements, especially in severely obese populations. Consequently, this does not comprise a large-scale anthropometric survey, and only studied a small scale sample of convenience of the target population. The proposed sample size for this survey was 16, stratified by sex and BMI; however this was eventually expanded to a sample size of 20, to account for increased variation in the population. The summary of participant strata is shown in Table 4. With this sample, the systematic error of the scanner was determined over a large range of possible measurements, prior to determination of agreement between manual and 3D scan extracted measures in obese participants. The ISO provided a sample size calculation according to the following formula:

$$n = \frac{s^2}{\delta^2} \times (1.96 + 1.65)^2 \quad (4)$$

Work performed prior to this study indicated that breadth measurements had a standard deviation of 4.2 mm, which was used for the sample *s* standard deviation. The sample size according to this calculation, that comprised the sample size for this preliminary study, where the ISO standard for allowable error for breadth measurements is 4 mm, is 15 participants. This was increased slightly to 20 to ensure a larger variety of body shapes could be captured by the study.

Table 4: Stratification of study participants

BMI	Males	Females	Total
< 18.5	1	2	3
18.5 to 24.9	3	5	8
25 to 29.9	3	2	5
30 +	4	0	4

3.1.1. Recruitment

Recruitment of participants, as approved by the ethics proposal submission to the Dalhousie University Health Sciences Research Ethics Board, was performed through posters distributed on the Dalhousie University campus. Participants consisted of adults between the ages 18 and 65 and who were able to hold their breath underwater for 20 seconds. A full disclosure of all processes was made to participants, and each participant signed an informed consent waiver.

3.2. Data Collection

All participants underwent the same measurement protocol consisting of one landmark identification station and three measurement stations, as shown in Figure 3. Attempts were made to schedule participants to undergo measurements in tandem to better utilize research assistants' time and reduce idle time.

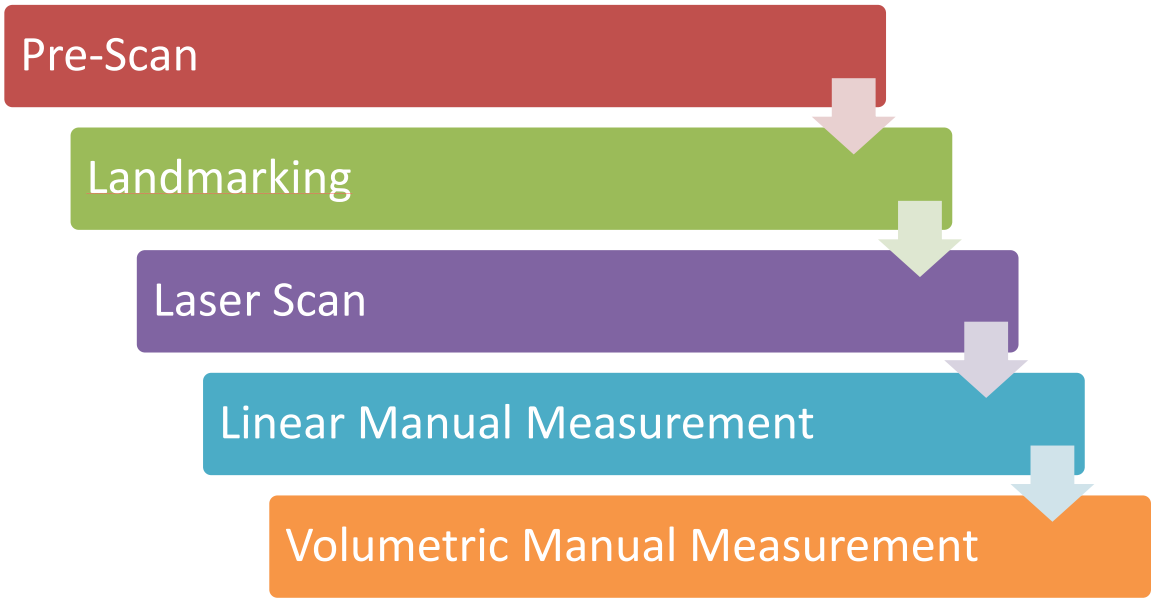

Figure 3: Flowchart of human testing procedures

3.2.1. Station 1: Landmark Identification

Prior to entering the first station, participants underwent landmark marking using a non-toxic "permanent" marker. The participants were asked to change into standard garments provided by the technicians. Males wore white boxer briefs, and females wore white undergarments, or spandex shorts, and a white sports (or

other) brassiere. Each of the landmarks listed in Table 5 were palpated by a technician, and identified with a small "X." This process took approximately 20 minutes.

Table 5: Anthropometric landmarks identified

Number	Landmark Name
1	Apex of Head
2	Glabella
3	Eye (left corner)
4	Spinous process of the 7th cervical vertebrae (C7)
5	Below bulge of thyroid cartilage
6	Right Acromion
7	Left Acromion
8	Right Front Scye Crease (no marking)
9	Left Front Scye Crease (no marking)
10	Maximum Circumference Upper Arm
11	Right Olecranon
12	Left Olecranon
13	Right Ulnar Styloid
14	Left Ulnar Styloid
15	Midpoint of Nipple Line
16	Omphalion
17	Right Iliocristale
18	Left Iliocristale
19	Right Greater Trochanter
20	Left Greater Trochanter
21	Right Gluteal Fold
22	Left Gluteal Fold
23	Crotch (no marking)
24	Right Lateral Femoral Epicondyle
25	Left Lateral Femoral Epicondyle
26	Right Lateral Malleolus
27	Left Lateral Malleolus

(Chamberland, Carrier, Forest, & Hachez, 1998), (STANDARD & ISO, 2008), (Zatsiorsky & Seluyanov, 1983)

3.2.2. **Station 2: Scanning**

The participants then proceeded to the laser scanner and instructions were provided by the technician who allowed the opportunity to ask questions. The scanner technician then applied markers over the previously identified landmarks, such that the centres of the markers were adjacent with the "X" markings. The

technician instructed the participants to stand still and assume a posture "as if their height was undergoing measurement." Furthermore, the participant was instructed to breathe normally, as it may have been difficult to hold their breath for the duration of the scan. The participant entered the scanner, stepped onto the scale, and assumed the posture shown in Figure 4. The participant indicated readiness to the technician, scanned a barcode under the reader at the front of the scanner, and remained still while the laser scanner performed the scan. This scan process proceeded three times in total. Once each scan had completed, the participant proceeded to the third station – manual measurement. The participant alternated between scan and manual measurement stations as there was a waiting period between scans such that the scan was processed. Total scan process took approximately 30 minutes.

Figure 4: Participant posture within scanner

3.2.3. Station 3: Manual Measurement – Circumferences, Breadths, and Lengths

After scanning, the participant proceeded to the manual measurement station that involved the measurement of circumferences, breadths, and lengths. Each

measurement was be collected three times, such that the final value was the average of the measured values. All limb measurements were taken on the participants' left side. All measurements shown in Table 6 were defined using documented standards and are described in detail.

Table 6: Manual measurements to be collected

Measurement Type	Measurement	Method Obtained	Standard Used
Volumes	Head and Neck Volume	Calculated measure	(Zatsiorsky & Seluyanov, 1983)
	(Left and Right) Upper Arm Volume	Direct measure	(Zatsiorsky & Seluyanov, 1983)
	(Left and Right) Lower Arm Volume	Direct measure	(Zatsiorsky & Seluyanov, 1983)
	(Left and Right) Hand Volume	Direct measure	(Zatsiorsky & Seluyanov, 1983)
	Torso Volume	Direct measure	(Zatsiorsky & Seluyanov, 1983)
	(Left and Right) Thigh Volume	Direct & calculated measure	(Zatsiorsky & Seluyanov, 1983)
	(Left and Right) Leg Volume	Direct & calculated measure	(Zatsiorsky & Seluyanov, 1983)
	(Left and Right) Foot Volume	Direct measure	(Zatsiorsky & Seluyanov, 1983)
Circumferences	Neck Circumference	Direct measure	(Chamberland et al., 1998)
	Chest Circumference	Direct measure	(STANDARD & ISO, 2008)
	Waist Circumference	Direct measure	(Chamberland et al., 1998)
	Hip Circumference	Direct measure	(Chan et al., 2003)
Lengths	Stature	Direct measure	(STANDARD & ISO, 2008)
Breadths	Chest Breadth	Direct measure	(Chamberland et al., 1998)
	Hip Breadth	Direct measure	(Chamberland et al., 1998)
Depths	Chest Depth	Direct measure	(Chamberland et al., 1998)
	Waist Depth	Direct measure	(Chamberland et al., 1998)
Other Relevant Data	Weight	Direct measure	(Chamberland et al., 1998)
	Body Mass Index	Calculated measure	(Chamberland et al., 1998)
	Age	Participant reported	-
	Sex	Participant reported	-

3.2.3.1. Linear Measurements

To measure vertical lengths from the ground, such as stature, and C7 height, a stadiometer was used, and participants were measured three times to the nearest milometer. To measure lengths between landmarks, an anthropometer was used with straight tips, and measurements were taken three times to the nearest millimeter. Breadth and depth measurements also utilized the anthropometer; however, as some depth measurements lie concave relative to adjacent anatomical structures, a curved tip was utilized.

3.2.3.2. Circumferential Measurements

All circumferences were taken at the landmark locations described in Table 7. A flexible cloth or metal measuring tape was used to collect circumference measurements to the nearest millimeter. Each circumference measurement was taken three times.

Table 7: Manual circumferential measurements to be collected

Number	Measurement	Landmarks
1	Neck Circumference	Circumference taken at the C7 landmark
2	Chest Circumference	Circumference taken at midpoint of nipple line
3	Waist Circumference	Circumference taken at omphalion
4	Hip Circumference	Circumference taken at trochanterian landmarks

3.2.4. Manual Measurement – Volumes

Manual volume measurements were collected on the body segments outlined in Table 8. To perform these measurements, apparatus was constructed to allow for obese populations. A full description of the development of volumeters can be seen in Appendix A. The strategy used involves the measurement of the volume of water displaced by the measured body segment. The entire segmental volume measurement process took approximately 45 minutes.

Table 8: Manual volumetric segmental measurements to be collected, with distal and proximal landmarks

Number	Segment Name	Distal Landmark(s)	Proximate Landmark(s)
1	Head and Neck	Apex of Head	C7, parallel to ground
2	Torso	C7	Centre of crotch, passing horizontally through the segment
5	Thigh	Centre of crotch, passing horizontally through the segment	Lateral femoral epichondyle, parallel to ground
6	Leg	Lateral femoral epichondyle	Sphyrion landmark, parallel to ground
7	Foot	Sphyrion landmark	Ground
8	Upper Arm	Acromion, passing laterally to scye creases	Olecranon, normal to arm length
9	Lower Arm	Olecranon	Ulnar styloid, normal to arm length
10	Hand	Ulnar styloid	Distal tip of middle finger

3.2.4.1. Measurement Apparatus

To perform limb volume measurements, arm and leg segment volumeters were manufactured. The device was comprised of a polyethylene container placed on an AMTI force plate, shown in Figure 5.

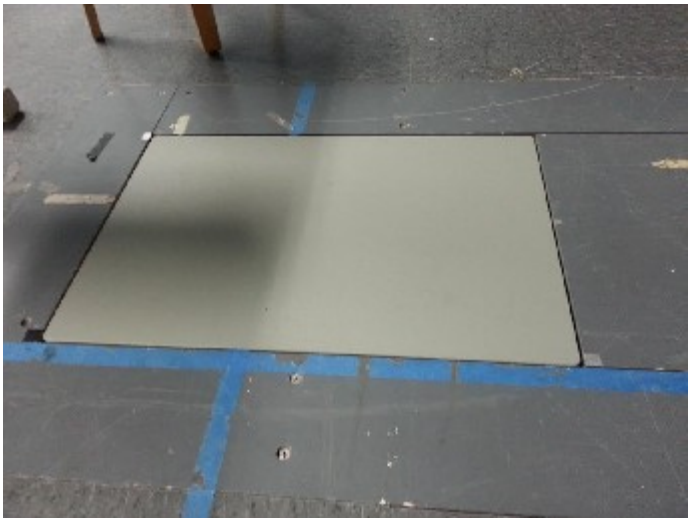

Figure 5: Force plate used for limb volumetry

The force plate was covered with a plastic sheet for protection from spillage. The volumeter was filled approximately two-thirds of the total volume such that a limb could be inserted without touching the walls, and also avoid overflowing of the water. The force plate was zeroed when it had stabilized, and prior to any limb submersion. In order to account for spillage reductions and/or loss of initial volume, the force plate amplifier was zeroed after every participant. The volumeter was validated according to the procedure discussed in Appendix A. In the case of the upper limb, the participant inserted his or her limb into the volumeter until the level intersected the landmark described in Table 8.

The participant's relaxed upper limb was placed into the volumeter. Five seconds of force plate data was collected at a frequency of 20 Hz. The volume of the limb segment was derived using the force and density of the displaced water. Each limb measurement was taken three times.

3.2.4.2. Torso and Thigh Volumes

The torso volume was measured using a full-body immersion method as described in the Review of Literature. Participants clothed in their personal bathing suit proceeded to the immersion tank, where a technician asked them to enter the tank and sit on the immersion chair. The participant performed a preliminary immersion

and was asked to remove all air bubbles from their hair, body surface as well as the air trapped within the bathing suit. The participants were asked to immerse themselves to the C7 landmark and breathe normally, in order to emulate the experience within the scanner. The force of the participant was collected and used to determine participant torso and limbs volume, using a AMTEK Chatillon CCR Series (CCR-220) force gauge, shown in Figure 6.

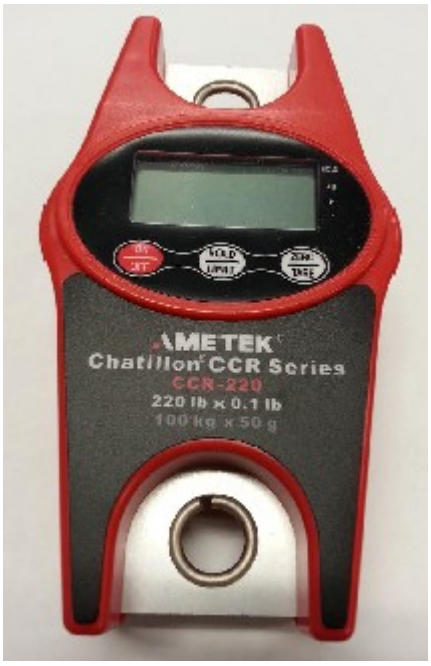

Figure 6: Force gauge used for torso, thigh, and head and neck volumetry

The limb volumes extracted prior were subtracted from this value to determine the torso value. Torso volumes were collected three times per subject. This provided a measure of the total body volume less the head and neck. From this, total volume the upper and lower limb volumes were subtracted to provide a measure of the torso. This measure was repeated three times per subject.

Participants were then asked to stand on the immersion chair, and lower themselves until the surface of the water intersected their crotch landmark. This was observed by the technician, but due to parallax as a result of viewing angle, the participants were asked to identify by sensation as well. The force value was

collected and by subtracting torso, upper limb, leg, and foot volumes, thigh segment volumes were computed.

3.2.4.3. Total Body Volume

To determine total body volume (TBV), the participants were then asked to inspire normally, and then lean forward to immerse themselves completely, again attempting to be compatible with what was experienced in the total body scanner. The force of the participant was then collected and used to determine participant volume. The final submerged weight value was not compensated for the residual volume of air in the lungs as the scan-extracted value was only a surface representation of the torso region; compensation would lead to scanner over-prediction of torso volume. Head and neck volume were calculated by subtracting total body volume from the torso and limb volume. Head and neck, as well as TBV were taken three times for each subject.

3.3. Scan Post-Processing

After the scans were collected, they were converted to a point cloud of three dimensional data points. The conversion software was supplied by Unique Solutions. Custom software developed in the lab was used to identify landmark markers, and begin the measurement process.

3.3.1. Linear Measurements

Custom software identified the distal and proximal landmarks of the length measurements in Table 6 and measured the distances between them. In the case where the ground is the terminal point of the measurement, the lowest data point on the foot functioned as the "ground" measurement.

3.3.2. Circumferential and Volumetric Measurements

Another application developed in the lab used the landmark markers described in Table 8 to create planes dividing sections of data comprising the body segments described. These segment volumes were measured according to the procedure

discussed in Chapter 5, discussing software development. Total body volume was calculated by summing segmental volumes.

3.4. Statistical Analyses

The data (linear, circumferential, and volumetric) collected using manual measurement methods and extracted using three-dimensional imaging was compared statistically to confirm agreement between the two measurement methodologies. All data from the manual and scanner was tested for normality using the Shapario-Wilkes test. The critical alpha required for the test was set to $\alpha = 0.1$.

3.4.1. Validity via Correlation and T-Test

Two measurement techniques that perform the same measurement should be highly correlated and not differ in overall mean scores. A Pearson Product Moment Correlation Coefficient was calculated for each measurement across all participants to represent the strength of the relationship between the two measures.

However, because correlation can only test the linearity of a relationship between two modes of measurement, and cannot account for bias, a t-test determined if there is a systematic error between the two measurement strategies. The "paired" t-test was used because the same participant population was used for both measurement methodologies.

3.4.2. Agreement

If two measurement methodologies are compared over a wide range of "true" values, a larger correlation coefficient can be determined; if the range of measurement validation is narrowed, the relative error between measurements is higher. Furthermore, an increase in sample size may indicate a better strength of relationship between the scan-extracted and manual measures than actually exists.

A Bland-Altman Agreement test was also used to determine the limits of agreement of the two strategies within a 95% confidence interval. The difference between the

measurements taken from 3D scans and manual techniques were plotted against the manual values. Ideally, these differences should be randomly distributed; however, if a systematic error was found, it was accounted for, and the data adjusted accordingly. This test also determined if the 95% confidence interval of linear measurements are within the maximum allowable error as discussed in ANSUR (Robinette, 2006), and maximum allowable errors outlined in ISO 20685 (STANDARD & ISO, 2010).

3.4.3. **Volumetric Considerations**

As the ISO has not published standards for segmental volume measurements, Wang's volume measurements of mannequins have served as a preliminary basis of comparison (Wang et al., April 2006). However, a more reasonable standard for acceptability, especially at this early stage in the research program, should be based on the intended clinical population. Clinical significance will be discussed in section 3.5.

3.4.4. **Regression**

Finally, due to the presence of systematic errors in many of the scan-extracted measurements when compared to manual methodologies, regression analysis was used to improve the prediction of the laser scanner for acquiring anthropometric measurements. In the regression, shown in Equation 5, M is the regressed segment volume value, S is the scan-extracted value, β_1 is the coefficient of the scan-extracted measurement term, C is the constant offset of the regression, and err is error not accounted for by the regression.

$$M = C + \beta_1 S + err \tag{5}$$

In some cases, standard healthcare-related measurements of manual stature and manual mass were used as predictors in the regressions of scan-extracted measurements, if they were significant coefficients in a backwards stepwise linear regression ($\alpha = 0.1$). The format for this regression followed Equation 5, and is

shown in Equation 6 below where m and s are manual mass and stature terms, and β_2 and β_3 are coefficients for the manual mass and stature terms of the regression.

$$M = C + \beta_1 S + \beta_2 m + \beta_3 s + err \quad (6)$$

Coefficients of determination (R^2) were reported for every regression, as were the p values for each included variable.

The residuals of these regressions were then correlated to the manual measurements in order to determine if there was a significant linear error. The 95th percentile confidence intervals of residuals of the regressed measurements were then substituted for differences when comparing to ISO standards for human anthropometry for allowable confidence intervals of difference values. Finally, a single sample t-test was then used to determine if the mean value was significantly different from zero.

3.5. **Clinical significance**

There is a general consensus in obesity literature that "clinically important" weight loss comprises a decrease in body weight of ≥5% (Douketis, Macie, Thabane, & Williamson, 2005). Therefore, while a measurement tool may have sensitivity to read with high precision, and measure differences *statistically* significant (according to section 3.4), such measurements may not comprise *clinical* significance; however, it is important that any tool with an intended clinical application related to obesity at least attain this standard.

It has been shown that for a decrease in adipose tissue due to a calorie-deficit diet, 75% of weight loss is a result of a decrease in adipose tissue, and 25% of weight loss is a decrease in fat-free mass (Klein et al., 2004). Many of the measurements collected in this study were volumetric measurements, and therefore it is important to recognize that there will be a decrease in volume that coincides with a decrease in mass. Siri's equation (Siri, 1956), which forms the foundation of body fat approximation, approximates the density of fat-free mass (m_{ff}) to be 0.9 g/cm^3, and

the density of fat-mass (m_f) to be 1.1 g/cm^3. Computing using the above proportions, a 5% decrease in mass would result in a 5.3% decrease in volume. As the intended clinical population of the research, those undergoing weight-loss by way of calorie-deficit diet and other lifestyle changes as well as potential surgical intervention, this was used as the standard for clinical significance for this pilot investigation.

Chapter 4. Preliminary Work

Precision error in assessing human measurements can be quite high, as the identification of human anthropometric landmarks can be challenging, and the suppleness of flesh, respiration, and short term physiological changes can cause measurement variability. Consequently, the identification of sources of systematic error in measurement instruments, such as the scanning apparatus intended for use in this body of research, can be equally as challenging. As a result, the scanner must be validated for measurements extracted from scans of a rigid imaging phantom of known dimensions, such that variation of measurements collected by the scanning device can be associated with systematic errors within the device itself. Initially, access to two different scanning devices was granted by Unique Solutions for evaluation for use in health research applications, a millimetre wave scanner, and a laser scanner.

4.1. Millimetre Wave Scanner

The first scanner investigated was the millimeter wave scanner. Human participants were scanned in the millimeter wave scanner located at Unique Solutions, in a variety of limb configurations approved in a prior ethics submission. Visual inspection of the output scans can be seen in Figure 7.

Figure 7: FOG file output from millimetre wave scanner

The fog (3D voxel positions with assigned intensity values) files seen above were operated upon by a conversion application supplied by Unique Solutions in order to convert the above to a point cloud, seen below in Figure 8 that can be used by OEAB Lab developed software.

Figure 8: Point cloud output of converted millimeter wave FOG file

It becomes apparent that centrally located data points are much better represented in the scanner output than are those located peripherally. Lateral surfaces of the arms can be clearly seen, however medial surfaces are not well-represented by data points in the point cloud. The inability for the scanner to extract meaningful measurements from certain peripheral regions of the human participants is problematic for circumferential and volumetric measurements. As a result, the OEAB Lab, despite limitations, decided to focus efforts on the laser scanner, discussed below. This decision was vindicated retrospectively, as the literature demonstrated decreased precision with this scan modality (H. Daanen & Ter Haar, 2013).

4.2. Laser Scanner

The second evaluated imaging device was the laser scanner, for which a series of validation studies were designed. This photonic imaging device was originally designed for the garment industry, but because photonic imaging has recently shown much promise in ergonomics and health research applications, this scanner is undergoing validation across a wider variety of measurements relevant to these fields.

The laser technology utilized in this work was the Unique Solutions laser scanner, for which access was provided to the Occupational Ergonomics and Biomechanics Laboratory on an ongoing basis as part of an industrial partnership with the common goal of validating the device for healthcare-related applications. The scanner was provided with built-in software that processed point cloud data from sixteen scan heads and produced an output file of automatically-extracted measurements of length and volume relevant to the garment industry. Figure 9 outlines the process flow of the Unique Solutions software as it existed at the outset of the partnership with the OEAB Lab.

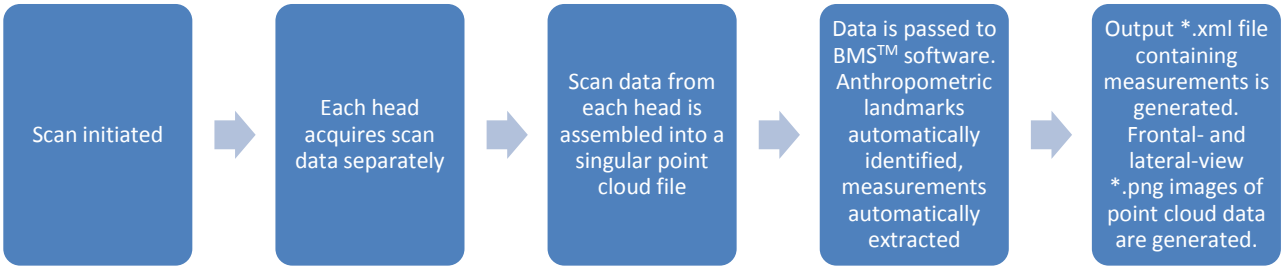

Figure 9: Flowchart of point cloud generation with Unique Solutions three-dimensional laser scanner

The first phase of the evaluation of the scanner assessed the onboard software for its utility for health-related applications. Given the increasing importance of percent body fat assessment in obese populations, the ability for the proprietary software to extract volumetric measurements from the point cloud data for percent body fat calculation was evaluated in a small pilot study of four participants.

4.2.1. Pilot Trial

Each participant was asked to wear light-coloured snug-fitting undergarments, and a scan cap to cover hair. The participant was then asked to enter the scanner, scan their barcode under a barcode reader to initiate the scan process, and assume a standardized posture and breathe normally. The scan took approximately 30 seconds. The point cloud was passed digitally to the proprietary software which automatically extracted total body volume (TBV) information.

Once the scan concluded, the participant was then asked to change into swimming garments and was directed to a hydrostatic weighing tank, where they sat on a submerged chair that was suspended by a force gauge. The participant was asked to take a normal breath and submerge for ten seconds while the force of the submerged participant was measured. The difference between the participants' dry land weight and the submerged force was used to calculate the buoyant force which

was then used to calculate TBV. The hydrostatic and scan-extracted TBV results were compared and are shown in Table 9 below.

Table 9: Results of initial pilot study

Participant Number	3D Scanner Volume (L)	Hydrostatic Weighing Volume (L)	Absolute Difference
1	49.01	47.02	2.0
2	75.4	76.3	0.9
3	136.1	120.7	15.4
4	146.03	59.48	86.6

As is evident in Table 9, there are significant errors with increasing volumes. Visual observation of scan-extracted point cloud data in point cloud viewer software availed distortion errors, as well as body sections unrepresented by point cloud data. A representative image can be seen below.

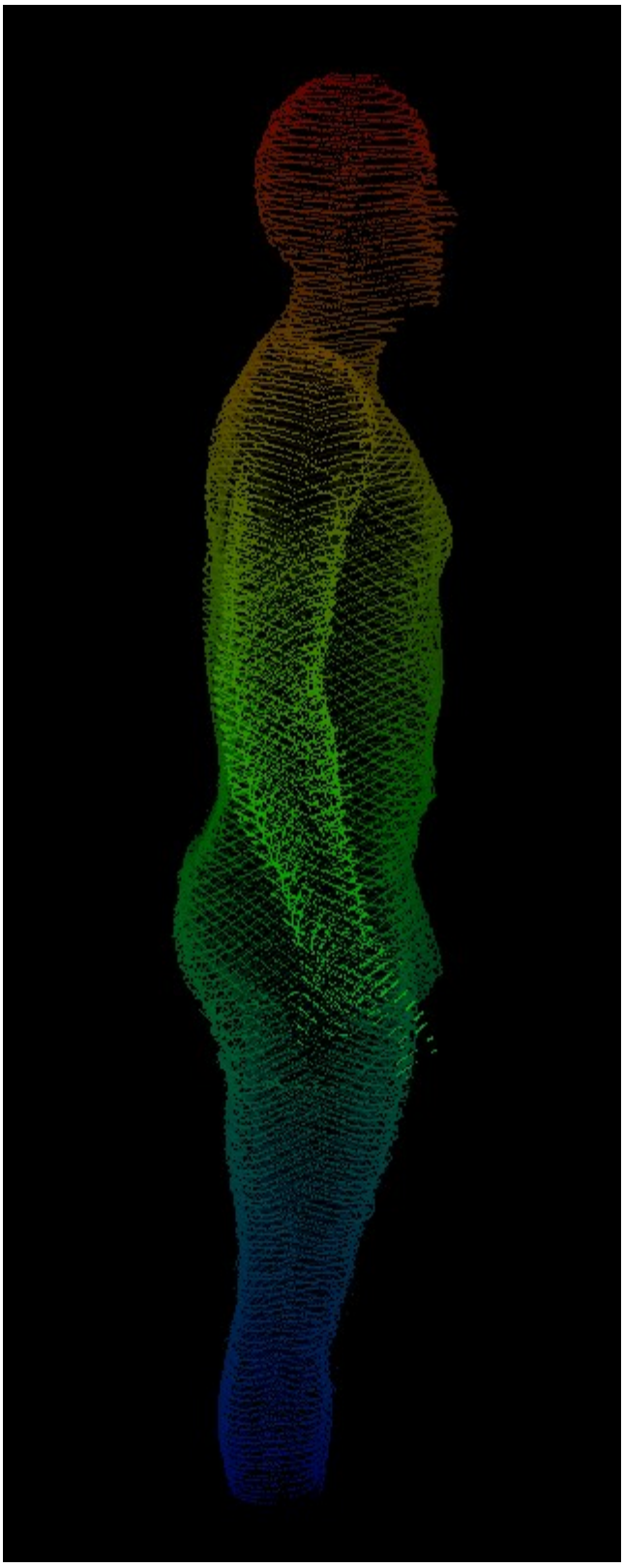

Figure 10: Distortions on side view of human scan

The results of this pilot study demonstrated a number of limitations associated with not only the software extracting and processing the point cloud, but also limitations associated with the hardware and set-up of the mechanical components of the three dimensional scanner. To correct for these sources of error, a series of hardware and software- related improvements were undertaken

4.2.2. **Mechanical limitations**

The most obvious limitation that became evident during this pilot study was the lack of data points below the ankles of participants' scans, and at the apex of their heads. This particular source of error was due to an insufficient field of view of the four lower scan heads. A custom acrylic bracket (shown in Figure 11 and Figure 12,) was designed that attached to the bolts on the back of the scan head, and also to the scan head mount, such that the scan head could be tilted forward, collecting an increased field of view. The effect of this tilt was an increase in a vertical field of view at the midpoint of the scanner of approximately 2-3 cm. Further adjustments to the brackets were not feasible so adjustment to the lower level of the scanner were made through the use of a small platform. This correction was useful for participants of shorter stature, but would not work for taller individuals.

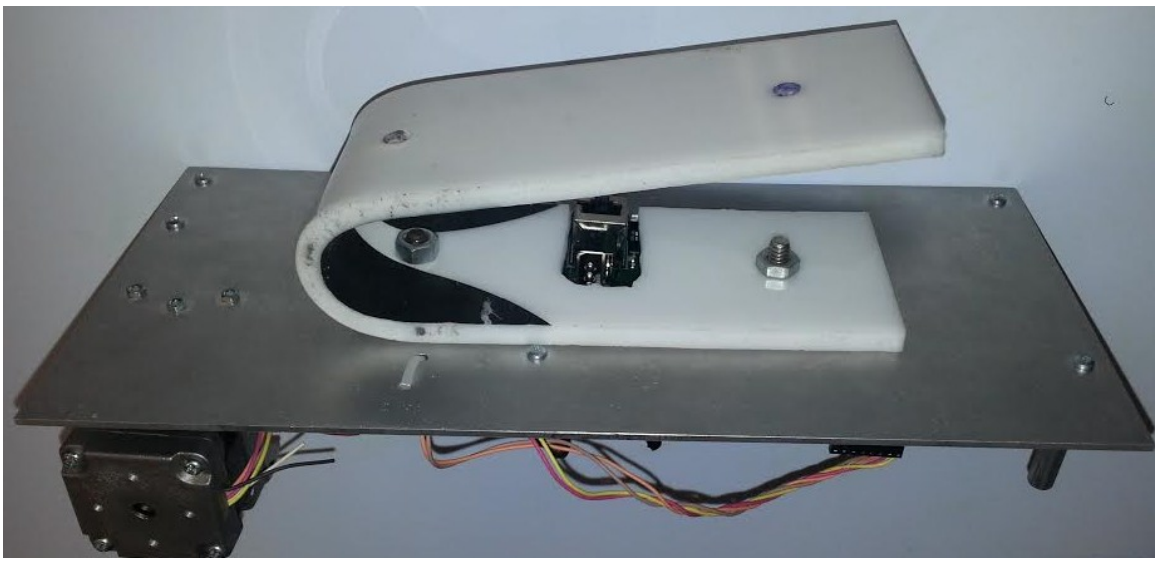

Figure 11: Photo of custom bracket mounted on scan head

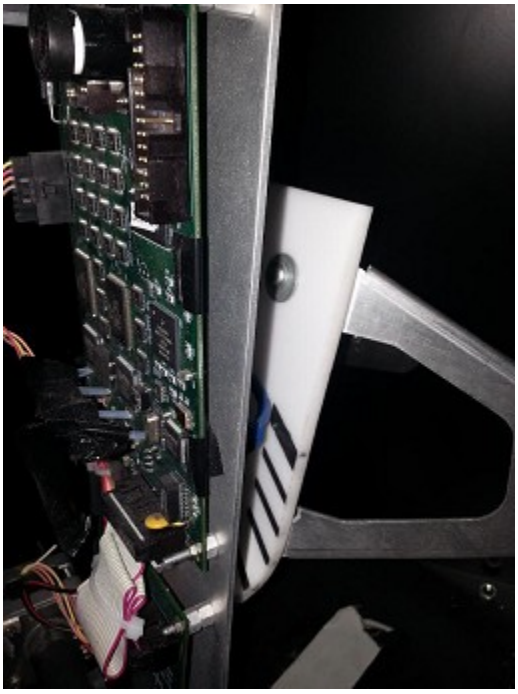

Figure 12: Photo of custom bracket mounted in situ

Further adjustments to the brackets were not feasible so adjustment to the lower level of the scanner were made through the use of a small platform. This correction was useful for participants of shorter stature, but would not work for taller individuals. The platform – painted black such that it did not reflect sufficient laser light that representative data points were generated, seen in Figure 13 – was placed on the floor of the scan booth. This allowed participants to step into the field of view of the scan heads.

Figure 13: Photo of platform for scanned participants

It was important, however, that both imaging devices on the lower scan heads be able to view sufficient portion of the calibration target such that the extrinsic characteristics of the scan heads could be determined, and correction for camera perspective could be performed. Rotating the scan heads forward to increase their lower field of view decreased scan coverage in the abdominal region of the participant. Furthermore, the centre of the calibration target, shown in Figure 14, had to be visible in all imaging devices for the scanner to calculate correct extrinsic parameters.

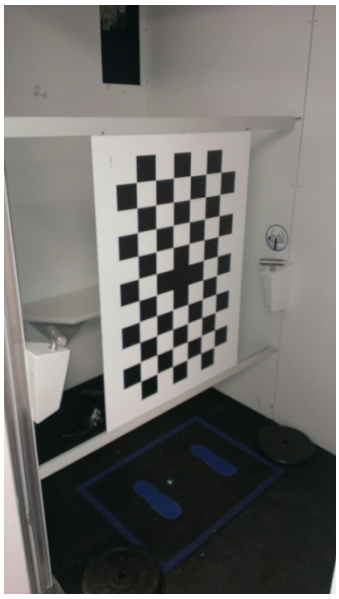

Figure 14: Calibration target

However, the subject could not simply be lifted to accommodate the reduced field of view. Despite this lower improvement, a large number of participants were unable to be completely scanned as partial omission of data points in the region of the head was common in tall participants.

4.3. Phantom-Related Validation Work

A phantom is a device of regular topography used to validate a medical imaging tool. Regularly shaped objects (mannequins, spheres, etc.) have been employed in the literature as a means of validating landmark marker location, and the quality of linear and volumetric measurements (Kouchi et al., 2012). The first phantom used here was constructed to imitate the torso and legs of a human participant, a photo of which can be seen in Figure 15. The materials utilized consisted of a plastic pail, several lengths of ABS sewer pipe and associated caps, as well as feet constructed using spruce lumber. The entire surface was coated with white spray paint such that the dark colours would best reflect the red lasers output by the scanner.

Figure 15: Laser imaging phantom

Visual observation of scan data on proprietary software owned by Unique Solutions, Point Cloud Browser, demonstrated sagittal plane distortion approximately below the knees and above shoulders in prior experiments. Anthropometric markers created from 1 cm white beads were placed along the length of the leg in order to localize the initial point of distortion, and validate frontal plane accuracy. The markers, seen in Figure 15, were measured linearly from the ground, and from visual observation, the distortion occurs at approximately 0.49 meters above the floor. The phantom was lifted 0.85 m by several boxes in order to determine that the upper limit of sagittal plane distortion occurs at approximately 1.44 m above the floor. The upper threshold distortion can be seen in Figure 16.

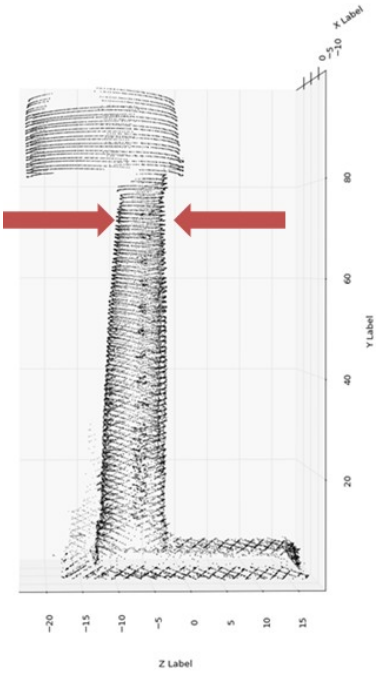

Figure 16: Upper threshold of scanner sagittal-plane distortion

The implication of this distortion is that there is a range of only approximately 0.95 metres where measurements can be reliably measured in the sagittal plane.

4.3.1. Cylinder

The distortion observed on the output scans of the above imaging phantom led to the development of another measurement phantom, a 25.4 cm diameter cardboard concrete piling form that was coated in white paper.

4.3.1.1. Linear Measurement Validation

Measurements were taken with a Holtain™ anthropometer in the medial-lateral and anterior-posterior directions at 10 cm increments along the vertical axis. The heights of these measurements marked with black landmark markers 3.8 cm on a side. The cylinder, seen in Figure 17, was scanned, and processed using lab-developed software, discussed in Section Chapter 5.

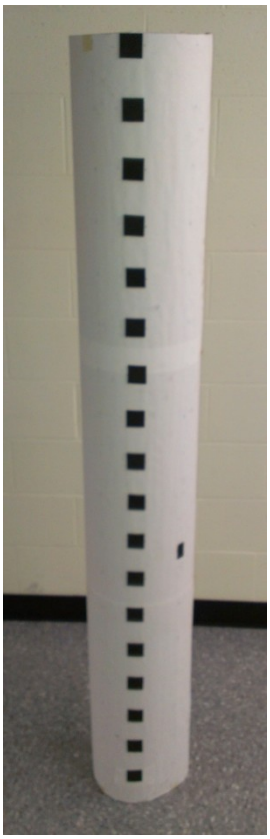

Figure 17: Cylinder for laser scanner validation

The differences between manual and scan-extracted measurements were calculated in order to determine error in both the X and Z-axis directions. These errors were then plotted with respect to Y-axis height. It became immediately clear, as shown in

Figure 18, that there was a systematic under-prediction of X and Z-axis measurements at the upper and lower regions of measurement.

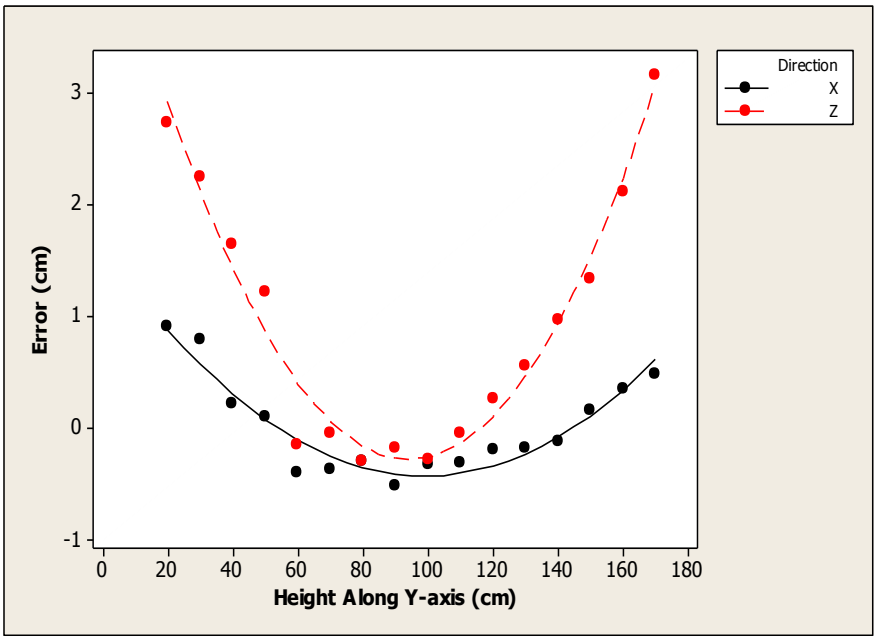

Figure 18: X and Z length errors with respect to the vertical position

The error was modeled with a 2nd order polynomial in both X and Z-axis directions as the systematic error appeared to take on parabolic characteristics. A correlation was performed between the polynomial predicted values and the actual errors, yielding the results summarized in Table 10, below.

Table 10: Error correction polynomials with respective PPMC coefficients

Direction	Polynomial Fit Equation	Polynomial Fit PPMC Coefficient
X-axis	$err_x=1.63-0.0414y+0.000208y^2$	0.957
Z-axis	$err_z=4.88-0.109y+0.000581y^2$	0.983

Because the error along the vertical length of the cylinder was demonstrably non-linear and poorly suited to correlation tests, a Bland-Altman statistical test was applied to the error values in order to test the limits of agreement of the manual and scan-extracted methods. The results are summarized in Table 11. Subsequently, the formulae of the parabolic regressions in Figure 18 were used to correct the systematic effects in the scan-extracted data. The resulting error-corrected data can be seen in Figure 19.

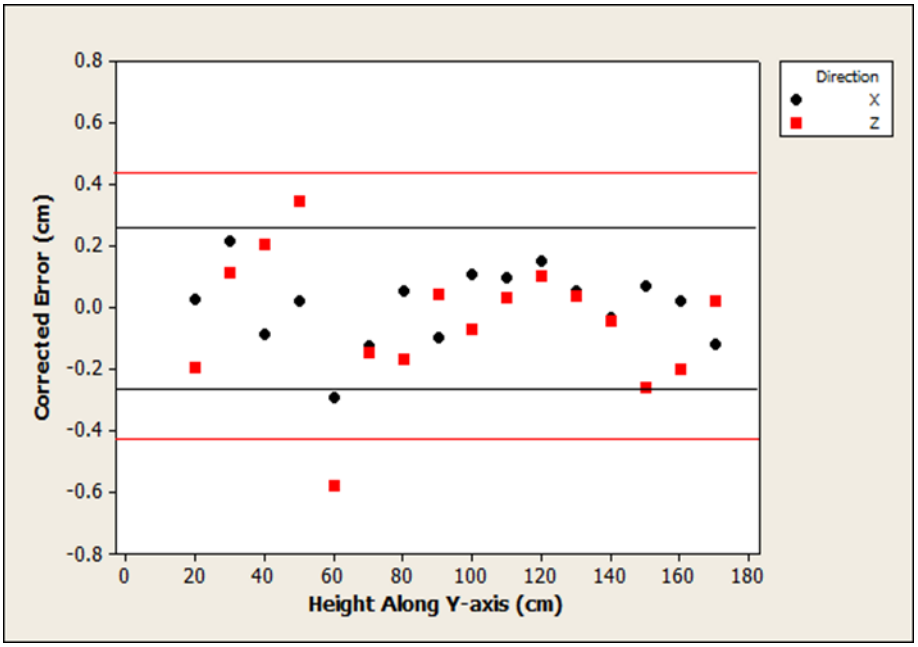

Figure 19: X and Z length errors with respect to the vertical position corrected for the systematic error

After correction, the magnitude of the error was reduced by almost an order of magnitude. The limits of agreement of the measurement methods were again tested with a Bland-Altman statistical test, the results of which are summarized in Table 11.

Table 11: Limits of agreement (95th percentile) between manual and scan-extracted linear measurements before and after correction

Direction	Before Correction	After Correction
X-axis	0.85 cm	0.25 cm
Z-axis	2.26 cm	0.42 cm

A summary of scanner error before and after correction can be seen in Table 12.

Table 12: Scanner mean error (and Standard Deviation) for linear measurements before and after correction

Direction	Before Correction	After Correction
X-axis	0.02 (0.43) cm	0.00 (0.13) cm
Z-axis	0.96 (1.15) cm	0.00 (0.21) cm

The resulting data shown in Figure 19 appears random, with little to no systematic effect. This was tested with a PPMC to determine if there was any remaining linear relationship after correction. The results of this test can be found in Table 13.

Table 13: PPMC between error-corrected scan data for linear measurements and Y-axis height

Direction	PPMC Coefficient
X-axis	0.03
Z-axis	-0.11

Work with the cylinder demonstrated that minor measurement errors associated with the scan data could be corrected to improve the overall device performance. Furthermore, the error after correction is within a reasonable margin. It has been hypothesized that with improved calibration procedures, this systematic error can be reduced without the need for systematic error correction.

4.3.1.2. Volumetric Measurement Validation

Using the X and Z diametric measurements (manual and scan-extracted) collected above as major and minor axes, an elliptic cylinder model was used to model the volume of the cylinder at each 10 cm increment level along the Y-axis. The area of each cross-sectional ellipse was calculated and multiplied by the segment height. The differences between manual and scan-extracted volume calculations of each 10 cm thick segment were plotted, as is shown in the image in Figure 20.

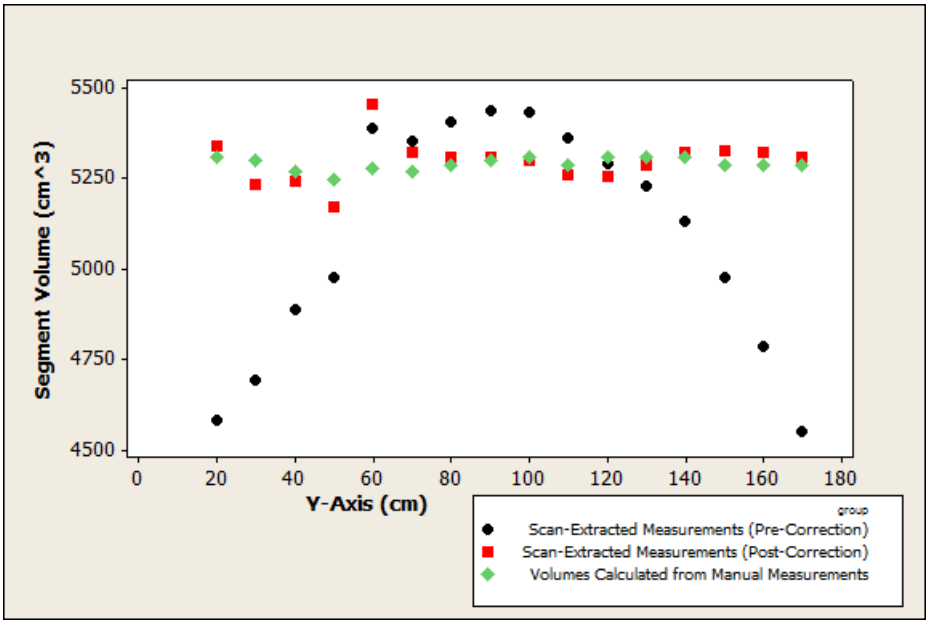

Figure 20: Segmental volumes - elliptical model

Marked, seemingly parabolic, distortion can be seen, similar to the linear plots shown above, as shown by the black points. As was performed in the diametric measurement data, the data was plotted after applying the parabolic corrections to the linear data. Table 14 shows the mean errors of the volumes of the segments with respect to manually calculated segment volumes before and after the linear corrections were applied. Note that volumes in this preliminary validation are measured in centimetres cubed, which is equal to one thousandth of a litre. For convenience, the majority of anatomical volume measurements in this document are presented in litres.

Table 14: Scanner mean error (and standard deviation) for volumetric measurements, before and after correction

Before Correction	After Correction
196 (315) cm^3	9 (60) cm^3

Table 15 shows the 95th percent limits of agreement between manual and scan-extracted volume measurements as determined using a Bland-Altman statistical test. The error-corrected data, with 95th percent confidence interval bars, can be seen in Figure 21.

Table 15: Limits of agreement (95th percent) between manual and scan-extracted volumetric measurements before and after correction

Before Correction	After Correction
$-421\ cm^3 \leq V \leq 813\ cm^3$	$-107\ cm^3 \leq V \leq 126\ cm^3$

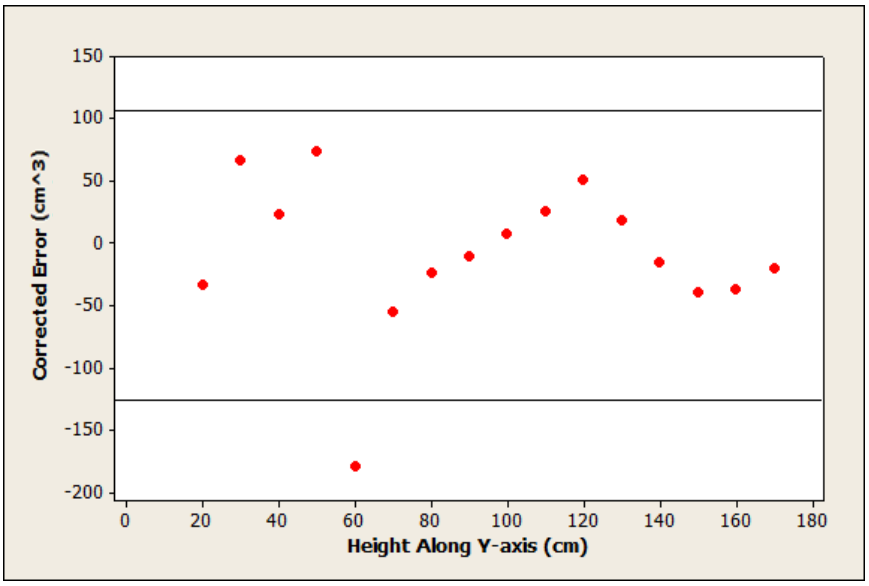

Figure 21: Segmental volume errors with respect to the vertical position corrected for the systematic error

The regression equations shown in Table 10, while valid for measurements taken at the medial-lateral and anterior-posterior axes along the surface of the cylinder, could not be applied as a global correction for all measurements within the scan volume. The overall modeled error was a composite of errors of each camera on each scan head. As a result, an investigation – discussed in Appendix A – was performed in order to determine if a correction for errors intrinsic to each camera's properties might correct this quantifiable systematic effect.

Chapter 5. Software Development

As was discussed prior, the intended design of the Unique Solutions laser scanner, and accompanying software, was for use in the fashion industry, where scanned measurements can be used to determine sizing requirements for garments. The original intention of this thesis was to evaluate the measurements output by the on-board software, in anticipation for its use in clinical applications. Discussion with the industry partner revealed that the output measurement file of the on-board software, an example of which can be seen below, in Table 16, contained industry measurements related to garment design, not validated against an international standard for anthropometry.

Table 16: Example output of garment-related from onboard measurement software

Dimension	Magnitude (in)
Inseam on Leg	34.62
Left Outseam	42.04
Right Outseam	40.77
Left Lower Hip Depth	11.00
Left Lower Hip Front	15.97
Abdomen Location	7.05
Abdomen Measurement	30.24

Given the eventual clinical and anthropometric applications of the scanner, it was decided within the research group that new software should be developed that extracted measurements based on ISO and research standards such that the scanner could be validated based on compatible comparisons.

5.1. Design Requirements

The Unique Solutions software was bypassed, and the raw point cloud data was extracted from the scanner for custom software development. Before measurement extraction was be possible, software had to be developed that could process this point cloud data, identify anthropometric landmarks, and perform linear, circumferential, and volumetric measurements. Furthermore, a graphical user

interface (GUI) had to be developed that allowed non-technical users to interact with point cloud data.

5.2. GUI Dashboard

The GUI dashboard is the main workspace for user interaction with point cloud data. It displays the three-dimensional point cloud and allows users to select a series of anthropometric landmarks from the plot, from which measurements are extracted. Figure 22 shows an view of the dashboard, and is accompanied by Table 17 which describes the various critical functions of the software.

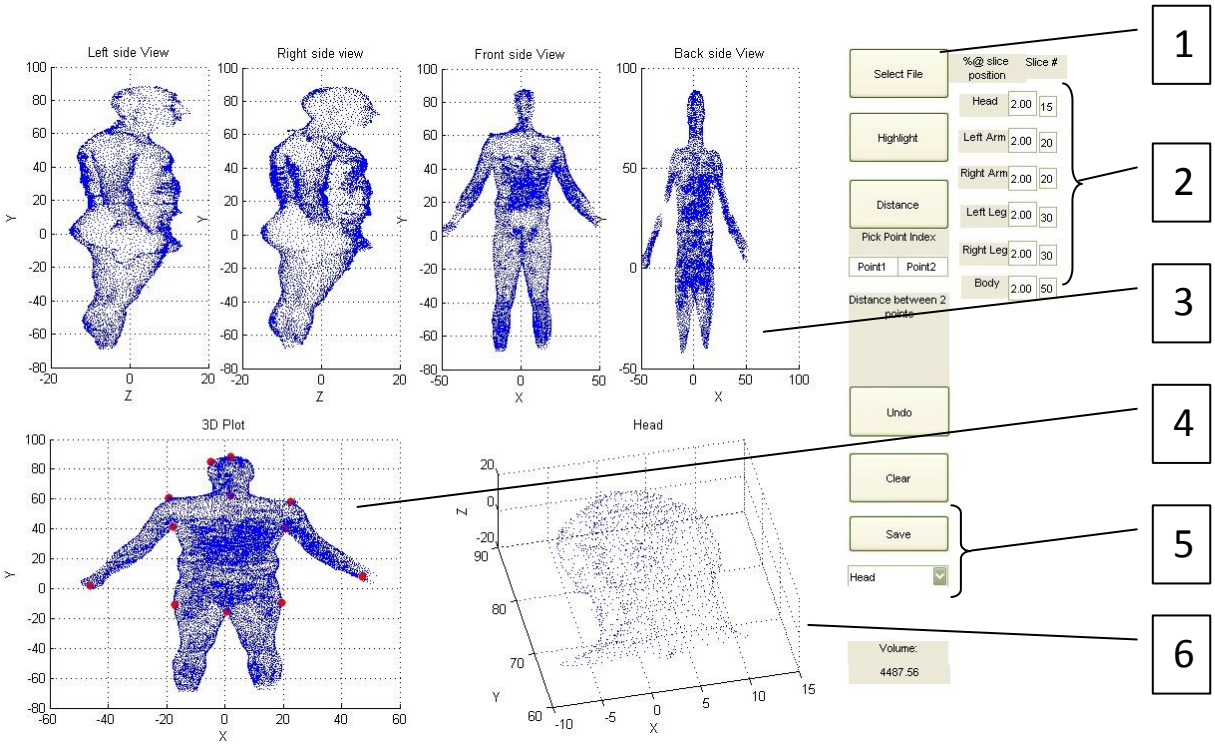

Figure 22: GUI dashboard for OEAB Lab *Scananalysis* software

Table 17: Description of *Scananalysis* functions

Numbered Location	Function
1	File selection; loads point cloud file
2	Slice thickness selection, by major segment
3	Frontal and sagittal view planes; view-only area
4	Anthropometric landmark identification field; workspace for identifying landmark markers
5	Save, and segment selection; selection of various segments allows them to appear for inspection in (6), the segment viewer. "Save" initiates the measurement generation process
6	Segment viewer; allows segment to be extracted

5.3. Software operation

Once the user loaded the point cloud file into memory, they then visually identified the 1-cm diameter landmark markers and clicked them in a pre-determined order. The index locations of the three-dimensional coordinates selected were automatically stored. Once the user had selected all 43 landmarks, the user inspected each of the major segments in the *segment viewer*, the selection of which separated segmented each point cloud segment into a separate file for measurement and if necessary. For all segments measured, the vertical (superior-inferior) axis was the Y-axis, the anterior-posterior axis was the Z-axis, and the medial-lateral axis was the X-axis. Because arm segments were abducted in the standard posture, an algorithm in the custom software calculated the abduction angle, and rotated the local long axes of these segments to be aligned with the global Y axis, orienting the arm segments vertically.

5.4. Measurement generation

Upon selecting "Save," a series of algorithms process the point cloud, and generates two output files; one contains the values for segmental volume, the other: linear and circumferential values. A separate algorithm processes each linear, circumferential, and volumetric measurement as described below.

5.4.1. **Linear**

To calculate linear measurements, Euclidian distances were calculated between three-dimensional coordinates of appropriate three-dimensional landmarks stored in the index file.

5.4.2. **Circumferential**

As each major segment was viewed, as shown in Figure 23, below, 1-cm transverse slices of body segments were taken along each long axis and each slice was "flattened" into a two-dimensional cross-section.

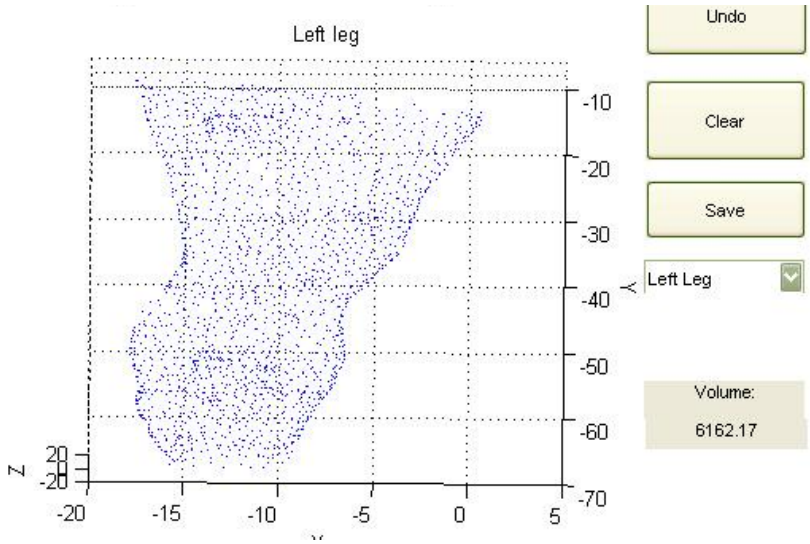

Figure 23: Example left leg point cloud representation

An algorithm identified the vector connecting the maximally displaced data points as the major axis of the slice, and rotated the slice data such that aligned with the horizontal axis. This allowed the cross-section to be divided horizontally into two independent sets of data. Raw slice data, and the subsequent operations can be seen in Figure 24, and Figure 25.

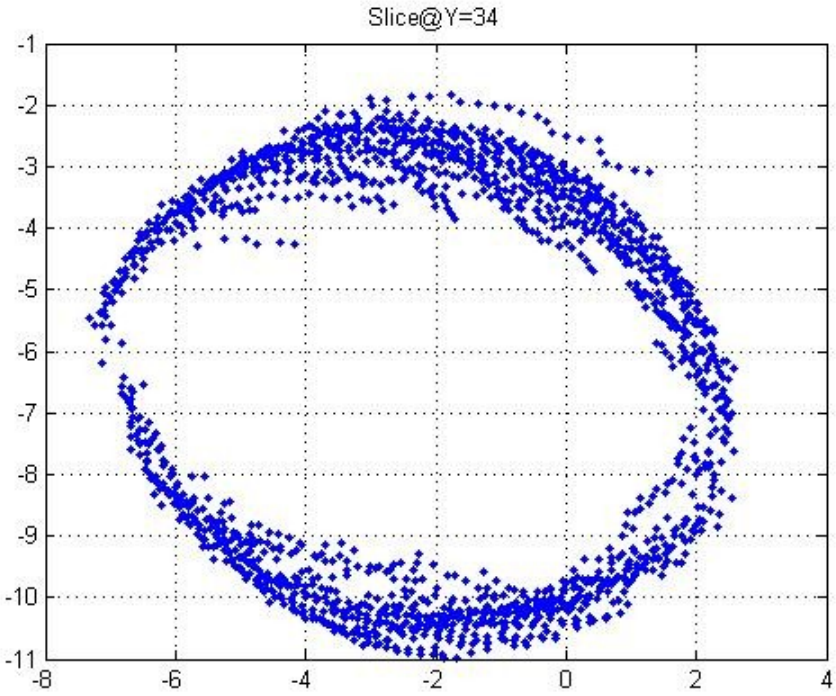

Figure 24: Cross-section (1 cm thick) of lower arm segment (cm)

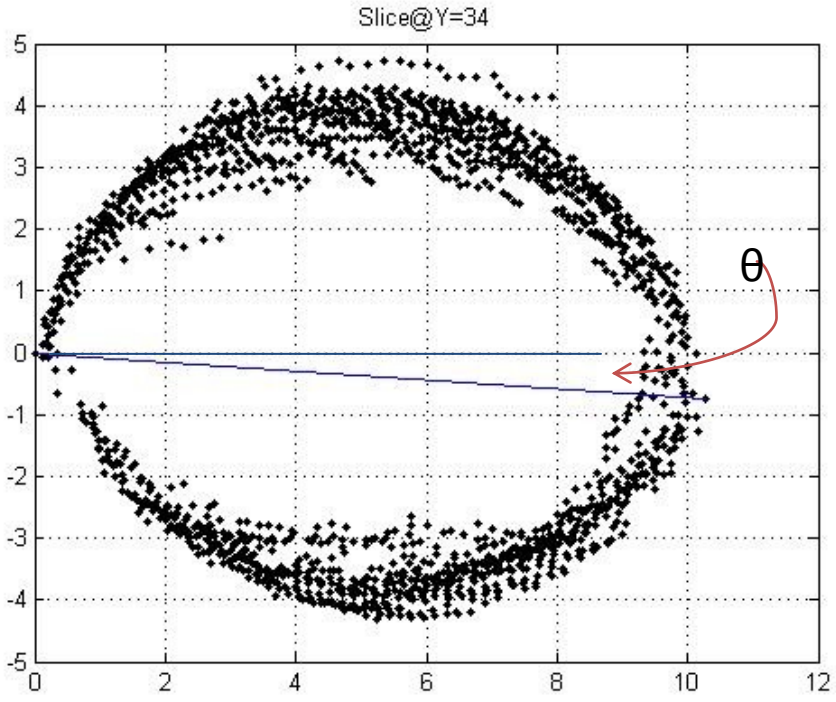

Figure 25: Identification of long axis, and rotation angle, for point cloud cross-section (cm)

The upper and lower regions of each slice were the automatically fit to an 8th order polynomial, in order to account for the contours of the various body surface, while reducing the risking of over-fitting the data. An image of the cross section of the torso can be seen in Figure 26. The complex curvature drove the decision to use an 8th order polynomial to model the upper and lower regions separately.

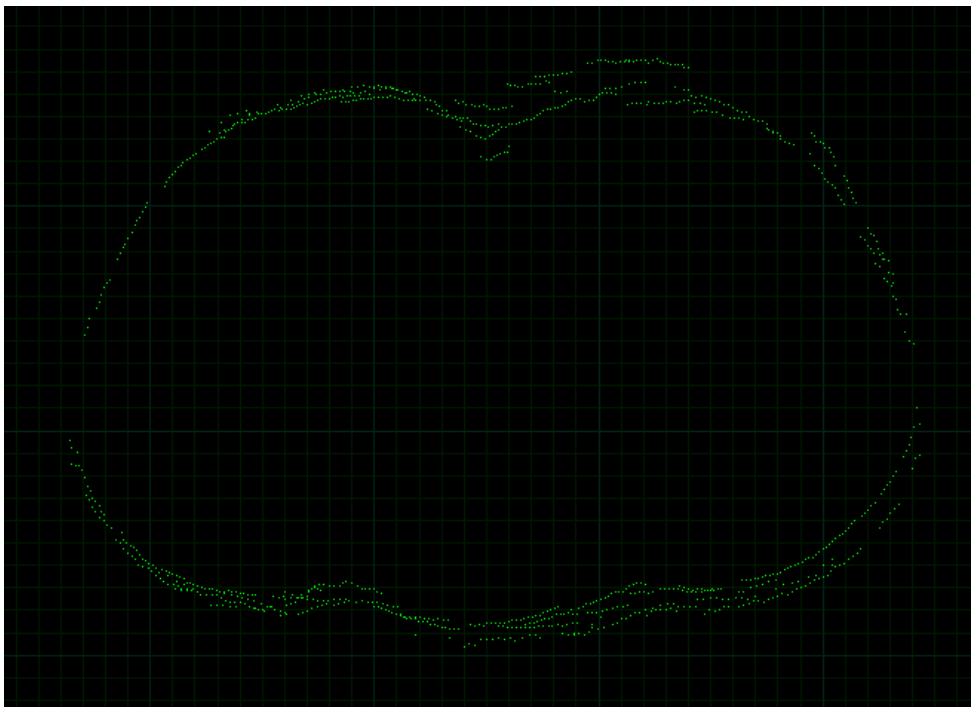

Figure 26: Cross section of the torso, viewed in Point Cloud Browser

The arc length of each polynomial was extracted and summed to approximate the circumference of that slice. The arc length of a polynomial can be calculated according to the Equation (7) (Larson, Hostetler, & Edwards, 2008).

$$s = \int_a^b \sqrt{1 + [f'(x)]^2}\,dx \qquad (7)$$

The lower and upper limits of integration in the case above were defined to be the origin of the X-Z plane, and the X-axis value farthest from the origin, respectively. Also, it is important to note that in the cases where the upper and lower regions would be discontinuous at the end of the curves away from the origin, a straight line

fit was calculated between the distal points, and the length was added to the total circumference. The curve-fits of an example slice can be seen in Figure 27, a and b.

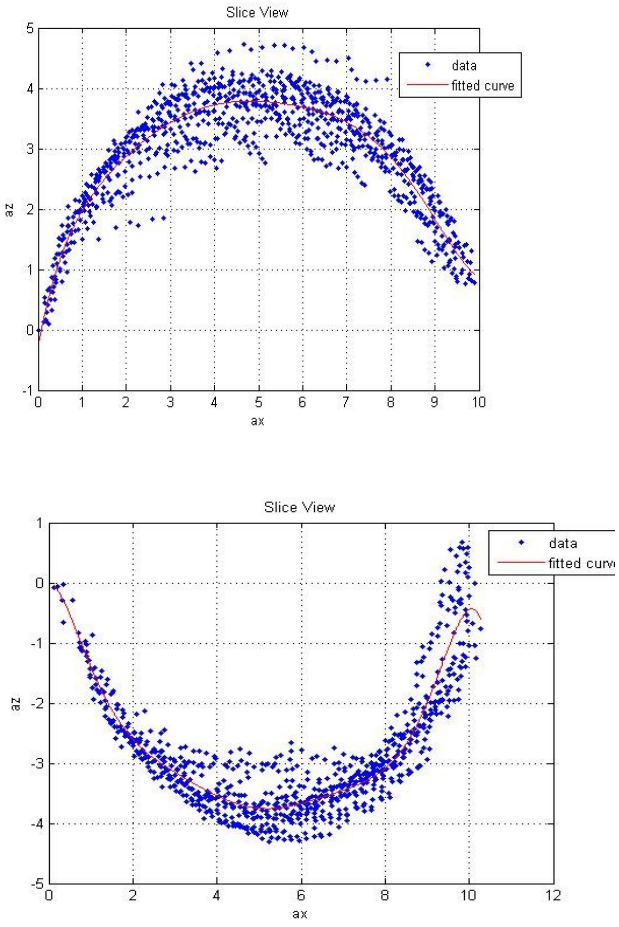

Figure 27a and 23b: Upper and lower sections of lower arm segment point cloud cross-section (cm)

Periodic visual inspections of 8th order fits were made during the course of development of the software. While not every slice was checked, the 8th order polynomial was perceived to be appropriate for this application.

Using the index positions of the identified landmark markers, the anthropometrically relevant circumferences were extracted and reported in the "lengths and circumferences" output file.

5.4.3. **Volumetric**

The slices that were generated above were further operated on by the segment volumes algorithm. The 8th order polynomial fits for the upper and lower regions of each slice were operated on by a definite integral. Refer to Equation (8)

$$Area = \int_u^v f(x)dx \tag{8}$$

The limits of integration in this case were the same as those used for the arc length calculation for circumference. As this represented the area between the major axis, and the curve's approximation of the segment's surface, the upper and lower areas of each slice were summed. The total area of each slice was multiplied by the slice thickness (1 cm) to approximate slice volume. The index points representing the anthropometric endpoints of each body segment identified which slices would be summed –similar to a rectangular integral – to generate a value for segment volume. These volume values were reported in the "segment volume" output file.

Chapter 6. Human Trials - Results

After the assessment of the point cloud data using multiple trials on imaging phantoms, a study was designed for 20 participants that would utilize the software that had been concurrently developed in lab to determine if clinically valid measurements could be collected using the Unique Solutions three dimensional laser scanner. To do so required a series of separate experiments to determine and correct for systematic errors, and quantify the remaining random error. The results of each of these steps will be presented in the order list.

6.1. Participant Trials

For each linear anthropometric measurement and segment volume measurement, a scatterplot was prepared for visual inspection prior to any statistical analysis. Following visual inspection, the Pearson product moment correlation coefficient of the manual versus scan data was calculated, summarized in Table 18. Note: for all torso and thigh volume measurements, one participant was too heavy for manual measurement methods, and was excluded from all data sets. Table 19 contains the p-values and significance output from paired-T tests used to determine whether the manual and scan-extracted volume values were statistically significant. Please note that where an asterisk (*) appears next to "Torso Volume" in the results tables below, there were two outlier excluded from the computed data sets, for reasons discussed subsequently.

Table 18: Pearson Product Moment Correlation coefficients, and related p-values for manual vs. scan-extracted measurements

Segment	$\bar{x}_{man}$	s_{man}	$\bar{x}_{scan}$	s_{scan}	PPMC	p-Value
Head and Neck Volume (L)	5.69	0.84	4.57	0.82	0.374	0.104
Torso Volume (L)	45.31	18.79	37.59	7.64	0.104	0.671
Torso Volume* (L)	39.83	9.38	38.38	7.65	0.876	0.000
Left Upper Arm Volume (L)	2.00	0.64	1.93	0.72	0.790	0.000
Right Upper Arm Volume (L)	2.06	0.66	2.03	0.70	0.908	0.000
Left Lower Arm Volume (L)	0.97	0.41	1.45	0.51	0.941	0.000
Right Lower Arm Volume (L)	0.98	0.39	1.24	0.49	0.976	0.000
Left Hand Volume (L)	0.40	0.14	0.80	0.28	0.378	0.100
Right Hand Volume (L)	0.43	0.16	0.74	0.28	0.344	0.137
Left Thigh Volume (L)	6.52	3.40	5.89	1.73	0.886	0.000
Right Thigh Volume (L)	6.62	3.11	5.81	1.58	0.915	0.000
Left Leg Volume (L)	3.42	0.94	3.31	1.14	0.770	0.000
Right Leg Volume (L)	3.34	0.84	3.26	0.96	0.981	0.000
Left Foot Volume (L)	0.87	0.20	0.54	0.13	-0.244	0.300
Right Foot Volume (L)	0.87	0.22	0.55	0.16	-0.338	0.144
Stature (cm)	172.4	9.3	170.2	8.2	0.929	0.000
Chest Breadth (cm)	34.0	4.7	35.3	4.4	0.938	0.000
Hip Breadth (cm)	35.3	4.4	36.9	4.6	0.986	0.000
Chest Depth (cm)	21.5	4.5	22.6	4.5	0.935	0.000
Waist Depth (cm)	21.7	6.0	23.3	6.5	0.995	0.000
Neck Circumference (cm)	36.2	5.6	53.6	23.0	0.825	0.000
Chest Circumference (cm)	96.8	17.4	100.2	18.6	0.983	0.000
Waist Circumference (cm)	91.5	18.9	92.6	19.7	0.996	0.000
Hip Circumference (cm)	99.1	14.0	101.4	14.0	0.985	0.000

Table 19: P-values of paired-t tests performed on manual vs. scan-extracted measurements

Measurement	T-Test P-Value
Head and Neck Volume	0.000
Torso Volume	0.102
Torso Volume*	0.208
Left Upper Arm Volume	0.484
Right Upper Arm Volume	0.623
Left Lower Arm Volume	0.000
Right Lower Arm Volume	0.000
Left Hand Volume	0.000
Right Hand Volume	0.000
Left Thigh Volume	0.208
Right Thigh Volume	0.063
Left Leg Volume	0.525
Right Leg Volume	0.090
Left Foot Volume	0.000
Right Foot Volume	0.000
Stature	0.013
Chest Breadth	0.002
Hip Breadth	0.000
Chest Depth	0.000
Waist Depth	0.000
Neck Circumference	0.001
Chest Circumference	0.000
Waist Circumference	0.023
Hip Circumference	0.001

It is apparent that that the segments at the distal extremities (head and neck, feet, and hands) of the sample population were not well correlated and limb and body segment volumes appeared to be relatively well correlated in comparison. One-dimensional measurements appeared to present the best correlation between manual and scan-extracted measurements.

Differences between manual and scanned measurements were calculated (the difference being defined as manual minus scan values) and plotted against manual measurements in a *Bland-Altman Plot*, each of which is shown in Appendix B. In order to determine if any linear systematic trends between the differences and manual measurement data existed, a PPMC coefficient was calculated for the Bland-

Altman plot. A significant positive correlation means an increasing (or decreasing, with a negative correlation coefficient) amount error with an increasing magnitude of measurement. Table 20 summarizes these PPMC coefficients and respective P-values.

Table 20: Pearson Product Moment Correlation coefficients, and related P-values for difference vs. manual measurements

Measurement	PPMC	P-Value
Head and Neck Volume	0.576	0.008
Torso Volume	0.921	0.000
Torso Volume*	0.588	0.013
Left Upper Arm Volume	0.151	0.524
Right Upper Arm Volume	0.083	0.729
Left Lower Arm Volume	-0.342	0.140
Right Lower Arm Volume	-0.633	0.003
Left Hand Volume	0.120	0.614
Right Hand Volume	0.228	0.333
Left Thigh Volume	0.918	0.000
Right Thigh Volume	0.933	0.000
Left Leg Volume	0.091	0.718
Right Leg Volume	-0.458	0.042
Left Foot Volume	0.878	0.000
Right Foot Volume	0.879	0.000
Stature	0.492	0.027
Chest Breadth	0.342	0.14
Hip Breadth	-0.129	0.589
Chest Depth	0.196	0.407
Waist Depth	-0.594	0.006
Neck Circumference	-0.717	0.000
Chest Circumference	-0.263	0.262
Waist Circumference	-0.391	0.088
Hip Circumference	0.113	0.635

From Table 20 above, the strongest correlations between difference and manual measurements appeared to be foot volumes (r = 0.88) and torso volumes prior to outlier removal (r = 0.92). Furthermore, there was a moderately strong significant correlation between error values and neck circumference magnitude (r = -0.72).

As was described in ISO20685:2010(E), 3D laser scanners are evaluated based on 95% confidence intervals, calculated using the standard error of the differences between manual and scan data, as calculated above. Mean differences, standard errors, and standard deviations are plotted for each segment volume and linear measurement in Table 21, accompanied by the Bland-Altman confidence intervals, and the ANSUR allowable error ranges to which they were compared. The Bland-Altman plots can be seen in Appendix B. Bland-Altman intervals for volume are provided for information only, as no standard exists for the reference range. Furthermore, none of the linear measurements fell within the ANSUR reference range, and as a result, further statistical analysis was performed. The 95th percentile confidence intervals of the differences as described in the ISO document are shown in context, later in this chapter, in Table 27.

Table 21: Mean differences between manual and scan-extracted measurements, and respective standard errors and standard deviations

Measurement	Mean difference	Standard Error	Standard Deviation	Bland-Altman 95th % CI (cm)
Head and Neck Volume (L)	1.1	0.2	0.9	(-0.7,2.9)
Torso Volume (L)	7.7	4.5	19.5	(-30.5, 46.0)
Torso Volume * (L)	1.5	1.1	4.6	(-7.5, 10.4)
Left Upper Arm Volume (L)	0.1	0.1	0.4	(-0.8,0.9)
Right Upper Arm Volume (L)	0.0	0.1	0.3	(-0.5, 0.6)
Left Lower Arm Volume (L)	-0.5	0.0	0.2	(-0.8, -0.1)
Right Lower Arm Volume (L)	-0.3	0.0	0.1	(-0.5, 0.0)
Left Hand Volume (L)	-0.4	0.1	0.3	(-0.9, 0.1)
Right Hand Volume (L)	-0.3	0.1	0.3	(-0.8, 0.2)
Left Thigh Volume (L)	0.6	0.5	2.0	(-3.4, 4.6)
Right Thigh Volume (L)	0.8	0.4	1.8	(-2.7, 4.3)
Left Leg Volume (L)	0.1	0.2	0.7	(-1.3, 1.5)
Right Leg Volume (L)	0.1	0.0	0.2	(-0.3, 0.5)
Left Foot Volume (L)	0.3	0.1	0.3	(-0.2, 0.9)
Right Foot Volume (L)	0.3	0.1	0.3	(-0.3, 0.9)
Stature (cm)	2.7	0.8	3.7	(-4.6, 9.9)
Chest Breadth (cm)	-0.1	0.4	1.6	(-3.3, 3.1)
Hip Breadth (cm)	-1.6	0.2	0.8	(-3.1, -0.1)
Chest Depth (cm)	-1.1	0.4	1.6	(-4.3, 2.1)
Waist Depth (cm)	-1.5	0.2	0.8	(-3.2, 0.1)
Neck Circumference (cm)	-17.4	4.2	18.6	(-53.9, 19.2)
Chest Circumference (cm)	-3.4	0.8	3.6	(-10.4, 3.6)
Waist Circumference (cm)	-1.0	0.4	1.9	(-4.7, 2.6)
Hip Circumference (cm)	-2.3	0.5	2.4	(-7.1, 2.5)

The confidence intervals demonstrated an unacceptable magnitude of error, and none of the linear measurements met the ANSUR allowable error thresholds, nor did they meet ISO standards. Therefore, a linear regression of manual to scan values was applied to each measurement in the form shown in Equation 5, in section 3.4.4, to attempt to predict the measurements in the presence of systematic error.

The regressions for each measurement are available for review in Table 22, which also shows the p-values of the constants and regression coefficients and R^2 values for the regression.

Table 22: Regression equations for scan-extracted measurements in terms of manual measurements

Measurement	Regression Formula	Scan Value P-Value	Constant P-Value	Regression R-Squared Value
Head and Neck Volume (L)	M = 3.93 + 0.385•S**	0.104	0.001	14.0
Torso Volume (L)	M = 35.7 + 0.257•S	0.671	0.135	1.1
Torso Volume * (L)	M = -1.42 + 1.07•S	0.000	0.815	76.8
Left Upper Arm Volume (L)	M = 0.653 + 0.699•S	0.000	0.023	62.5
Right Upper Arm Volume (L)	M = 0.325 + 0.856•S	0.000	0.120	82.4
Left Lower Arm Volume (L)	M = -0.149 + 0.769•S	0.000	0.154	88.5
Right Lower Arm Volume (L)	M = 0.0135 + 0.779•S	0.000	0.806	95.3
Left Hand Volume (L)	M = 0.255 + 0.185•S	0.100	0.011	14.3
Right Hand Volume (L)	M = 0.283 + 0.194•S	0.137	0.010	11.8
Left Thigh Volume (L)	M = -3.72 + 1.74•S	0.000	0.017	78.5
Right Thigh Volume (L)	M = -3.81 + 1.79•S	0.000	0.004	-
Left Leg Volume (L)	M = 1.31 + 0.638•S	0.000	0.012	59.3
Right Leg Volume (L)	M = 0.527 + 0.864•S	0.000	0.001	96.2
Left Foot Volume (L)	M = 1.07- 0.374•S	0.300	0.000	6.0
Right Foot Volume (L)	M = 1.13 - 0.472•S	0.144	0.000	11.5
Stature (cm)	M = - 6.1 + 1.05•S	0.000	0.739	84.4
Chest Breadth (cm)	M = -1.26 + 0.998•S	0.000	0.687	88.0
Hip Breadth (cm)	M = 0.15 + 0.952•S	0.000	0.918	97.3
Chest Depth (cm)	M = 0.23 + 0.941•S	0.000	0.907	87.4
Waist Depth (cm)	M = 0.461 + 0.914•S	0.000	0.401	98.9
Neck Circumference (cm)	M = 25.4 + 0.202•S	0.000	0.000	68.1
Chest Circumference (cm)	M = 5.02 + 0.916•S	0.000	0.241	96.6
Waist Circumference (cm)	M = 3.10 + 0.955•S	0.000	0.114	99.2
Hip Circumference (cm)	M = - 1.19 + 0.989•S	0.000	0.781	97.0

**S stands for the scan-extracted volume measure

As has been demonstrated with other statistical tests, the regressions of head and neck, hand, and foot volumes demonstrated a very poor fit to presented data, as demonstrated by the coefficient of determination (R^2). In each case, the scan value was not a significant predictor of the true value. The strongest relationships appeared within the one-dimensional measurements.

In order to test the residuals of the regressions for linear trends not accounted for by the calculated regressions, a PPMC coefficient was calculated for each measurement, the summary of which can be found in Table 23.

Table 23: Pearson Product Moment Correlation coefficients, and related P-values, for residuals of regressions of scan-extracted measurements

Measurement	PPMC	P-Value
Head and Neck Volume (L)	0.927	0.000
Torso Volume (L)	0.995	0.000
Torso Volume * (L)	0.482	0.050
Left Upper Arm Volume (L)	0.613	0.004
Right Upper Arm Volume (L)	0.419	0.066
Left Lower Arm Volume (L)	0.339	0.143
Right Lower Arm Volume (L)	0.217	0.358
Left Hand Volume (L)	0.926	0.000
Right Hand Volume (L)	0.939	0.000
Left Thigh Volume (L)	0.464	0.053
Right Thigh Volume (L)	0.404	0.086
Left Leg Volume (L)	0.638	0.004
Right Leg Volume (L)	0.195	0.411
Left Foot Volume (L)	0.970	0.000
Right Foot Volume (L)	0.774	0.000
Stature (cm)	0.395	0.085
Chest Breadth (cm)	0.346	0.135
Hip Breadth (cm)	0.165	0.488
Chest Depth (cm)	0.355	0.125
Waist Depth (cm)	0.103	0.667
Neck Circumference (cm)	0.564	0.010
Chest Circumference (cm)	0.185	0.435
Waist Circumference (cm)	0.087	0.714
Hip Circumference (cm)	0.174	0.463

There is substantial evidence, by way of strong significant PPMC values, that there is remaining systematic error captured, especially in the head and neck volume ($r = 0.93$), hand volume ($r = 0.93$ and $r = 0.94$ for left and right hands respectively, and foot volume ($r = 0.97$ and $r = 0.77$, for left and right feet respectively) segments. Moderate correlations can be found in left upper arm volumes ($r = 0.61$), and left leg volumes ($r = 0.64$), as well as in neck circumferences ($r = 0.56$).

In order to maximize the amount of variation captured by the regression, identify sources of systematic error, and possibly improve on the quality of the regressive relationships, standard manual measurements of height and mass were included as predictive variables. A stepwise linear regression with backwards elimination of non-significant factors was computed for each segmental volume, the form of which is shown in Equation 6 in section 3.4.4,

A summary table of the multi-term regressions can be found below, in Table 24, followed by Table 25, which contains the p-values for the regression coefficients and the R^2 value for each regression.

Table 24: Regression equations for scan-extracted measurements in terms of manual measurements, including manual mass and stature as predictive terms

Measurement	Equation
Head and Neck Volume (L)	M = -0.89 - 0.141S + 0.0162m + 0.0347s***
Torso Volume (L)	M = 18.1 - 0.485S+0.641m
Torso Volume * (L)	M = - 4.28 + 0.375S + 0.447m
Left Upper Arm Volume (L)	M = - 5.47 + 1.25S - 0.0234m + 0.0398s
Right Upper Arm Volume (L)	M = - 2.30 + 0.699S +0.0171s
Left Lower Arm Volume (L)	M= -0.170 + 0.311S + 0.00888m
Right Lower Arm Volume (L)	M = 0.0260 + 0.447S + 0.00588m
Left Hand Volume (L)	M = 0.151 + 0.056S + 0.00268m
Right Hand Volume (L)	M = 0.186 - 0.037S +0.00349m
Left Thigh Volume (L)	M = -3.72 + 1.74S
Right Thigh Volume (L)	M = -4.27 + 1.41S + 0.0367m
Left Leg Volume (L)	M = 1.31 + 0.638S
Right Leg Volume (L)	M = 0.527 + 0.864S
Left Foot Volume (L)	M = -1.13 - 0.070S +0.00289m + 0.0105s
Right Foot Volume (L)	M = -1.33 - 0.036S +0.00354m + 0.0113s
Stature (cm)	M = 22.5 + 0.837S + 0.0982m
Chest Breadth (cm)	M = 9.42 + 0.514S + 0.0834m
Hip Breadth (cm)	M = - 12.0 + 1.07S + 0.0595s - 0.0338m
Chest Depth (cm)	M = - 15.0 + 0.831S + 0.102s
Waist Depth (cm)	M = 0.461 + 0.914S
Neck Circumference (cm)	M = 22.6 + 0.0903S + 0.115m
Chest Circumference (cm)	M = 22.4 + 0.552S +0.249 m
Waist Circumference (cm)	M = 3.10 + 0.955S
Hip Circumference (cm)	M = -20.0 + 0.935S + 0.141s

***s stands for manual stature; m stands for manual mass

Table 25: Significance of coefficients in regressions of scan-extracted measurements in terms of manual measurements, including manual mass and stature as predictive terms

Measurement	Scan Value P-Value	Constant P-Value	Mass P-Value	Stature P-Value	Regression R-Squared Value
Head and Neck Volume (L)	0.600	0.837	0.158	0.175	64.8
Torso Volume (L)	0.091	0.127	0.000	-	79.9
Torso Volume * (L)	0.436	0.262	0.031	-	83.5
Left Upper Arm Volume (L)	0.006	0.023	0.058	0.012	75.2
Right Upper Arm Volume (L)	0.000	0.126	-	0.081	85.4
Left Lower Arm Volume (L)	0.009	0.022	0.000	-	95.1
Right Lower Arm Volume (L)	0.002	0.598	0.013	-	96.8
Left Hand Volume (L)	0.598	0.101	0.017	-	39.2
Right Hand Volume (L)	0.798	0.067	0.023	-	35.6
Left Thigh Volume (L)	0.000	0.017	-	-	78.5
Right Thigh Volume (L)	0.000	0.001	0.015	-	88.8
Left Leg Volume (L)	0.000	0.012	-	-	59.3
Right Leg Volume (L)	0.000	0.001	-	-	96.2
Left Foot Volume (L)	0.740	0.121	0.061	0.028	72.2
Right Foot Volume (L)	0.842	0.076	0.027	0.021	76.9
Stature (cm)	0.000	0.215	0.006	-	90.1
Chest Breadth (cm)	0.004	0.027	0.003	-	93.0
Hip Breadth (cm)	0.000	0.045	0.068	0.048	97.9
Chest Depth (cm)	0.000	0.034	-	0.027	90.7
Waist Depth (cm)	0.000	0.401	-	-	98.9
Neck Circumference (cm)	0.046	0.000	0.003	-	81.0
Chest Circumference (cm)	0.000	0.001	0.002	-	98.1
Waist Circumference (cm)	0.000	0.114	-	-	99.2
Hip Circumference (cm)	0.000	0.066	-	0.061	97.0

Substantial improvement across most measurements was shown by improved coefficient of determination values; however, head and neck volume and hand volumes only showed marginal improvement, and still have no significant predictor variable. Foot volumes markedly improved, likely due to the inclusion of stature as a significant predictor variable, as did the neck circumference. The left leg volume regression did not improved at all, as regression was not improved by either stature or mass. The left upper arm coefficient of determination has improved substantially with the inclusion of both mass and stature as significant predictors ($\alpha = 0.1$).

Again, as was performed for the single-term regressions, a PPMC coefficient of the residuals of each regression tested for linear trends not accounted for by the regressions, displayed in Table 26. Additionally, single sample T-tests were performed on regression residuals, testing for a significant difference between manual and regressed scan-extracted values. The data would have been presented in table format, however, every p-value was calculated to be greater than 0.999, indicating no significance between manual and regressed scan-extracted measurements.

Table 26: Pearson Product Moment Correlation coefficients, and related P-values, for residuals of regressions of scan-extracted measurements, including manual mass and stature as predictive factors

Measurement	PPMC	P-Value
Head and Neck Volume (L)	0.593	0.006
Torso Volume (L)	0.449	0.054
Torso Volume * (L)	0.406	0.106
Left Upper Arm Volume (L)	0.498	0.025
Right Upper Arm Volume (L)	0.382	0.096
Left Lower Arm Volume (L)	0.222	0.347
Right Lower Arm Volume (L)	0.180	0.448
Left Hand Volume (L)	0.780	0.000
Right Hand Volume (L)	0.802	0.000
Left Thigh Volume (L)	0.464	0.053
Right Thigh Volume (L)	0.334	0.162
Left Leg Volume (L)	0.638	0.004
Right Leg Volume (L)	0.195	0.411
Left Foot Volume (L)	0.528	0.017
Right Foot Volume (L)	0.480	0.032
Stature (cm)	0.315	0.176
Chest Breadth (cm)	0.264	0.261
Hip Breadth (cm)	0.143	0.546
Chest Depth (cm)	0.306	0.190
Waist Depth (cm)	0.103	0.667
Neck Circumference (cm)	0.436	0.055
Chest Circumference (cm)	0.139	0.559
Waist Circumference (cm)	0.087	0.714
Hip Circumference (cm)	0.157	0.510

The remaining significant ($\alpha = 0.05$) correlations between residuals of regressions and manual measurements are the same as those in the previous regressions, with the exception of neck circumference, for which the inclusion of mass as a predictive variable has improved the quality of regression fit (R2 = 0.81) and made the PPMC coefficient of residuals weak and non-significant. However, despite the significant correlations, much reduction in the PPMC value can be seen for head and neck volume (r = 0.59), hand volumes (r = 0.78 and 0.80 for left and right hands respectively), left upper arm volume (r = 0.50), and foot volumes (r = 0.53 and 0.48 for left and right feet respectively). Left leg volume (r = 0.64) remains unchanged as

there was no significant improvement in regression due to the inclusion of stature and mass as predictive variables.

The limitations of the scanner have been well-documented, as was explained prior, and the ISO method of using differences between manual and scan-extracted values to evaluate scanner performance demonstrated an unacceptable amount of error. As such, the means and standard error values of the residuals of the multi-factor regressions were used to calculate 95th percentile confidence intervals about the mean of the residuals, and are summarized in Table 27. Unlike the Bland-Altman confidence intervals, which employed standard deviation, the ISO confidence intervals utilized standard error. It is quickly apparent that there is substantial overall improvement in the quality of the regressed measures.

Table 27: 95th percentile confidence intervals of scanned measurements, compared to ISO standard

Measurement	Manual Meas. Mean	CI Before Regression	CI After Regression	Standard	Actual
Head and Neck Vol. (L)	5.69 L	(0.72, 1.53) L	(-0.22, 0.22) L	5.3%	3.9%
Torso Vol. (L)	45.31 L	(-1.04, 16.52) L	(-3.67, 3.67) L	5.3%	8.1%
Torso Vol.* (L)	39.83 L	(-0.72, 3.62) L	(-1.81, 1.81) L	5.3%	4.5%
Left Upper Arm Vol. (L)	2.00 L	(-0.13, 0.27) L	(-0.14, 0.14) L	5.3%	7.0%
Right Upper Arm Vol. (L)	2.06 L	(-0.10, 0.16) L	(-0.13, 0.13) L	5.3%	6.4%
Left Lower Arm Vol. (L)	0.97 L	(-0.56, -0.40) L	(-0.04, 0.04) L	5.3%	4.2%
Right Lower Arm Vol. (L)	0.98 L	(-0.32, -0.20) L	(-0.03, 0.03) L	5.3%	3.1%
Left Hand Vol. (L)	0.40 L	(-0.51, -0.28) L	(-0.05, 0.05) L	5.3%	11.5%
Right Hand Vol. (L)	0.43 L	(-0.43, -0.20) L	(-0.06, 0.06) L	5.3%	12.9%
Left Thigh Vol. (L)	6.52 L	(-0.31, 1.56) L	(-0.73, 0.73) L	5.3%	11.2%
Right Thigh Vol. (L)	6.62 L	(0.01, 1.61) L	(-0.47, 0.47) L	5.3%	7.0%
Left Leg Vol. (L)	3.42 L	(-0.22, 0.45) L	(-0.28, 0.28) L	5.3%	8.1%
Right Leg Vol. (L)	3.34 L	(-0.01, 0.18) L	(-0.07, 0.07) L	5.3%	2.2%
Left Foot Vol. (L)	0.87 L	(0.22, 0.45) L	(-0.05, 0.05) L	5.3%	5.4%
Right Foot Vol. (L)	0.87 L	(0.18, 0.46) L	(-0.05, 0.05) L	5.3%	5.4%
Stature (cm)	172.4 cm	(0.6, 3.9) cm	(-1.3, 1.3) cm	(-0.4,0.4) cm	0.7 cm
Chest Breadth (cm)	34.0 cm	(-2.0, -0.6) cm	(-0.5, 0.5) cm	(-0.4,0.4) cm	1.6 cm
Hip Breadth (cm)	35.3 cm	(-2.0, -1.3) cm	(-0.3, 0.3) cm	(-0.4,0.4) cm	0.8 cm
Chest Depth (cm)	21.5 cm	(-1.8, -0.4) cm	(-0.6, 0.6) cm	(-0.5,0.5) cm	2.8 cm
Waist Depth (cm)	21.7 cm	(-1.9, -1.2) cm	(-0.3, 0.3) cm	(-0.5,0.5) cm	1.2 cm
Neck Circ. (cm)	36.2 cm	(-25.5, -9.2) cm	(-1.1, 1.1) cm	(-0.4,0.4) cm	3.0 cm
Chest Circ. (cm)	96.8 cm	(-4.9, -1.8) cm	(-1.1, 1.1) cm	(-0.9,0.9) cm	1.1 cm
Waist Circ. (cm)	91.5 cm	(-1.9, -0.2) cm	(-0.7, 0.7) cm	(-0.9,0.9) cm	0.8 cm
Hip Circ. (cm)	99.1 cm	(-3.4, -1.2) cm	(-1.0, 1.0) cm	(-0.9,0.9) cm	1.0 cm

Because the ISO documentation only applies to linear measurements only the linear measures were compared. There were 3 of 9 linear measurements that met the ISO requirement for acceptable error. Yet another 3 of the 9 linear measurements were close to meeting the standard (defined here as falling within two times the acceptable limit). The remaining three grossly exceeded the ISO standard. A summary of the validation can be seen in Table 28 below.

Table 28: Summary of measurement validation

Criterion	Linear Measurements	Volumetric Measurements
Met Standard	Hip Breadth Waist Depth Waist Circumference	Head and Neck Left Lower Arm Right Lower Arm Torso* Right Leg
Close to Standard (< 2 times Std)	Chest Breadth Chest Depth Chest Circumference Hip Circumference	Left Upper Arm Right Upper Arm Left Leg Left Foot Right Thigh Right Foot
Grossly Exceeded Standard	Stature Neck Circumference	Left Hand Right Hand Left Thigh

While some of the relative errors of segment volumes were large when compared to the magnitude of the segments (hand volumes, foot volumes, etc.), an analysis of absolute error of body segments, and error normalized to total body volume, would provide a better picture of the severity of the error of the various segments. A summary of regressed body segments' absolute 95th percent confidence limits of agreement can be seen in Table 29 alongside the upper-end normalized to mean total body volume (manual, in litres), excluding the three largest participants (one was completely excluded due to inability to manually measure thigh and torso volumes, two were excluded due to algorithmic issues associated with torso volume measurement).

Table 29: TBV-normalized limits of agreement

Measurement	Absolute CI (L)	CI Relative to Segment Magnitude	CI Relative to TBV
Head and Neck Volume	(-0.22, 0.22)	3.9%	0.33 %
Torso Volume *	(-1.81, 1.81)	4.5%	2.66 %
Left Upper Arm Volume	(-0.14, 0.14)	7.0%	0.21 %
Right Upper Arm Volume	(-0.13, 0.13)	6.4%	0.20 %
Left Lower Arm Volume	(-0.04, 0.04)	4.2%	0.06 %
Right Lower Arm Volume	(-0.03, 0.03)	3.1%	0.05 %
Left Hand Volume	(-0.05, 0.05)	11.5%	0.07 %
Right Hand Volume	(-0.06, 0.06)	12.9%	0.08 %
Left Thigh Volume	(-0.73, 0.73)	11.2%	1.08 %
Right Thigh Volume	(-0.47, 0.47)	7.0%	0.69 %
Left Leg Volume	(-0.28, 0.28)	8.1%	0.41 %
Right Leg Volume	(-0.07, 0.07)	2.2%	0.11 %
Left Foot Volume	(-0.05, 0.05)	5.4%	0.07 %
Right Foot Volume	(-0.05, 0.05)	5.4%	0.07 %

It should be clear from the above table, that the greatest contributors to total error are torso volume and thigh volume measurements. Furthermore, the regressed segments with the largest errors relative to the average segment magnitude (hands, feet, head and neck volumes) had relatively small errors when normalized against total body volume, compared to larger segments such as thigh and torso volumes.

Finally, the mean of total body volume values was computed from the unregressed scan extracted segment parameters, neglecting the three participants discussed above. Mean manual TBV was determined by hydrostatic weighing to be 67.34 L, while the scan-extracted value was slightly over-predicted at 68.18 L. This resulted in a error of approximately 1.2%.

Chapter 7. Discussion

Broadly speaking, there are three related research foci related to the application of human anthropometry. *Engineering anthropometry* relies on the application of linear and circumferential measures to improve human function in workspace design, and can be applied to product and personal protective equipment design to improve user-device interaction and safety. In the OEAB Lab, anthropometric measurements are also used in *biomechanics and body composition* research, evaluating kinematics and kinetics of human motion, as well as determining body fat percentage in human subjects. Finally, the third extension of the study of anthropometry in the OEAB lab is *health research,* where the literature shows an increasing amount of evidence that anthropometric measurements of shape and volume can be algorithmically related to the risk for different diseases. This area forms the primary purpose of this study and the discussion.

In preparation for the discussion of this research, it is important to re-state that the primary goal of this research was to validate the quality of scan-extracted measurements, more specifically to health related measures; however, some reference to the other two areas is important. The validity of the measures is greatly influenced by the quality of scanned images, software developed for the measures and the experimental methods employed for the study. Major alterations to the scanner and scanner related software were limited based on the proprietary licensing of the elements and was beyond the scope and timelines of this research.

The ultimate outcome of this work was twofold: firstly, a three-dimensional laser imaging apparatus was validated not only for linear and circumferential measurements, but also for segmental volumes. Secondly, and more importantly, a systematic method for comparisons of anthropometric measurements to digital measurement methodologies was designed and validated.

This study is novel in terms of the method of acquiring anthropometric measurements from 3D scans, a novel method of validating the measurements, and

presents a quantification of errors associated with the scan of human participants, which to this point has be notably absent from the literature. Finally, this document provides explanation for the sources of these errors, and recommends further work that would improve the quality of scan-extracted measurements.

7.1. Manual Measurement Collection

The first step in developing a novel method of comparing manual to scan-extracted measurements was to develop a method of manually collecting anthropometric values. In the case of manual measurements of length and circumference, the ISO standard methodology was employed: repeated (three) measures using an anthropometer, stadiometer, or cloth measuring tape, depending on the measurement collected.

The more complicated measurements to measure were the segment volumes, for which new measurement devices had to be acquired by the lab and testing procedures developed. Initially, such algorithmic segment approximation strategies as employed by Hanavan (Hanavan Jr, 1964), which serves as a standard for limb parameter (centre of mass, volume, etc.) in biomechanics, was ruled out for applications related to obese populations. Hanavan used a frustum model for limb segments, which is a poor approximation for segment parameters in all but the most ideal body shapes. The literature demonstrates an abundance of piecewise manual segment volume measurement strategies, such as Contini and Drillis, who measured arm and hand volumes (Drillis & Contini, 1966), and Dempster (Dempster, 1955), who developed a variety of volumeters for different body segments. Furthermore, hydrostatic weighing is the "gold standard" for total body volume measurement. However, the population under consideration in this study is obese, and the apparatus must be suitable for a variety of body shapes. The commonality of all of these strategies was the use of the displacement of water for the measurement medium.

The work performed in the OEAB Lab used a hybrid of the methods described in the literature, but provided a robust apparatus that allowed a large variety of human participants to be measured. Small segment (arms, feet, legs, hands) parameters were measured separately than larger volumes (head and neck, torso, and thighs).

7.1.1. **Small Segments**

Historically, limb volume measurement has been procedurally complicated and often relied on measurement of displaced water from one vessel to another for volume measurement. The use of a force plate and single container has been shown to accurately collect limb measurements with demonstrated effectiveness, while being a simple and robust enough system to accommodate a wide variety of segment magnitudes. Furthermore, while literature has shown methodologies, little has been done to show the error in volumetric measurement of limbs over a population sample, which will be subsequently discussed.

The height of the limb volumeter was designed to capture greater than 95% of participants by leg length, and as such was usable by the entire sample utilized in this study. Rather than pure displacement volumetry, where displaced water is collected in a separate container which is measured separately, this method measured the change in volume of the volumeter through measurement of mass change by force plate, averaged over a five second collection time. This meant less water was lost during transfer between containers, and a faster collection time.

The error within this methodology was quantified from 0 to 4 L, as shown in Appendix A. The volumeter was validated for relative and absolute error by standardizing polyethylene terephthalate (PET) bottles with water from a 200 mL beaker, and capturing force plate data at 500 mL increments as the bottles are inserted into the volumeter. The resulting relative error (2.3 %) was not only less than the threshold for clinically relevant weight loss (5.3%) (Douketis et al., 2005), but also within the tolerance of the beaker used to measure the water (±5%).

7.1.2. Larger Segments

The OEAB Lab has access to a total-body hydrostatic weighing tank, which was used to collect large segment volumes of head and neck volume, torso volume, and thigh volume. Thigh volume was calculated by measuring total left and right lower limb volume, dividing in half, and subtracting leg and foot volumes. This resulted in the possibility of errors from one side propagated to the other, which is one limitation of the apparatus; unique errors for thigh volume are possibly caused by errors in the leg and foot volume measurements. Head and neck volume is calculated by calculating the difference between measurements taken for total body volume and the measurements taken with the participants submerged only to the C7 landmark. Finally, torso volumes are calculated by subtracting limb volumes from the C7 volume measurement mentioned above.

One limitation with torso volume measurement is the breathing artifact, which results in changes in body density, resulting in errors in volume calculation. Participants were asked to breathe normally for the C7 volume measurement, and take and hold, a normal breath prior to total body immersion. The literature approximates average tidal lung volume in adult human participants to be 500 mL (Saladin, 2007). As this is only 1.3% of torso volume, and 0.7% of total body volume for the participants in this study, less than the clinically relevant 5.3% threshold, and 2.3% error for limb volume measurement, this error source is negligible in comparison. Furthermore, the participants in the laser scanner under comparison were also asked to breathe normally during the scan process, in an attempt to match the methodologies and reduce error. This may also have been a source of error for circumference measurements in the torso region (chest circumference).

7.2. Image Quality Improvement

Observation of the scans yielded a source of error related to limitations of field of view. A hard-coded algorithm in the scanner software was designed to exclude data points at the limit of the scan volume in order to ensure that data points representing the walls of the scanner are not included in the participant's scan file.

Often this resulted in the truncation of hand segment data points (see Figure 29). Furthermore, due to the placement of the scan heads, a resulting reduction of field of view was observed at the upper and lower regions of the scan volume along the vertical Y-axis. Despite some mechanical alterations to the scanner hardware, the field of view was only increased a small amount. This resulted in the removal of data points in the region of some participants' heads and feet (see Figure 28).

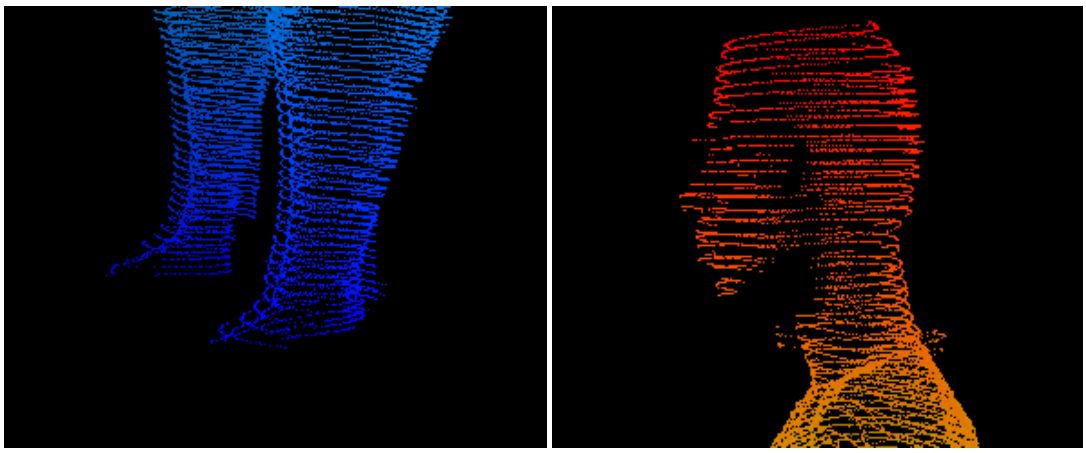

Figure 28: Head and foot truncation by FOV limitations

While this was a known limitation of the scans after analysis, the truncated segments were included in the regressions because this evaluation serves as the measure of the performance of the scanner as it currently exists. Furthermore, while this contributed to increased error in these segments, head and foot volume is unlikely to become clinically relevant, and the overall absolute error for these smaller segments are less important when compared to the acceptable amount of error in the torso region. Furthermore, without improving the quality of the scans, exclusion criteria can be designed that will prevent users over a certain height to be measured in the scanner. (~1.8 m)

Aside from mechanical improvements used to increase the scanner's field of view, discussed earlier, several sources of error in the acquisition of scan images were also identified. Radial distortion was most notable at the periphery of the scan

volume, an artifact first recognized in the preliminary work on the imaging phantoms. While this was not directly corrected by improving the quality of the scan itself, the regression of scanned measurements substantially improved the quality of the measurements at the periphery (head and neck volume, foot volume, and hand volume). It is apparent though, that the hand volumes retain the largest amount of relative error. A point cloud representation of a hand can be seen in Figure 29.

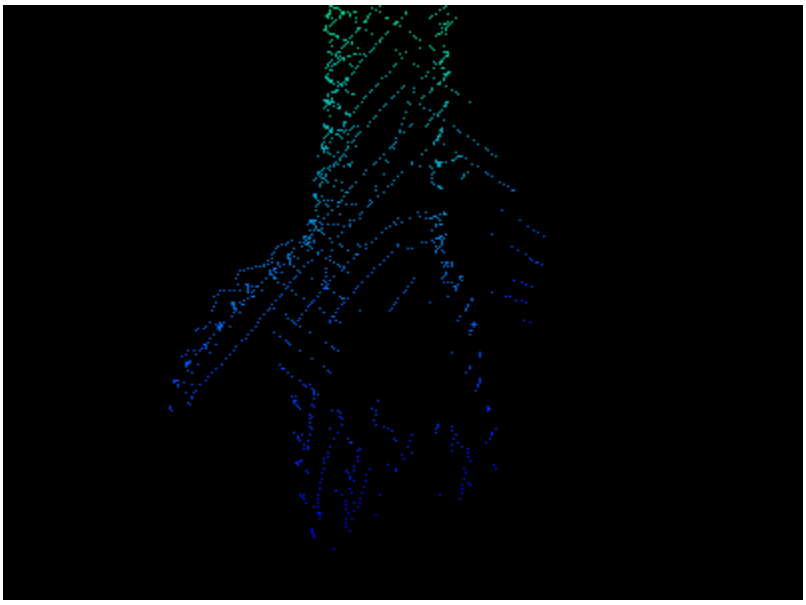

Figure 29: Point cloud rendering of a participant's hand

Despite the large amount of relative error, the absolute error in litres (~ 0.3 L) of these segments is very small when compared to the absolute error more clinically relevant measurements or of total body volume (~67 L) or that of the larger individual segments, such as torso volume (29 to 99 L). Appendix D contains a more comprehensive discussion of issues associated with radial distortion.

Based on the early work using the phantom, it was clear that radial distortion was a problem in the images. This is an example of an error that is camera specific and should and normally is, corrected for early in the measurement process. However, a licensing agreement between Unique Solutions and Dalhousie could not be reached during the timeline of this research allowing radial distortion artifacts to be

resolved on the front end. As such, rather than attempting to correct the quality of the images, which was not the objective of the research, a systematic regression was employed to compensate for the distortion across participants, and the results were validated. This is not to say that the distortion did not have an impact on the quality of the measurements, however, the quality of the measurements could be greatly improved through the use of systematic linear regression. The effects of scanner limitations was most notably experienced at the periphery of the scan volume, as seen in the head, foot, and hand segment volume measurements. There is in fact little mention in the literature of these errors or their effect if any on the scan quality of prior studies (Wang et al., April 2006). Thus, it is not known if the error was not present in their measures or what of any processes were used to minimize their effects.

7.3. Comparison of Scan-Extracted and Manual Measurements

The research was further extended into another area that is undergoing rapid investigation: the development of health indices for obese populations. Incorporated into this validation was a set of one-dimensional measurements relevant to the quantification of obesity. The goal of this pilot work to determine if the scanner could acquire measurements that could be used to develop novel health indices based on surface measurements that better predict metabolic disorders than the current landscape (eg. BMI, waist to hip ratio etc.).

The current literature landscape has shown ample evidence that some obesity related, metabolic diseases can be better predicted by combinations of measurements that incorporate more than the traditional one-dimensional measurements. The HI (health index) developed out of Chang Gung Medical Centre in Taiwan incorporates measures of area in a multi-factor formula that predicted several indicators of metabolic syndrome better than traditional BMI measurements (J. D. Lin et al., 2004). It follows that because adiposity is deposited volumetrically, and that body mass – a component of the measure of BMI – is proportional to body

volume, that a health index incorporating regional volumes might improve on health indices in the literature.

Prior to regression, many of the difference calculations, especially those such as torso volume and thigh volume that would possibly be used in the prediction of obesity-related disease, grew as the magnitude of the measurement grew as measured through significant PPMC coefficients. This was problematic as the intended population of this research would be larger than many of the participants measured. However, once stepwise linear regressions were used to model the scanned measurements, and the residuals were subjected to the same PPMC test, many of these correlations became non-significant. Several of the segment measurements that were, after regression, significant were the head and neck volume and foot volumes. This was most likely caused by the threshold issue discussed prior, where for taller people, part of the head segment and foot segments were not within the field of view of the scanner resulting in increased error values. However, volume measurements in these regions are not likely to be clinically relevant, and the errors of such should not be critically analysed to the same degree as measurements associated with the torso and thigh regions.

In the case of the two participants for whom measurements were taken, representing the largest body mass index values, torso volume was greatly under-predicted by 68.2 L and 50.2 L respectively, resulting in their exclusion from the regressed data set. This has strong implications for the future of this technology's use for the obese populations, and the cause of this under-prediction was possibly due to algorithmic computation of segment volumes. Despite this volumetric error, circumferential measurements in similar regions did not result in similar error magnitudes.

Several research groups have employed 3D laser imaging in the collection of segment and total body volumes, and have published their work; however, notably absent from the literature is a validation of these measurements beyond mannequin measurements, and large segment volumes; in 2006, Wang published results of

repeated measures on a single mannequin (Wang et al., April 2006). However, until this point, no comprehensive study has been performed that compares segment volumes acquired through manual methodologies to those computationally extracted from 3D scans on a sample of human participants, or even on a variety of body shapes. This validation is essential to determine the reliability of 3D laser scanning apparatus, as its eventual application is a clinical environment.

7.3.1. Other Sources of Scan-Extracted and Manual Testing Errors

The primary error sources in this the process can be separated into five major types: image quality and radial distortion, field-of-view (FOV) limitations, and manual volumetry issues – all discussed prior – as well as motion artifacts (sway, breathing), and post-scan digitization.

7.3.1.1. Motion Artifacts

Once the door of the scanner is closed, there can be no visual interaction between the technician and the participant. As a result, any position or motion-related errors by the participant within the scanner would result in increased error in the resulting measurements and cannot be easily detected. Motion can be caused by the postural sway of the participant, or by breathing artifacts (H. A. M. Daanen, Brunsman, & Robinette, 1997). Furthermore, it was observed in early pilot work that participants under scanning measurement assume postures such as slouching during a scan, which was not observed during manual measurement of stature. These errors occurred during the scan process, and there is no way for retrospective analysis to be performed. These errors will be assumed to contribute both a constant and a random error inherent to the scan process and will affect comparisons with the annual measures.

7.3.1.2. Landmark Detection

Unlike some work in the literature, which employed automatic, or semi-automatic, landmark detection during three-dimensional laser scanning (Burnsides et al., 2001), in this study anthropometric landmarks were digitized manually using

custom software. In some cases, the identification of anthropometric landmarks posed difficulty due to participants' anatomical features, or sparse distribution of data points. This was especially true in the identification of scye creases and crotch landmarks, shown in Figure 30.

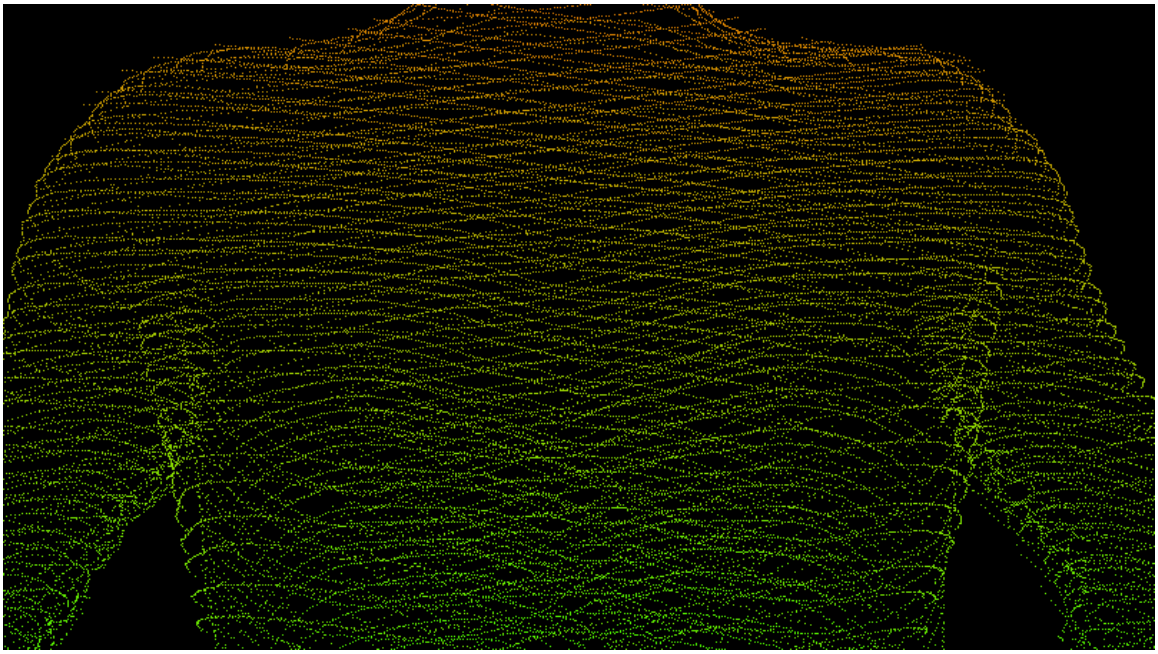

Figure 30: Point cloud rendering of the left and right scye creases of a human participant

The averaging of measurements from multiple digitisations and some post-processing exclusion of outliers (a process discussed in detail in Appendix C) improved the quality of the measurements; however, the magnitude of the user error has not yet been quantified, and will be assumed to contribute to the random error associated with measurement. This has been an artifact of manual landmark detection in the literature (H. A. Daanen, Taylor, Brunsman, & Nurre, 1997).

7.3.2. Stepwise Analysis of Statistical Validation Process

While the above sections spoke to broader observations of the human trials, following sections discuss notable results in greater detail, reflecting on the prior discussion.

7.3.2.1. Correlations

From the correlation relationships between measurement methods, it was apparent that one-dimensional scan-extracted measurements were better correlated to manual measurements than most segment volumes. It must be remembered that volumetric measurements propagate one-dimensional errors in three axes, effectively cubing the order of magnitude of the error present in one-dimensional measurements. Furthermore, the weakest or non-significant correlations existed in volumes at the periphery of the scan volume: in the hand segments, foot segments, and head and neck segments.

The source of this uncorrelated data may be twofold. Firstly, point cloud data is under heaviest influence of radial distortion (See Appendix D) at the periphery of the scan volume, for each imaging apparatus. Furthermore, as was mentioned prior, field of view issues arose at all sides of the scan volume, partially caused by camera angle limitations, but also by hard-coded algorithmic exclusion of sidewall data points. This combined effect caused the point clouds of participants whose peripheral segments extended into these areas to be truncated, decreasing the predicted volume values.

7.3.2.2. Differences

Bland-Altman analysis allows for analysis of trends in errors between measurement modalities, and to determine the limits of agreement between measurement modalities. When the differences were calculated between manual and scan extracted measurements, and confidence intervals were calculated (95% CI), the confidence intervals far exceeded the allowable range as presented in the ISO. Due to an inability to improve scan quality through improved intrinsic and extrinsic calibration techniques due to software licensing issues with the partner company, regression was used as a means of using scan-extracted measurements to predict the true measurements.

In addition to the ISO, ANSUR has provided a secondary standard for allowable error in human anthropometry – called “Maximum Allowable Error” (MAE) between

repeated linear manual measurements. Its application was originally applied to the repeated measurements of manual anthropometry: a measure of precision, not a validation across measurement methodologies, and was extended for use in the evaluation of the two scanners employed during the CAESAR studies (Robinette, Daanen, 2006). However, because this work comprises a validation of a technology that compares two measurement methodologies, not simply the precision of a single apparatus, this error standard is insufficient. Finally, as most of the measurements under evaluation were volumetric, and subject to *clinical* standards developed for this work, the ANSUR and ISO measurements only applied to the linear measurements under validation.

In addition to calculating confidence intervals, the Bland-Altman plots were used to determine trends between the magnitude of the error and the magnitude of true measurements. The strongest correlations can be seen in the foot volumes ($r = 0.88$ for both left and right foot volumes), the left and right thigh volumes ($r = 0.918$, 0.933 respectively), the torso volumes prior to outlier removal ($r = 0.921$), and the neck circumference measurements ($r = -0.717$), demonstrating that the magnitudes of the errors in these measurements increase as true measurements increase in magnitude. The likely cause of the highly correlated foot volume differences was a threshold issue in the scanner. The taller participants were asked to step off the platform raising participants into the scanner field of view, such that the majority of the body and head could be scanned. This caused several participants' feet to be truncated in scans as they were below the field of view of the scanner. The likely cause of the strong correlation for torso volumes was the inclusion of outliers, representing the two largest participants. This correlation was substantially reduced when the two largest values of torso volume were removed ($r = 0.588$). The strong correlation between neck circumference difference values and magnitude may have been brought on by the inclusion of beads in the circumference measurements, which presented most strongly in this smaller circumference measurement.

7.3.2.3. Regressions

A novel method of regression analysis was applied to the scan-extracted measurements, in order to improve the quality of predicted measurements. In place of difference calculations in the ISO documentation, the 95th percentile confidence interval was taken about the mean of the residuals of the regressions.

The first regressions measurements were simple, and only scan-extracted were used in the prediction of the true measurements. The residuals were then plotted against the true magnitudes, for which PPMC coefficients were calculated. Strong correlations were found, especially the head and neck volumes ($r = 0.927$), hand volumes (0.93 and 0.94, for left and right hands respectively), and foot volume measurement (0.97 and 0.77, for left and right feet respectively), demonstrating that there was remaining systematic error not accounted for by the simple regressions. This led to the inclusion of the manual measurements of mass and stature (frequently collected clinically) as predictive factors in the regressions, in order to test for a systematic effect caused by the size of the participant.

The resulting linear models incorporated the new variables almost exclusively additively to the regression equations, implying an under-prediction in the absence of the compensatory variables: as the mass and stature of the participants increased, the correction factors increased the compensatory effects in the by linearly increasing the magnitude of the predicted measurement (besides hip breadth, where mass was inversely proportional). The quality of fit (coefficient of determination) of the linear regressions improved markedly for almost all measurements, except for those for which manual mass and stature were not correlated to the manual measurement in the stepwise regression.

The correlations between residuals and manual measurements of most measurements were reduced in magnitude, and in some cases, non-significant, after manual stature and mass were included in the regressions – again besides those for which manual mass and stature were not included in the regression. The implication of this is that one-dimensional metrics of patient size easily captured

clinically, can substantially improve the quality of scans. Furthermore, some of the strongest remaining significant correlations are on segments at the periphery of the scan volume (hand volume, foot volume, etc.), for which known sources of error have been described.

Several limitations with these regressions should be noted. Firstly, the manual measurements of stature and mass are significantly and moderately correlated ($r = 0.754$, $p > 0.000$) across this sample. While the regressions that used these predictors may describe the sample recruited in this study, issues of multicollinearity may increase the volatility of these regressions if used as correction regressions for scan-extracted measurements in the future. Further testing of these regressions on another sample of participants is advised.

In several cases, non-significant scan-extracted measurements were inclouded in the model regressions, despite stronger relationships to predictor variables of mass and stature. This was most notable in the segment volumes of the head, hands, and feet, where issues associated with hardware and software have been previously identified.

7.3.2.4. Limits of Agreement:

In the initial work, Bland-Altman confidence intervals were compared the ANSUR standards to determine whether a linear scan-extracted measurement was valid; however, ANSUR maximum allowable error (MAE) values only apply to repeated manual measurements and the objective of this research is to compare across measurement methodologies. The ISO standard of comparison quantifies measurement validity, which is a combination of measurement accuracy and precision.

Whereas the Bland-Altman formula (applied to ANSUR standards) for determining limits of agreement utilized standard deviation, shown in Equation (9) the ISO standard utilized standard error to develop the limits of agreement between measurement methodologies, shown in Equation (10). Both ANSUR and ISO methods

were used to compare the limits of agreement of linear measurements to absolute thresholds of allowable error.

$$CI = \bar{x}_{err} \pm 1.96 s_x \quad (9)$$

$$CI = \bar{x}_{err} \pm 1.96 s_{\bar{x}} \quad (10)$$

Volume measurements employed the same ISO methodology for developing the limits of agreement; however, no standard exists for absolute allowable segment volume error. The clinical threshold for allowable error developed for this study was 5.3%, against which confidence intervals were converted to relative errors for comparison.

An examination of the results summary table – Table 28 – shows that most of the measurements were close to, or met, the criterion standards for each measurement. A brief discussion of those that did not follows.

It appeared, as expected from prior examination, that the hand and foot volumes did not meet the criterion of 5.3%; however, Table 29 shows that despite a relatively large amount of error relative to segment volume, hand and foot volume errors are very small when normalized relative to total body volume. This too applies when analysing arm and leg segments as well; however, the left thigh volume grossly exceeded the 5.3% standard. This may have been an issue in the manual collection of thigh segment volumes; it was often very difficult for the operator of the hydrostatic weighing tank to visualize the crotch landmark, and often required self-reported identification by the participants, due to some bathing wear obscuring the landmark. Furthermore, a left-right asymmetry is pronounced in as left thigh volumes meet the standard, and right thighs do not. Thigh volume was calculated as the difference between both lower limbs, divided and half, and the respective leg and foot volumes. This drives the consideration that the individually calculated leg and foot volumes are likely causing the asymmetry. An inspection of the raw data demonstrated that several participants had seemingly low measurements for manual thigh volumes. This could be caused by an artificially large volume measurement for leg volume, a result of a participant placing their foot

on the floor of the volumeter during manual leg measurement. Table __ demonstrates a summary of the data of one such participant.

Table 30: Example of left-right asymmetry on a single participant, leg and thigh volumes

Measurement	Manual (L)	Scan-Extracted (L)
Left Leg Volume	5.48	3.06
Right Leg Volume	3.12	2.93
Left Thigh Volume	1.60	5.35
Right Thigh Volume	3.95	5.39

This left-right asymmetry may also be a result of distortion in the scan heads. Each scan head collects point cloud data for a region of the participant separately, which is later compiled into a unified point cloud. If the scan head on the lower right side of the participant had significantly greater intrinsic parameter distortion than the lower left side, this could result in an asymmetry between the two lower limb volume measurements.

Again, unsurprising was the result that both stature and neck circumference grossly exceeded the ISO standard for linear measurement. One proposed source of neck circumference variability discussed prior is the inclusion of landmark markers in the circumference calculation. Again discussed prior was the effect in several taller participants where stature was under-predicted due to the truncation of the point cloud near the apex of the head.

While prior discussion has shown that breathing has little impact on the error in torso volumes, one study has shown that tidal breathing artifacts can affect circumference measurements by as much as 2.0 cm, greater than the ISO standard for allowable variation in chest circumference (Wade, O.L., 1954). This may explain the error in the linear measurements in chest depth, chest circumference and chest breadth.

In comparison to Wang's volume-related error analysis for laser anthropometry in the literature review, it becomes clear that despite substantially smaller relative error values (shown in Table 2), as compared to the measurement magnitudes

shown for this study in Table 27, the absolute magnitudes of measurements in Wang were substantially smaller. Wang's mannequin had an average total body volume of 23.62 L, as compared to this study's average TBV of 67.34 L. As several error sources in this work propagated with magnitude, one might expect that smaller volumes might be better predicted by laser imaging techniques. Perhaps this is because the smaller volumes are derived from more central location in the scan volume which has been shown to have less image distortion. Furthermore, the sampling of the participants in this study forms a much more realistic picture of human variability than literature-based validation.

Finally, Siri's body fat computation (Siri, 1956) is a function of total body density, directly proportional to total body volume. Because scan extracted values predict true values with a relatively low (1.2%) amount of relative error, this technology shows promise that with corrections of scan-extracted acquisition of torso volume values for obese populations, that percent body fat may be computed.

Chapter 8. Ethics

Prior to initiating the use of human participants in this body of research, a submission of an ethics document to the Research Ethics Board (REB) of Dalhousie University. As this is an engineering validation study, and not intended to demonstrate clinical efficacy in the pre-surgical population, a submission to the Capital District Health Authority Research Ethics Board will not be necessary; however, as clinical investigation with CDHA involvement will eventually be a desired outcome programmatically, a CDHA REB document should soon be pursued.

The Occupational Ergonomics and Biomechanics Lab at Dalhousie University filed an approved ethics application in 2011 that encompasses the use of laser imaging, millimeter wave imaging, and fully body hydrostatic weighing on a normal population. Additionally, it allows for the manual measurement of anthropometric measures sought in this project.

Chapter 9. Industrial Involvement

Unique Solutions, based in Dartmouth Nova Scotia, developed scanning apparatus and associated software to provide three-dimensional scans of human topography in order to optimize clothing fit within the apparel industry. Their recognition that the technology provided reasonable depictions of human topography led to their desire to enter the medical device marketplace. Unique Solutions loaned Dalhousie University's health and human performance department both a laser scanner and a millimetre wave scanner in order to test the technologies in the health field. Furthermore, Unique Solutions has provided software to visualize the point cloud scanner output files, and assistance in debugging both the hardware and the software involved in the scan process. They intend to continue their involvement through the clinical application of this work.

Chapter 10. Conclusion

While the original intent of this research was the validation of a closed-platform technology, the customization of some hardware and ground-up development of novel software utilizing innovative measurement techniques, yields this apparatus a custom device better-suited to laser anthropometry.

This research followed two simultaneous streams: the investigation and resolution of technological issues associated with the scanner and the validation of novel manual measurement methodologies. This culminated in the main experiment that formed the basis of the presented work: the validation of the scanning technology against manual measurement methods.

Prior to the human trials, two phases of scanner evaluation were performed. Firstly, technology selection procedures demonstrated that of mmWave scanning technology and the 3D laser scanner, that laser imaging proved to be superior for comprehensive imaging of participants. Secondly, Anterior-posterior and medial-lateral measurements in the transverse plane along the vertical axis were shown to be subject to systematic error. Further investigation demonstrated that modeling difference measurements with a second order polynomial was able to substantially improve the magnitude of the error.

Because the technology selection phase of scanner investigation demonstrated that on-board software neither captured standardized ISO or clinical measurements, nor did it capture segment volumes. As a result, custom software was developed that required testing on human participants. Manual volumetry methodology was subsequently developed and tested, with measureable effectiveness.

The results of this study have shown promise for the future of the use of this device for the acquisition of measurements related to obesity. When compared to ISO and clinical standards, the majority of the measurements collected were within, or close to, these standards. The implication of this is that the implementation of a small number of minor improvements may very quickly allow the scanner to collect

measurements on a clinical population. Furthermore, many of the volumetric measurements that did not meet the clinical standard (hand volumes, foot volumes, etc) are unlikely to be clinically relevant, and the absolute error of these measurements was often very small when normalized against total body volume, and compared to the more clinically relevant volumes of torso and thigh.

Several drawbacks exist with the scanner that will require further investigation before clinical application. Stature is used in the computation of the most commonly used measure of obesity: BMI. As such, it is important that any measurement methodology be able to accurately acquire this measurement. Due to a threshold "cut-off" as a result of the scanner's field of view, participants taller than approximately 1.8 m are unable to be scanned.

Aside from the historically significant circumference and breadth values, which were primarily used in this research as a demonstration of the compatibility of the technology with current measurement methods, the literature landscape would imply that like the clinically relevant circumference measurements of the trunk and thighs that are frequently used to predict disease, torso and thigh volumes may demonstrate improved relationships with metabolic disorders. This proves problematic when reflecting on the results of this study, as unique algorithmic deficiencies appeared in the calculation of torso volumes of participants with large values of BMI. While the removal of two outliers allowed torso volumes to be well predicted by the scanner for normal, overweight, and mildly obese, participants, the data points removed were those of the most obese participants. Furthermore, while the largest participants in this study had BMI values that were less than 40 $\frac{kg}{m^2}$; most candidates for bariatric surgery – the intended eventual population for clinical study – far exceed this BMI range. Additionally, right thigh volumes were not shown to be measured within or close to pre-determined standards; however, this may be due to methodological issues associated with manual thigh volume measurement.

10.1. Improvements to Scan Process

The first goal of this study was the validation of a commercial three-dimensional laser scanner. The intended use of the scanner for clinical applications, the custom nature of the *Scananalysis* software, and the novel application of the Unique Solutions scanner lead to a number of improvements for the future application of the three-dimensional laser scanner

Firstly, a licensing agreement should be developed between the OEAB Lab, and Unique Solutions, such that the algorithms related to image acquisition can be modified to accommodate improved intrinsic lens parameters, in an attempt to correct radial lens distortion, as discussed in Appendix D. This will impact all measurements; however, those at the most distal locations – such as the hands and feet – would likely experience the greatest increase in measurement quality. While improved intrinsic parameters may result in somewhat improved distortion, the replacement of the cameras on the scanners may further improve the quality of scan-extracted measurements.

In the measurement of smaller circumferences, such as the neck circumference, it would likely be beneficial to improve upon the design of landmark markers such that they do not interfere with the measurement of circumferential measurements.

Slight improvements to the field of view of upper scan heads may further improve the total field of view, and improve stature, and other head and neck measurements. Furthermore, increasing the hard-coded scan volume may also improve the quality of computed hand volumes.

Experimentation in the algorithm used to model circumference measurements, such as optimizing the order of polynomial, or incorporating spline fits into the circumference fits to scan data, may increase the quality of scan-extracted circumferential measurements. Finally, and most importantly, given that the eventual intended use of this technology is the measurement of obese populations,

improvements in data quality should be focused on improving the algorithm for torso volume measurement of larger participants.

10.2. Improvements to Methodology

Retrospective consideration of the second propose of this study, the validation of a process by which laser scanners can be validated, has given rise to several concerns that may require improvement in the future.

Firstly, participants were permitted to bring their own bathing garments, which were not pre-screened for fit. Loose-fitting lower limb bathing garments often obscured the technician's view of the crotch landmark during hydrostatic weighting. In the future, requesting that participants wear skin-tight bathing garments may improve the identification of this landmark.

Secondly, participants were instructed to breathe normally in the scanner; however, they were unable to breathe normally underwater. This may have introduced a small degree of error as patients were allowed to inspire a normal breath prior to submerging. Given the duration of the scan – 45 seconds – it would be unreasonable to expect all participants to hold their breath for an entire scan. If this device were to be eventually used as a substitute for underwater weighing for the approximation of percent body fat, the scan-extracted total body volume measurements would require compensation for lung volume. In addition, accuracy of the results would be based on assumptions between body density and percent body fat.

Given that the volume measurements of the lower arm segments met the standard for volumetric measurements, changing the standard participant posture within the scanner to move the most distal points of the hand within the scan volume may improve the quality of hand volume measurements.

Statistical methodologies have been shown to improve the predictive ability of three-dimensional laser imaging for measurements related to obesity. There remain some proprietary hardware and software issues related to the scan process

that have been identified and will likely require resolution before the scanner can be used for all measurements. With the limitations identified, the scanner is unlikely to become useful for hand and foot measurements in the near future; however, with minor modifications, clinically relevant measurements taken in the arm, torso and thigh regions will be the most useful measurements extracted by this scan system.

References

Alberti, K. G. M. M., Eckel, R. H., Grundy, S. M., Zimmet, P. Z., Cleeman, J. I., Donato, K. A., . . . Smith, S. C. (2009). Harmonizing the metabolic syndrome: A joint interim statement of the international diabetes federation task force on epidemiology and prevention; national heart, lung, and blood institute; american heart association; world heart federation; international atherosclerosis society; and international association for the study of obesity. *Circulation, 120*(16), 1640-1645. doi:10.1161/CIRCULATIONAHA.109.192644

Allen, B. (2003). The space of human body shapes: Reconstruction and parameterization from range scans. *ACM Transactions on Graphics, 22*(3), 587. doi:10.1145/882262.882311

Biaggi, R. R., Vollman, M. W., Nies, M. A., Brener, C. E., Flakoll, P. J., Levenhagen, D. K., . . . Chen, K. Y. (1999). Comparison of air-displacement plethysmography with hydrostatic weighing and bioelectrical impedance analysis for the assessment of body composition in healthy adults. *The American Journal of Clinical Nutrition, 69*(5), 898-903.

Bridger, R. S. (2009). *Introduction to ergonomics* (3rd ed.). Boca Raton, FL, USA: CRC Press.

Brozek, J., Grande, F., Anderson, J. T., & Keys, A. (1963). DENSITOMETRIC ANALYSIS OF BODY COMPOSITION: REVISION OF SOME QUANTITATIVE ASSUMPTIONS*. *Annals of the New York Academy of Sciences, 110*(1), 113-140. doi:10.1111/j.1749-6632.1963.tb17079.x

Burnsides, D., Boehmer, M., & Robinette, K. (2001). 3-D landmark detection and identification in the CAESAR project. Paper presented at the *3-D Digital Imaging and Modeling, 2001. Proceedings. Third International Conference On,* 393-398.

Chamberland, A., Carrier, R., Forest, F., & Hachez, G. (1998). Anthropometric survey of the land forces. *Defence and Civil Institute of Environmental Medicine (DCIEM-98-CR-15, 98-01897),*

Chan, D. C., Watts, G. F., Barrett, P. H. R., & Burke, V. (2003). Waist circumference, waist-to-hip ratio and body mass index as predictors of adipose tissue compartments in men. *QJM, 96*(6), 441-447. doi:10.1093/qjmed/hcg069

Daanen, H., & Ter Haar, F. (2013). 3D whole body scanners revisited. *Displays, 34*(4), 270-275.

Daanen, H. A., Taylor, S. E., Brunsman, M. A., & Nurre, J. H. (1997). Absolute accuracy of the cyberware WB4 whole-body scanner. Paper presented at the *Electronic Imaging'97,* 6-12.

Daanen, H. A. M., Brunsman, M. A., & Robinette, K. M. (1997). Reducing movement artifacts in whole body scanning. Paper presented at the *3-D Digital Imaging and Modeling, 1997. Proceedings., International Conference on Recent Advances In,* 262-265.

Dempster, W. T. (1955). Space requirements of the seated operator: Geometrical, kinematic, and mechanical aspects of the body, with special reference to the limbs.

Dempster, W. T., Gabel, W. C., & Felts, W. J. L. (1959). The anthropometry of the manual work space for the seated subject. *American Journal of Physical Anthropology, 17*(4), 289-317. doi:10.1002/ajpa.1330170405

Douketis, J., Macie, C., Thabane, L., & Williamson, D. (2005). Systematic review of long-term weight loss studies in obese adults: Clinical significance and applicability to clinical practice. *International Journal of Obesity, 29*(10), 1153-1167.

Drillis, R., & Contini, R. (1966). *Body segment parameters* New York University, School of Engineering and Science.

Gordon, C. C., Churchill, T., Clauser, C. E., Bradtmiller, B., & McConville, J. T. (1989). *Anthropometric Survey of US Army Personnel: Methods and Summary Statistics 1988,*

Hanavan Jr, E. P. (1964). *A Mathematical Model of the Human Body,*

Hertzberg, H. T. E., Dupertuis, C. W., & Emanuel, I. (1957). *Stereophotogrammetry as an anthropometric tool* Wright Air Development Center.

Hrdlicka, A. (1972). *Practical anthropometry* AMS Press.

Janssen, I., Katzmarzyk, P. T., & Ross, R. (2004). Waist circumference and not body mass index explains obesity-related health risk. *The American Journal of Clinical Nutrition, 79*(3), 379-384.

Jensen, R. K. (1978). Estimation of the biomechanical properties of three body types using a photogrammetric method. *Journal of Biomechanics, 11*(8–9), 349-358. doi:http://dx.doi.org/10.1016/0021-9290(78)90069-6

Kissebah, A. H., & Krakower, G. R. (1994). Regional adiposity and morbidity. *Physiological Reviews, 74*(4), 761-811.

Klein, S., Burke, L. E., Bray, G. A., Blair, S., Allison, D. B., Pi-Sunyer, X., . . . American Heart Association Council on Nutrition, Physical Activity, and Metabolism. (2004). Clinical implications of obesity with specific focus on cardiovascular disease: A statement for professionals from the american heart association council on nutrition, physical activity, and metabolism: Endorsed by the american college of cardiology foundation. *Circulation, 110*(18), 2952-2967. doi:10.1161/01.CIR.0000145546.97738.1E

Kouchi, M., Mochimaru, M., Bradtmiller, B., Daanen, H., Li, P., Nacher, B., & Nam, Y. (2012). A protocol for evaluating the accuracy of 3D body scanners. *Work: A Journal of Prevention, Assessment and Rehabilitation, 41*, 4010-4017.

Larson, R., Hostetler, R., & Edwards, B. (2008). In Cantin C., Galuardi P. and Carter K. (Eds.), *Essential calculus: Early trancendental functions*. Boston, MA: Houghton Mifflin Company.

Lin, J. D., Chiou, W. K., Weng, H. F., Fang, J. T., & Liu, T. H. (2004). Application of three-dimensional body scanner: Observation of prevalence of metabolic syndrome. *Clinical Nutrition, 23*(6), 1313-1323. doi:10.1016/j.clnu.2004.04.005

Lin, J., Chiou, W., Weng, H., Tsai, Y., & Liu, T. (2002). Comparison of three-dimensional anthropometric body surface scanning to waist–hip ratio and body mass index in correlation with metabolic risk factors. *Journal of Clinical Epidemiology, 55*(8), 757-766. doi:10.1016/S0895-4356(02)00433-X

Obesity Network. (2010). Weight loss surgery (WLS) information & handouts. Retrieved September, 2012, from http://www.cdha.nshealth.ca/obesity-network/weight-loss-surgery-wls-information-handouts-binder-information

Oxford english dictionary. (2011). Retrieved February 28, 2012, from http://www.oed.com/view/Entry/8444

Pheasant, S. (1996). *Bodyspace*. London: Taylor & Francis Ltd.

Robinette, K. M. (2006). Precision of the CAESAR scan-extracted measurements. *Applied Ergonomics, 37*(3), 259. doi:10.1016/j.apergo.2005.07.009

Saladin, K. (2007). The respiratory system. In K. A. Queck (Ed.), *Anatomy & physiology: The unity of form and function* (4th ed., pp. 874-875). New York, NY: McGraw-Hill.

Schneider, H. J., Friedrich, N., Klotsche, J., Pieper, L., Nauck, M., John, U., . . . Wittchen, H. (2010). The predictive value of different measures of obesity for incident cardiovascular events and mortality. *Journal of Clinical Endocrinology & Metabolism, 95*(4), 1777-1785. doi:10.1210/jc.2009-1584

Siri, W. (1956). *Body composition from fluid spaces and density: Analysis of methods.* (No. UCRL - 3349). Berkeley, California: University of California.

STANDARD, B., & ISO, B. (2008). ISO 7250-1: Basic human body measurements for technological design.

STANDARD, B., & ISO, B. (2010). ISO 20685:2010: 3-D scanning methodologies for internationally compatible anthropometric databases.

Vincent, H. K., Vincent, K. R., & Lamb, K. M. (2010). Obesity and mobility disability in the older adult. *Obesity Reviews, 11*(8), 568-579. doi:10.1111/j.1467-789X.2009.00703.x

Wang, J., Gallagher, D., Thornton, J. C., Yu, W., Horlick, M., & Pi-Sunyer, F. X. (April 2006). Validation of a 3-dimensional photonic scanner for the measurement of body volumes, dimensions, and percentage body fat. *The American Journal of Clinical Nutrition, 83*(4), 809-816.

Wells, J., Douros, I., Fuller, N., Elia, M., & Dekker, L. (2000). Assessment of body volume using Three-Dimensional photonic scanning. *Annals of the New York Academy of Sciences, 904*(1), 247-254.

Wells, J. C. K. (2007). Whole-body three-dimensional photonic scanning: A new technique for obesity research and clinical practice. *International Journal of Obesity, 32*(2), 232. doi:10.1038/sj.ijo.0803727

World Health Organization. (2014). Health topics: Obesity. Retrieved July 28, 2014, from http://www.who.int/topics/obesity/en/

Zatsiorsky, V., & Seluyanov, V. (1983). The mass and inertia characteristics of the main segments of the human body. *Biomechanics VIII-B, 56*(2), 1152-1159.

Zhengyou Zhang. (2000). A flexible new technique for camera calibration. *Pattern Analysis and Machine Intelligence, IEEE Transactions On, 22*(11), 1330-1334. doi:10.1109/34.888718

Appendix A Validation of Manual Displacement Volumeter

The goal of this thesis is to demonstrate agreement between laser scanning technology and more classical means of collecting anthropometric measurements. Because rulers, anthropometers, stadiometers, and cloth measuring tapes are all well-validated methods of measuring linear and circumferential measurements, it is unnecessary to demonstrate their efficacy in this context. Furthermore, the hydrostatic weighing method has also served as the "gold-standard" for the determination of total body volume and will not be validated for this work.

A variety of segmental volume measurement strategies have been presented in the literature. Early on, cadaveric sections were immersed and measured for volume using hydrostatic methods (Dempster, 1955). Dempster presented a displacement-overflow method, shown in an excerpt of his work, *Space Requirements of the Seated Operator*, that employed a filled tank that overflowed into a secondary collection tank when a segment was inserted. The water was collected and measured for displaced volume.

Volumeter Development

Dempster's method of segment volumetry required that the participant positions themselves in a variety of orientations that may be difficult for mobility-impaired participants. Due to the variety of the participants in this study, a flexible strategy that could accommodate a variety of body shapes was needed.

Four volumeters were underwent qualitative evaluation, in order to determine which would best accommodate the population, and effectively measure segmental volumes.

Faucet Volumeter

First in order to test the concept of displacement volumetry, a valve was attached to the top of a Rubbermaid™ polyethylene container such that when a segment was inserted into the container, the displaced water would flow through the open valve

into a collection tank. When the water had finished flowing, the valve could be closed, such that participant motion within the volumeter would not contribute error due to water sloshing through the opening, and into the collection tank. The displaced water would be measured to determine limb volume. An image of this proof-of-concept is show in Figure 31.

Figure 31: Proof of concept faucet volumeter

When tested, the insertion of the limb did not change the height of the water enough to cause substantial flow to exit the volumeter through the faucet, and the flow was too slow through the opening for efficient use of participant time, given the number of required measurements for each participant.

Channel Volumeter

In order to increase the flow of the water, second and third volumeters were developed – for upper and lower segments respectively – with wider channels and more study structure, to allow the participants to self-support during measurement.

In this case, the volumeters were filled until the water was about to flow over the channel, and the participant would slowly insert their limb into the volumeter. The displaced water would flow through the channel and down the trough into a collecting tank, where the water would be measured for volume. These new volumeters can be seen in Figure 32 and Figure 33.

Figure 32: Upper limb channel volumeter

Figure 33: Lower limb channel volumeter

Again, upon testing, the flow of the water through the channel was too slow for efficient measurement, despite the larger channel. Furthermore, when a small segment – such as a foot segment – was inserted into the lower limb volumeter, very little to no water would flow through the channel, due to surface tension at the channel's edge.

Force Plate Volumeter

It was evident from prior iterations of volumeter design that displacement volumetry alone was a time-consuming measurement process, heavily influenced by surface tension. As a result, a simple hybrid of classical hydrostatic weighing and displacement segment volumetry was developed.

This new strategy involved placing a polyethylene container on a force plate and filling it with a volume of water that the insertion of a limb would not cause the water to overflow, yet allow for the full submersion of the limb. The force plate was then zeroed prior to data collection. Each limb volume was then inserted into the volumeter, and force plate data was collected for five seconds at a rate of 20 Hz. The resultant z-direction (vertical) force vector was used to calculate the volume of the displaced limb, according to the following diagram (Figure 34) and subsequent expressions.

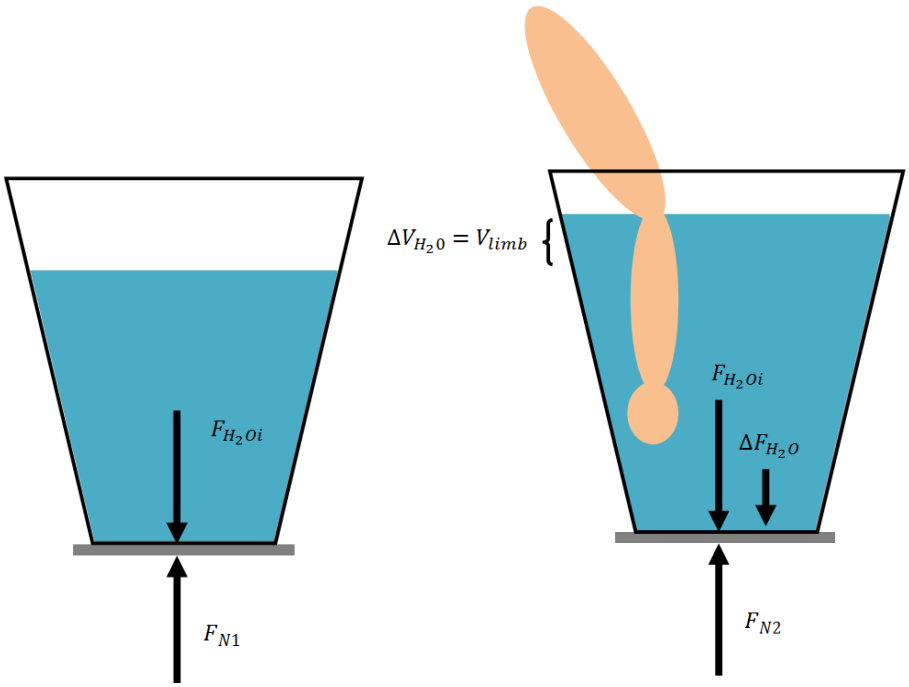

Figure 34: Manual volumetry diagram - theoretical

The z-direction normal force is equal to the force of the volume of water initially.

$$F_{N1} = F_{H_2Oi} \tag{a}$$

Once the limb is inserted, the apparent force at the force plate increased due to the increased volume in the container.

$$F_{N2} = F_{H_2Oi} + \Delta F_{H_2O} \tag{b}$$

Given the properties of liquids,

$$\gamma = \frac{m}{V} \tag{c}$$

and that the force exerted by the increase in volume in the container is due to its mass under the acceleration of gravity,

$$\Delta F_{H_2O} = \Delta m_{H_2O} g \tag{d}$$

and that the volume displaced in the container is equal to the volume displaced by the limb,

$$\Delta V_{H_20} = V_{limb} \tag{e}$$

it can be concluded that the vertical force measured by the force plate is equal to the initial force exerted by the water, and the density of the water (assumed to be 1000 $\frac{kg}{m^3}$ at STP).

$$F_{N2} = F_{H_2Oi} + \gamma V_{limb} g \tag{f}$$

Rearranging for limb volume, and assuming an initial zeroing of the force plate once the container was filled, the following expression can be produced. This describes the relationship between the force output from the force and the measured limb volume.

$$V_{limb} = \frac{F_{N2}}{\gamma g} \tag{g}$$

An image of the setup can be seen in Figure 35.

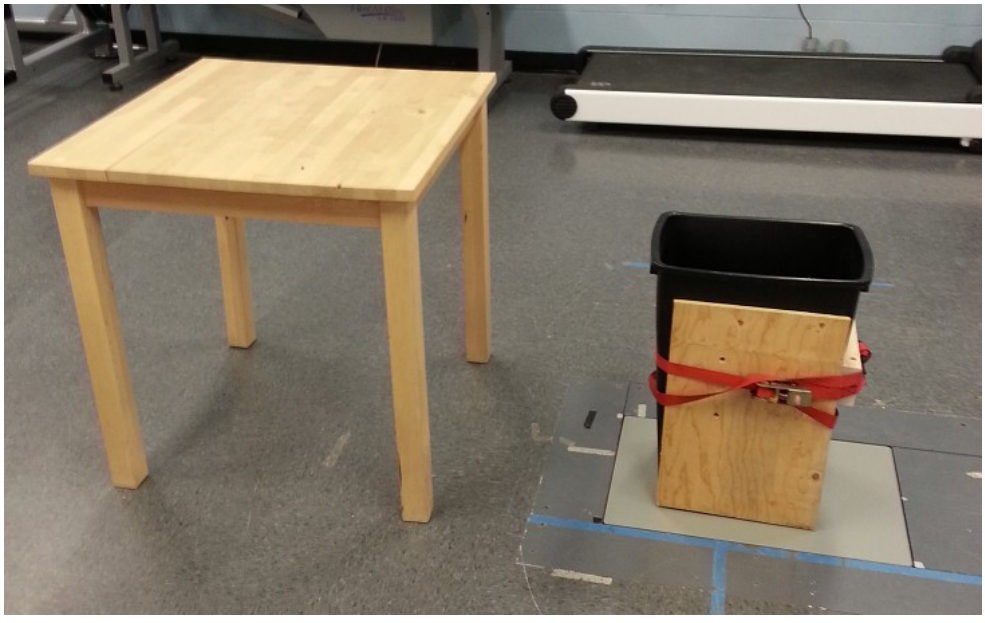

Figure 35: Experimental set-up for limb volume measurement

Initial Validation of Manual Volumes

As this was a new method of acquiring volumes, a validation experiment was designed. Using a standard 200 mL (+/-5%) beaker, a PET bottle was filled with pre-measured water, and manually graduated at 500 mL intervals (from 0 to 4 L). The thickness of the bottle was neglected.

The volumeter was placed on a force plate, and filled approximately two-thirds with room temperature water. The PET bottle was inserted vertically into the volumeter at each of the 500 mL graduations, and the force plate recorded 5 seconds of voltage data at 20Hz. As was performed in the human trials, each measurement was taken three times. The Z (vertical) axis force was calculated from the voltage data and averaged over the duration of the measurement. The resulting force values were used to compute the volume of each graduation, according to the principle explained in the introduction.

Results of Calibration Study

The difference between water-measured volume values and values calculated from force plate data were compared for volume values from 0 to 4 L and the summary of the data can be seen below in Figure 36.

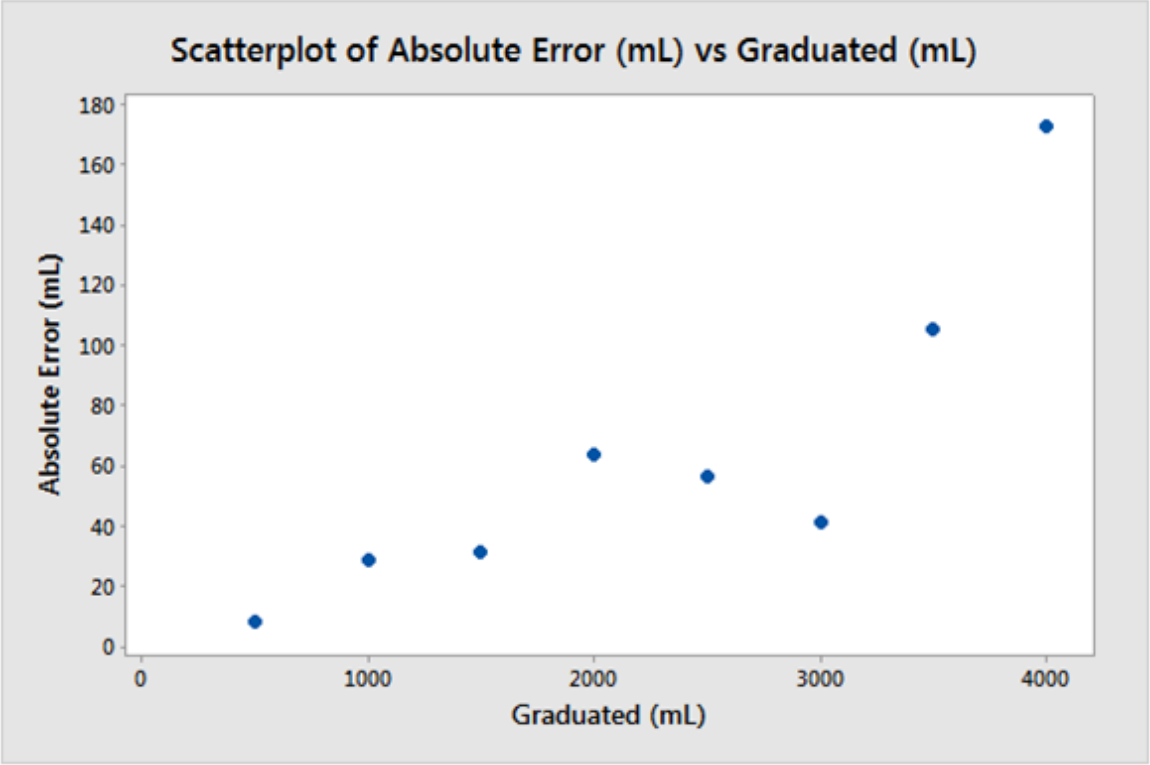

Figure 36: Difference values (absolute error) between graduated and force plate acquired volumes in volumeter validation

It is apparent that the force plate is consistently under-predicting the graduated volume value. The seemingly linear error was expressed as a percent of magnitude, and again plotted, as shown in Figure 37. The mean percent error was calculated to be 2.34 %.

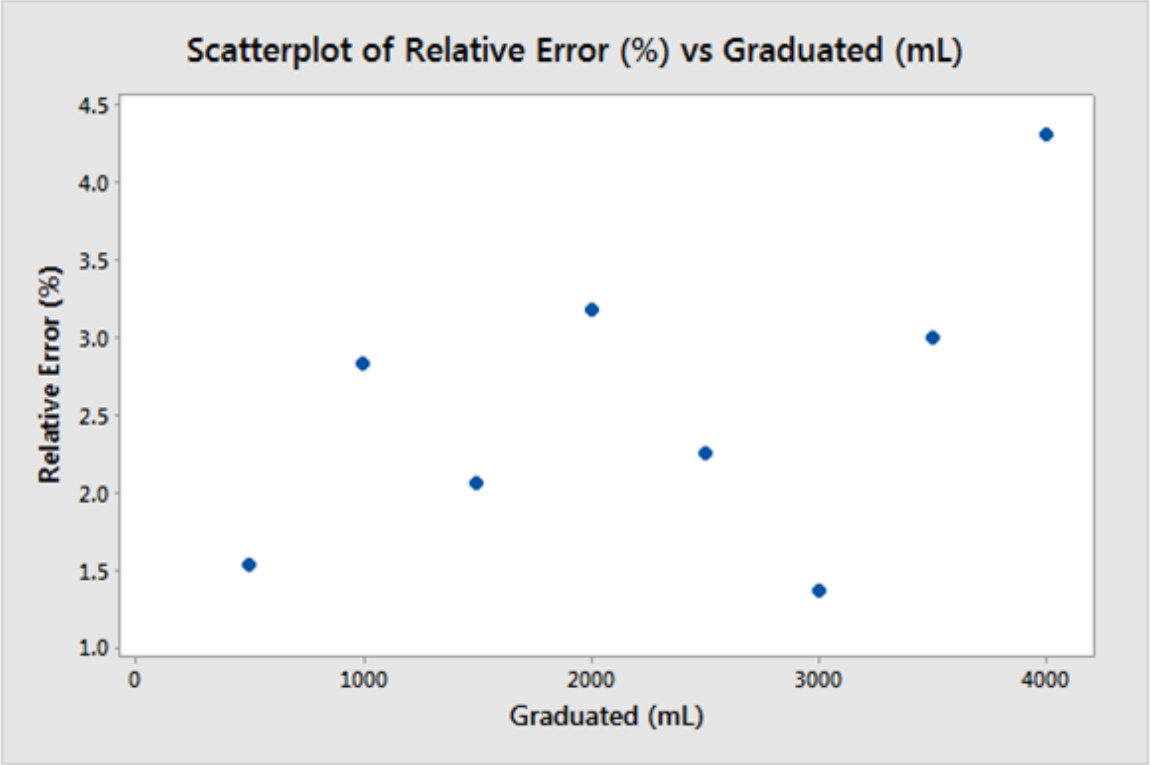

Figure 37: Relative error between graduated and force plate acquired volumes in volumeter validation

Calibration Study Discussion

The propagating error at larger volumes was likely caused by a systematic effect caused by expressed tolerance inscribed on the surface of the beaker of ±5% accuracy. Such error could have stacked with each volume measurement, propagating that error. Furthermore, while the volumeter was found to have a significant difference in measurement when compared to the water measured using the beaker, the average percent error margin is below clinical significance for the population for which the apparatus is subject to validation. The seemingly outlying absolute and relative error values for 0.5 L may have been caused by a significant contribution of the thickness of the PET bottle at the base, with respect to the volume of water measured.

Calibration Study Conclusions

Because the error was propagating as a ratio of the magnitude of the measurement taken, the likely source of error was the beaker used to measure the water in the graduated bottle. Given the tolerance of the beaker used to measure the water in the graduated bottles, and the indicated population for which this volumetry will be used, the level of error observed in this validation is acceptable.

Appendix B Bland-Altman Plots

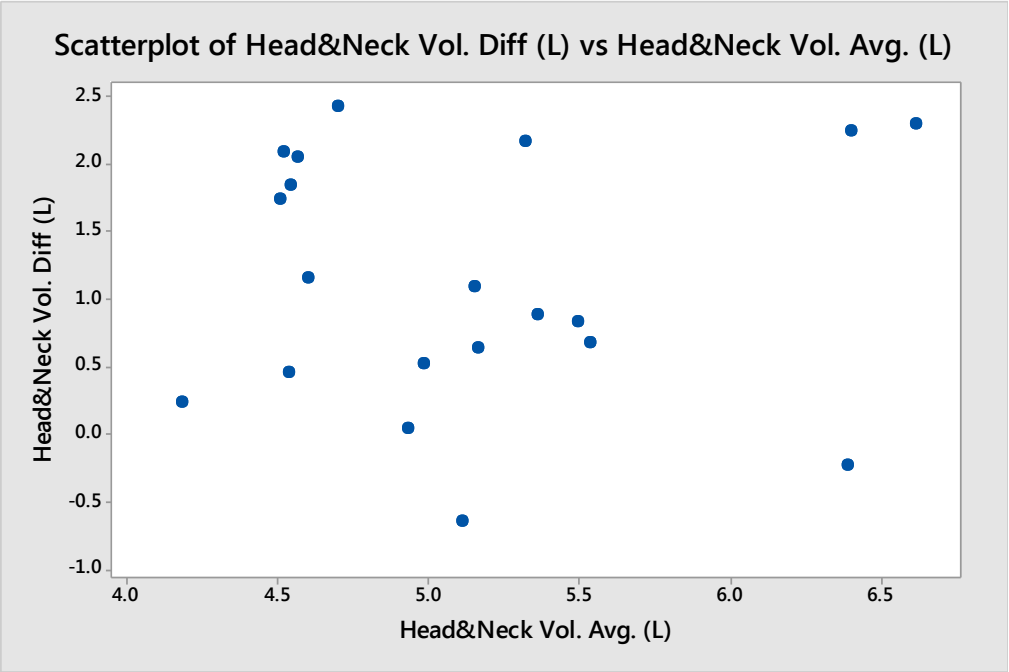

Figure 38:Bland-Altman figure for right upper arm volume - CI: (-0.7, 2.9) L

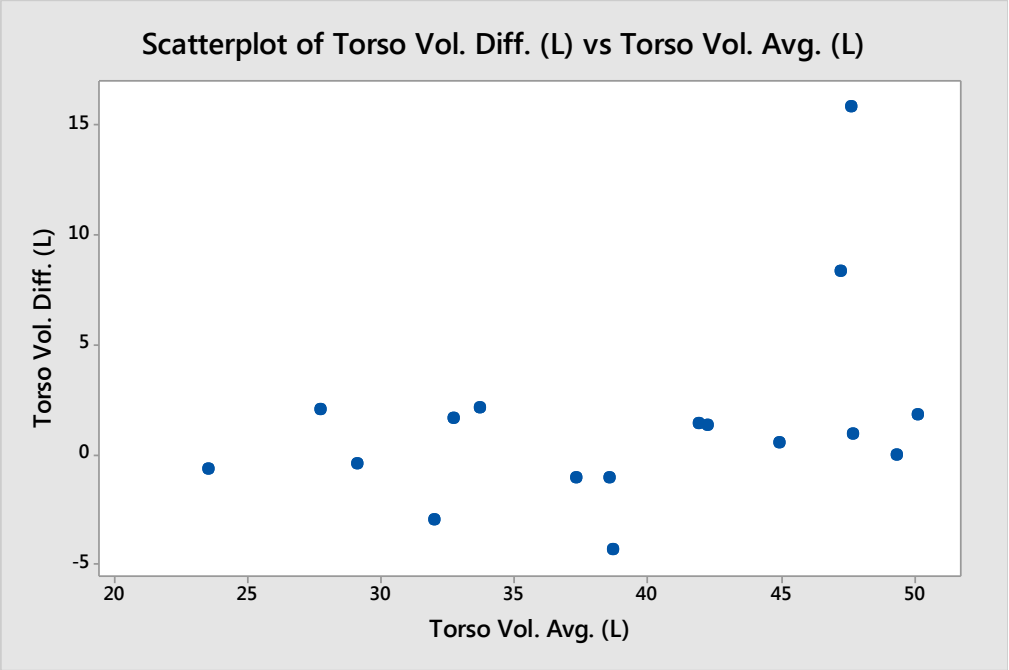

Figure 39 Bland-Altman figure for torso volume - CI: (-7.5, 10.4) L

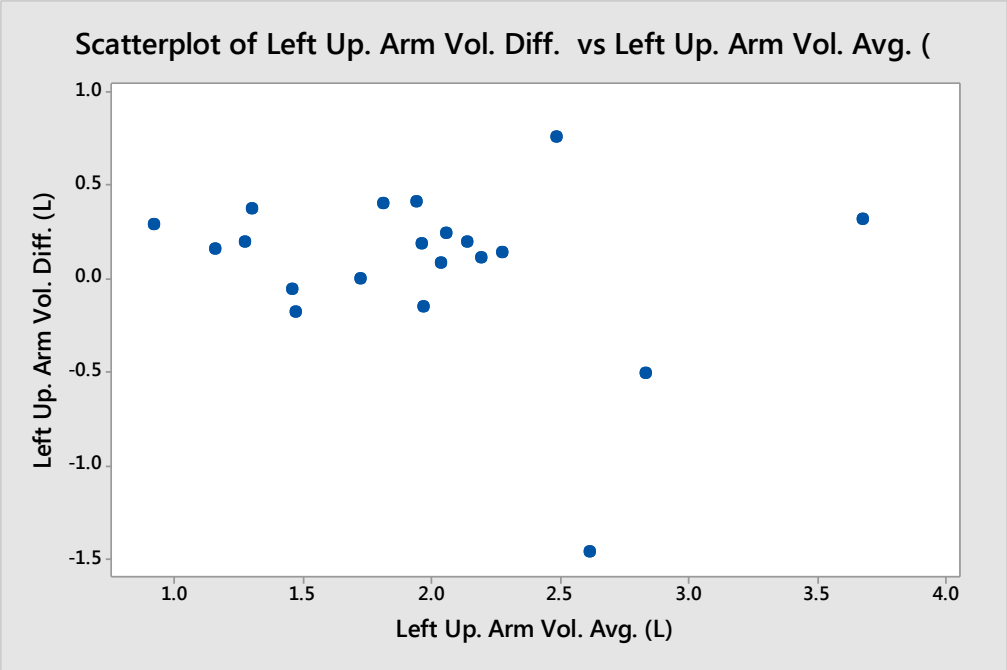

Figure 40: Bland-Altman figure for left upper arm - CI: (-0.8, 0.9)

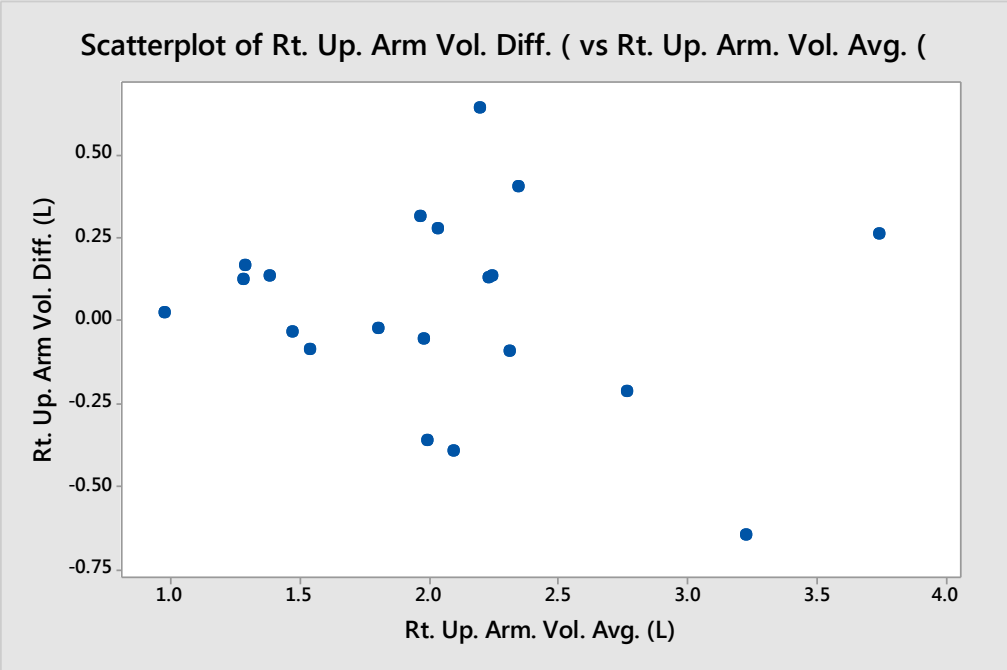

Figure 41: Bland-Altman figure for right upper arm volume - CI: (-0.5, 0.6)

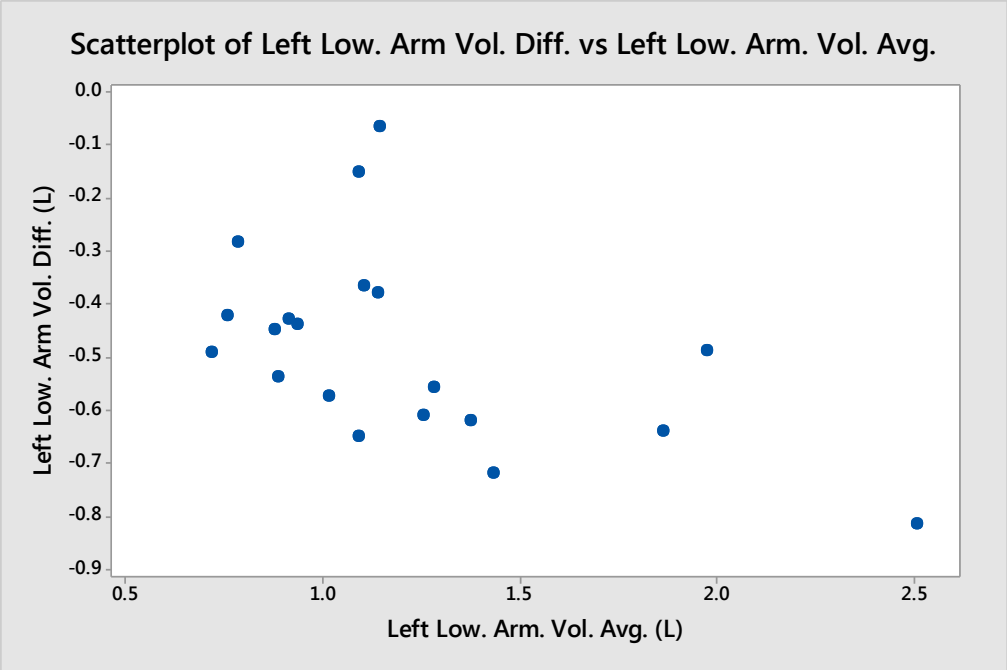

Figure 42: Bland-Altman figure for left lower arm volume - CI: (-0.8, -0.1) L

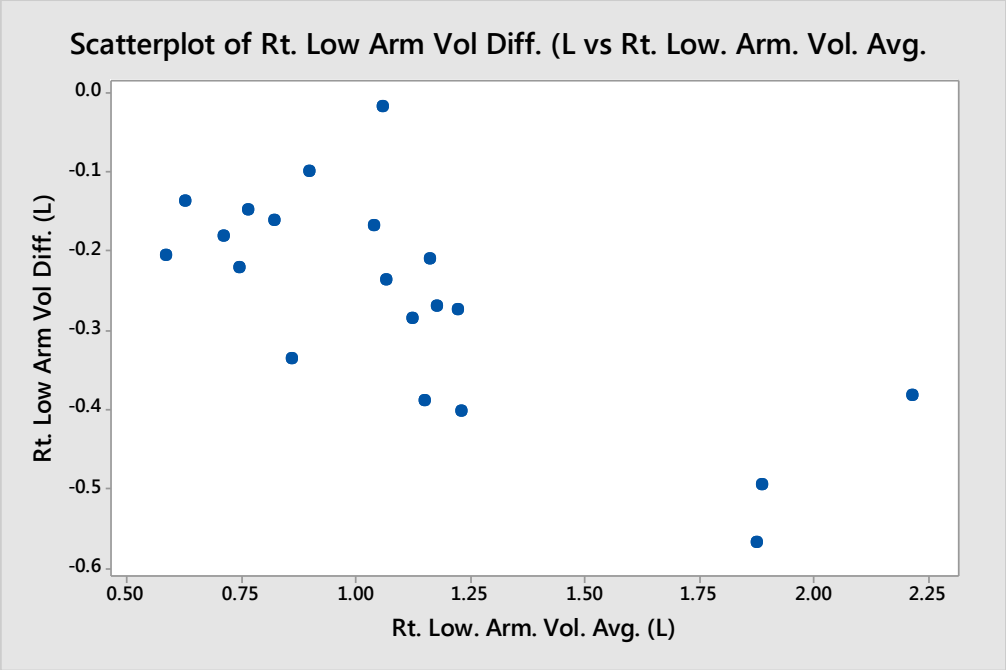

Figure 43: Bland-Altman figure for right lower arm volume - CI: (-0.5, 0.0) L

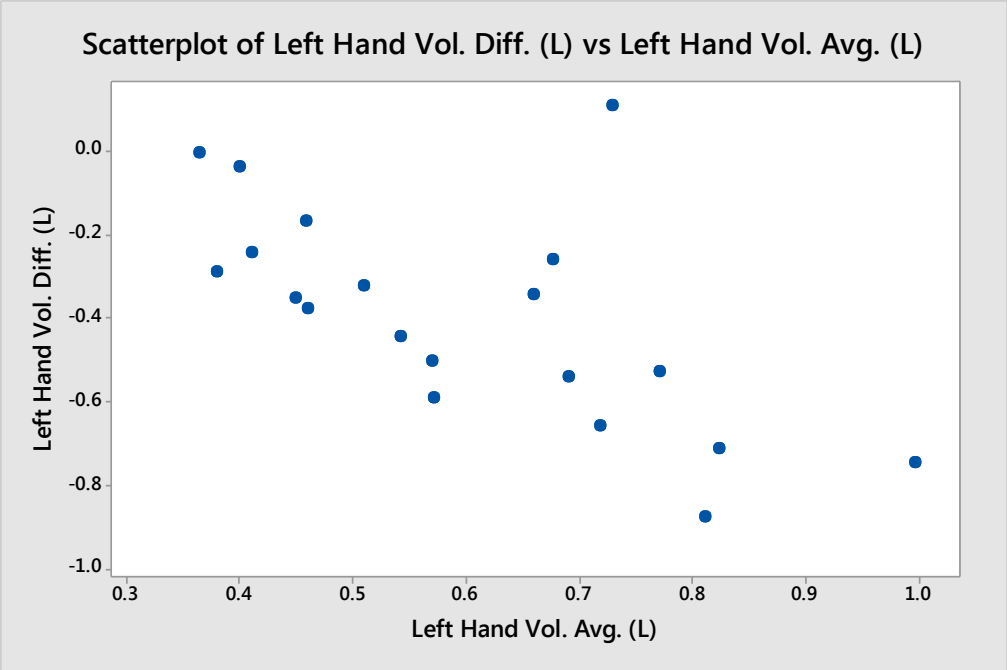

Figure 44: Bland-Altman figure for left hand volume - CI: (-0.9, 0.1) L

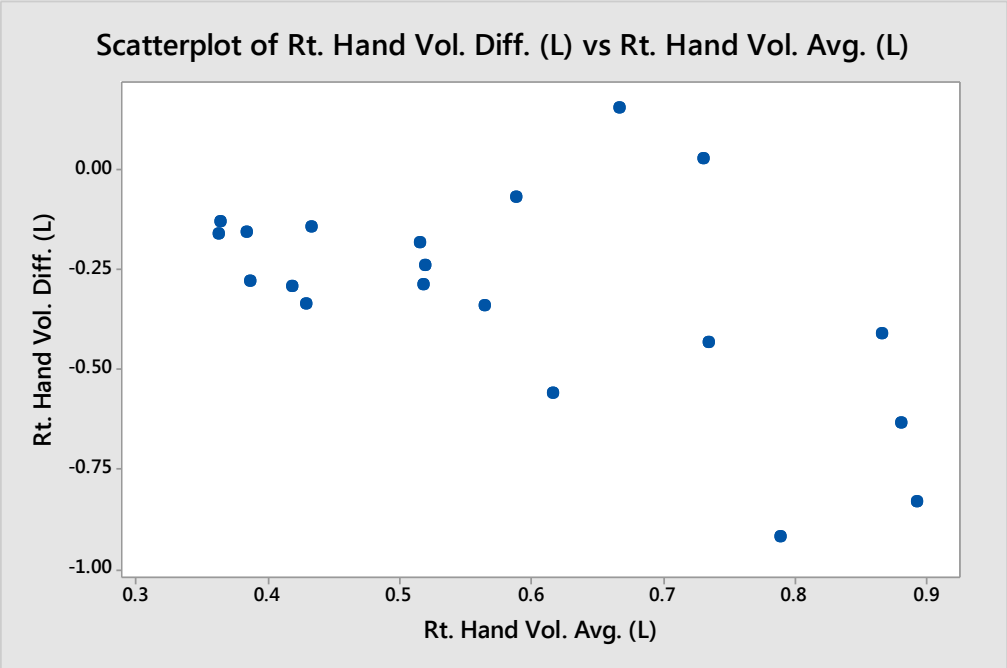

Figure 45: Bland-Altman figure for right hand volume - CI: (-0.8, 0.2) L

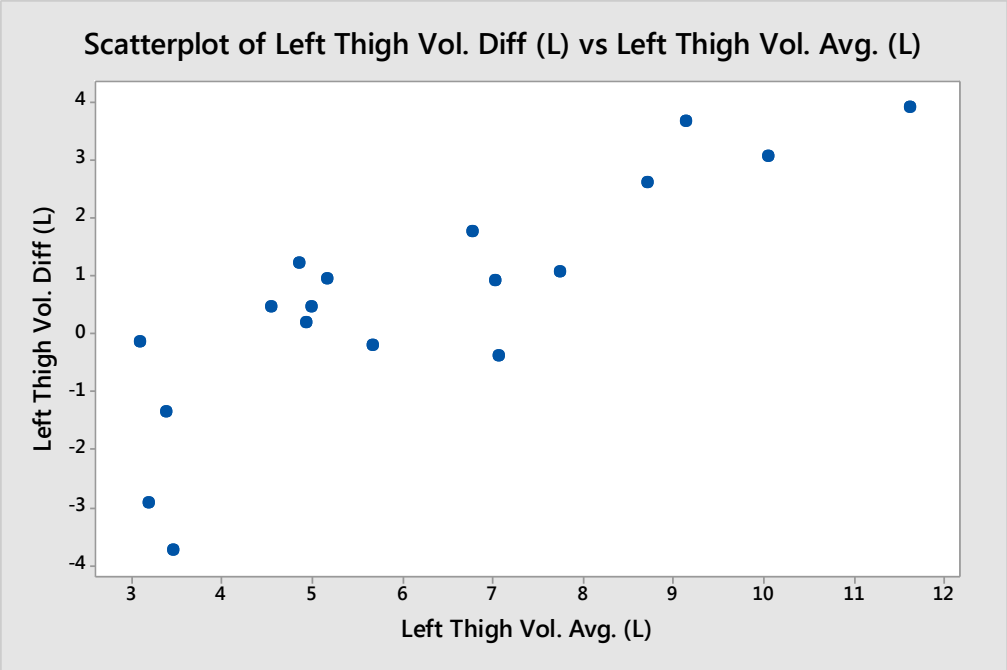

Figure 46: Bland-Altman figure for left thigh volume - CI: (-3.4, 4.6) L

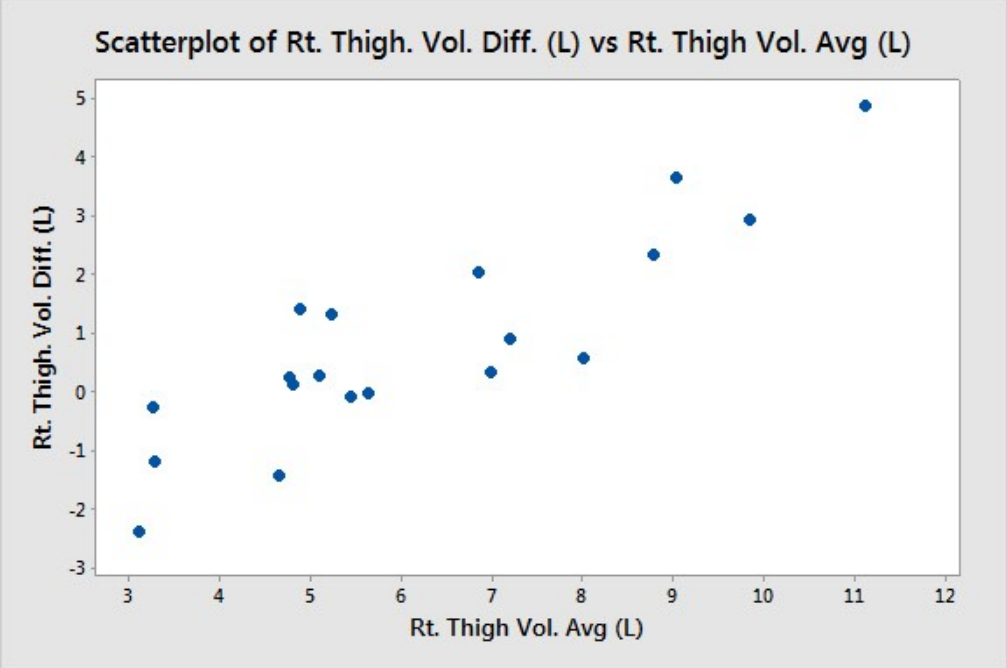

Figure 47: Bland-Altman figure for right thigh volume - CI: (0.2, 0.9) L

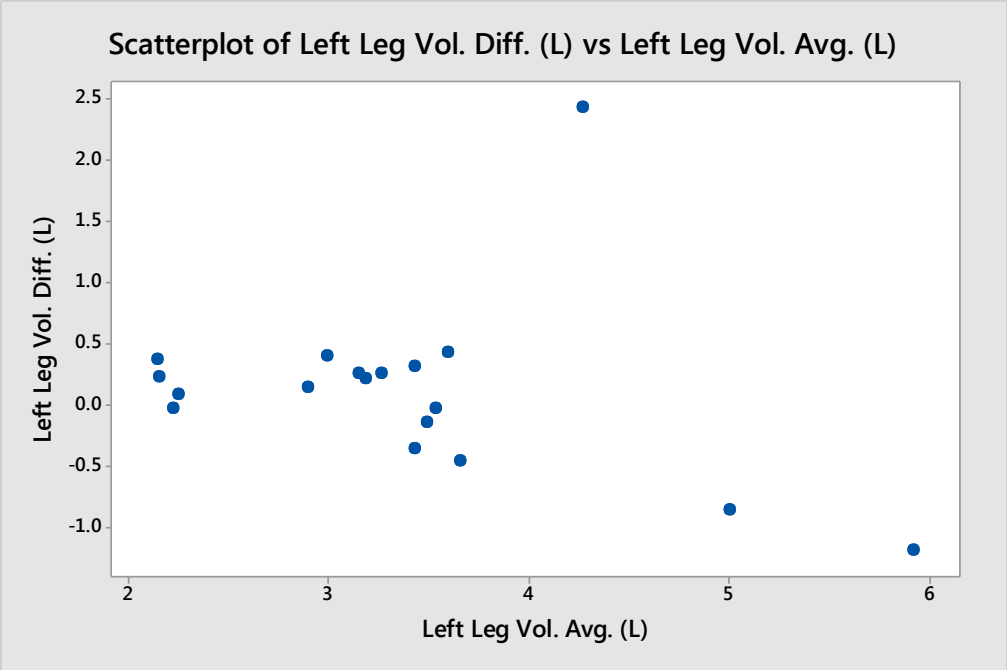

Figure 48: Bland-Altman figure for left leg volume - CI: (-1.3, 1.5) L

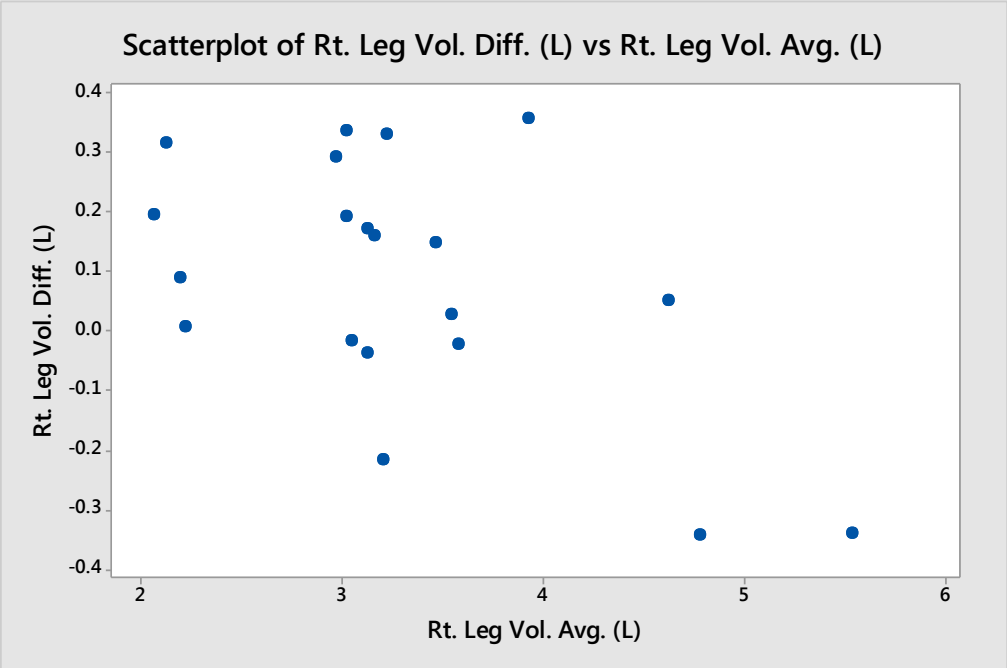

Figure 49: Bland-Altman figure for right leg volume - CI: (-0.3, 0.5) L

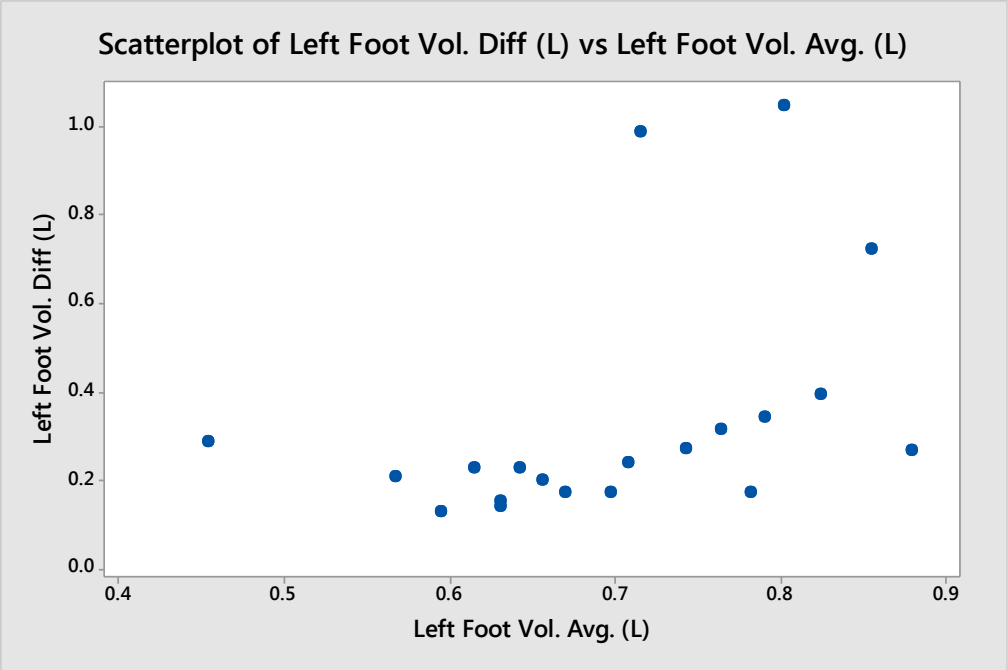

Figure 50: Bland-Altman figure for left foot volume - CI: (-0.2, 0.9) L

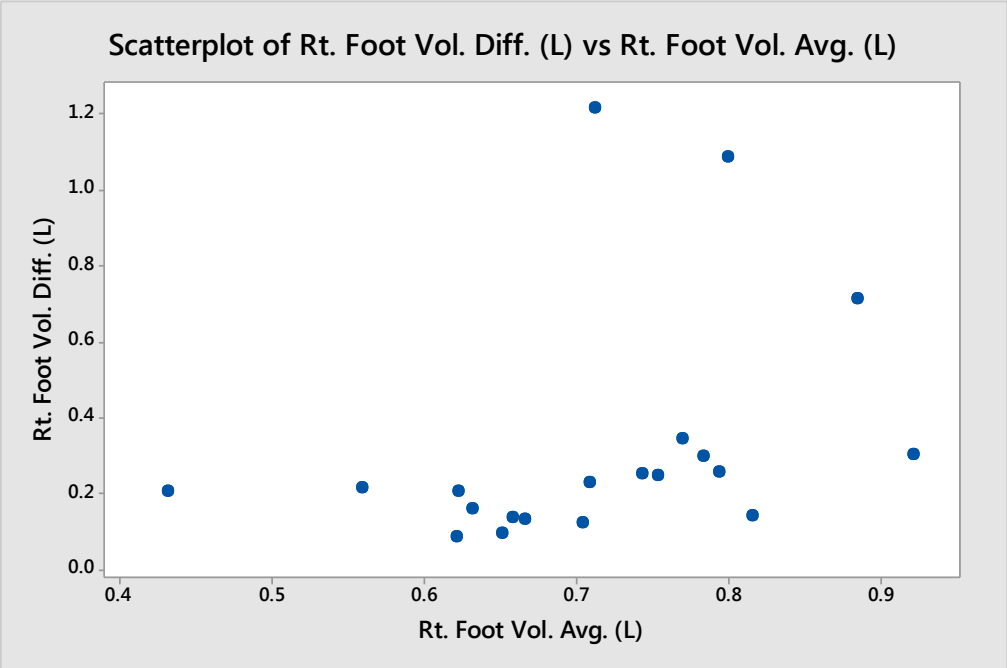

Figure 51: Bland-Altman figure for right foot volume - CI: (-0.3, 0.9) L

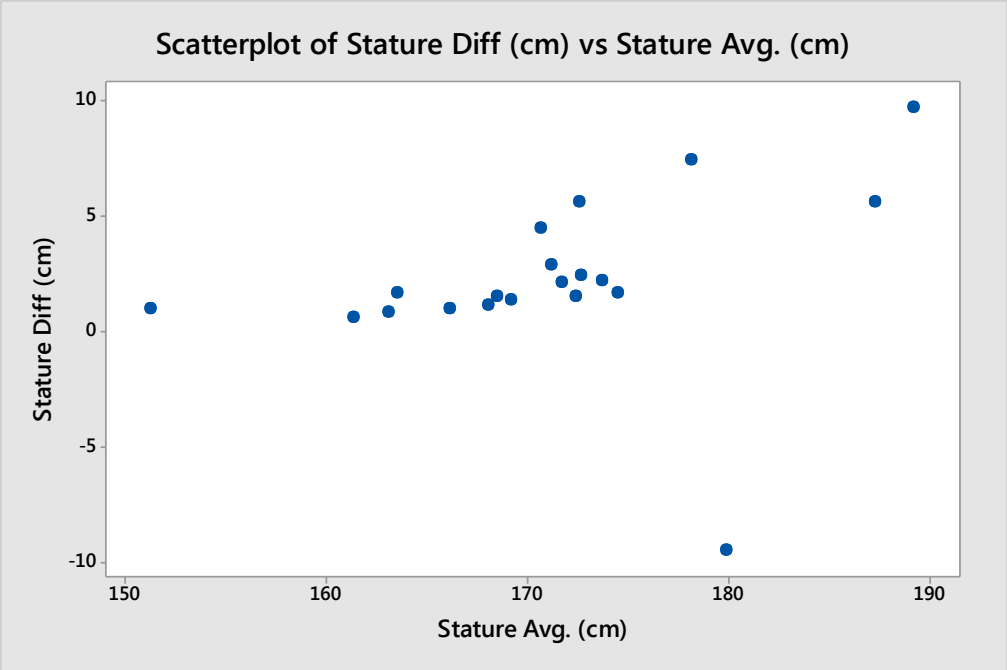

Figure 52: Bland-Altman figure for stature - CI: (-4.9, 9.9) cm

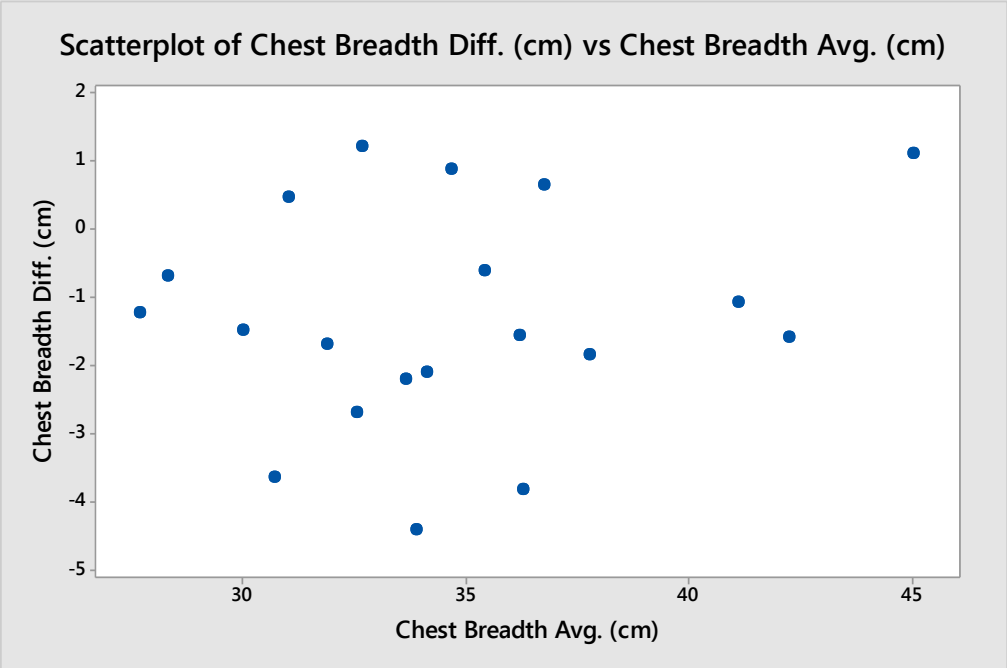

Figure 53: Bland-Altman figure for chest breadth - CI: (-3.3, 3.1) cm

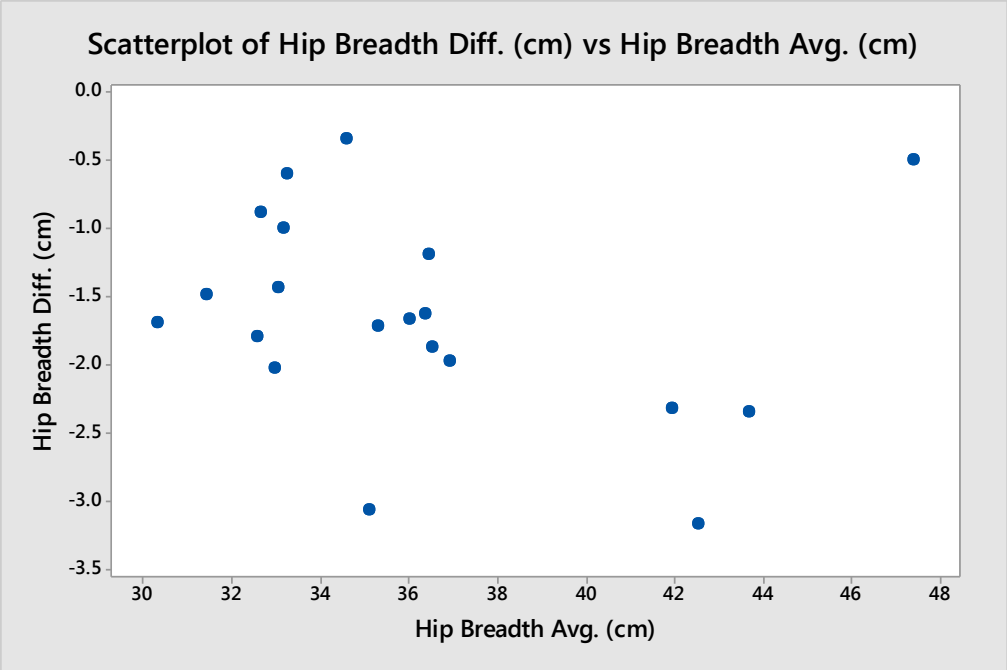

Figure 54: Bland-Altman figure for hip breadth - CI: (-3.1, -0.1) cm

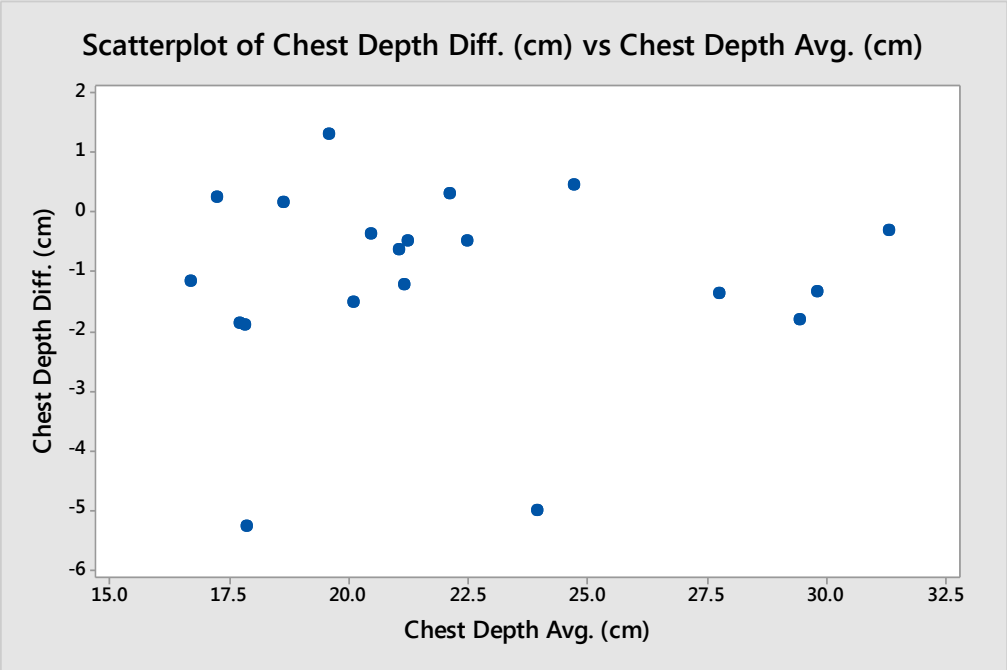

Figure 55: Bland-Altman figure for chest depth - CI: (-4.3, 2.1) cm

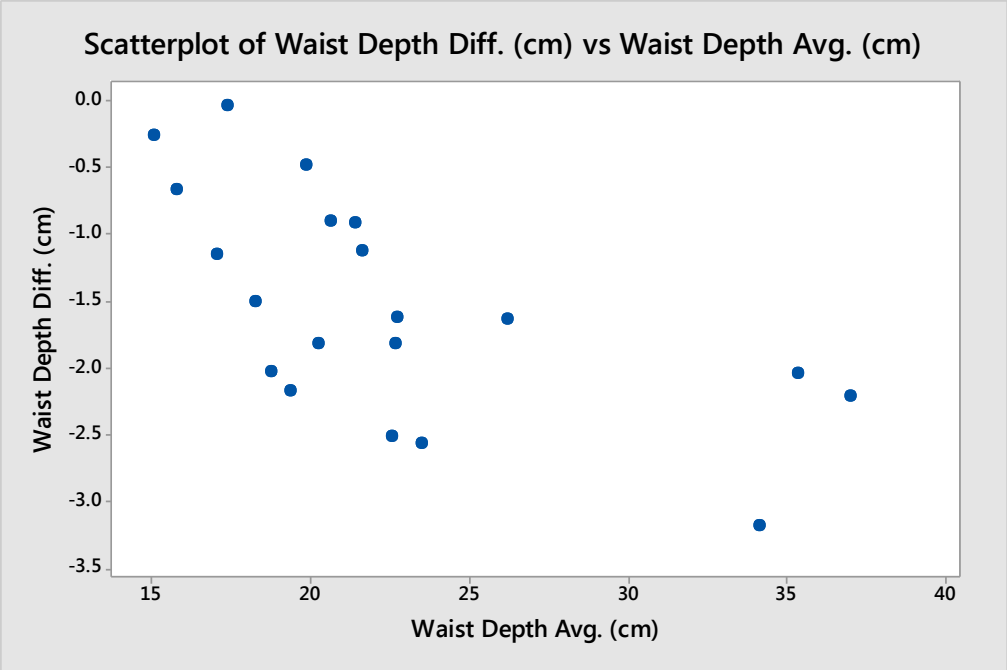

Figure 56: Bland-Altman figure for waist depth - CI: (-3.2, 0.1) cm

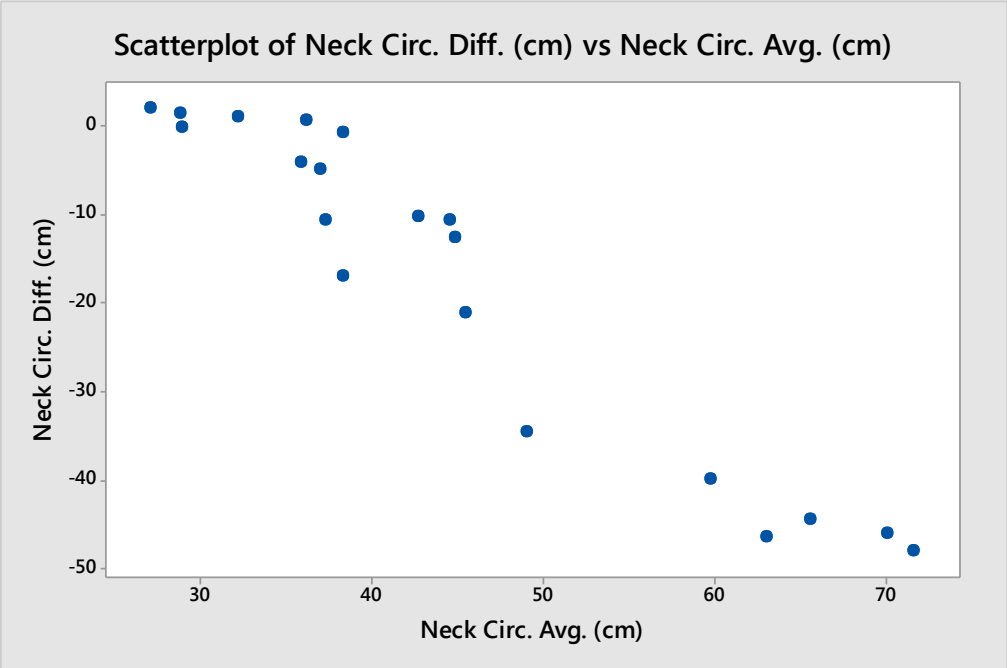

Figure 57: Bland-Altman figure for neck circumference - CI: (-53.9, 19.2) cm

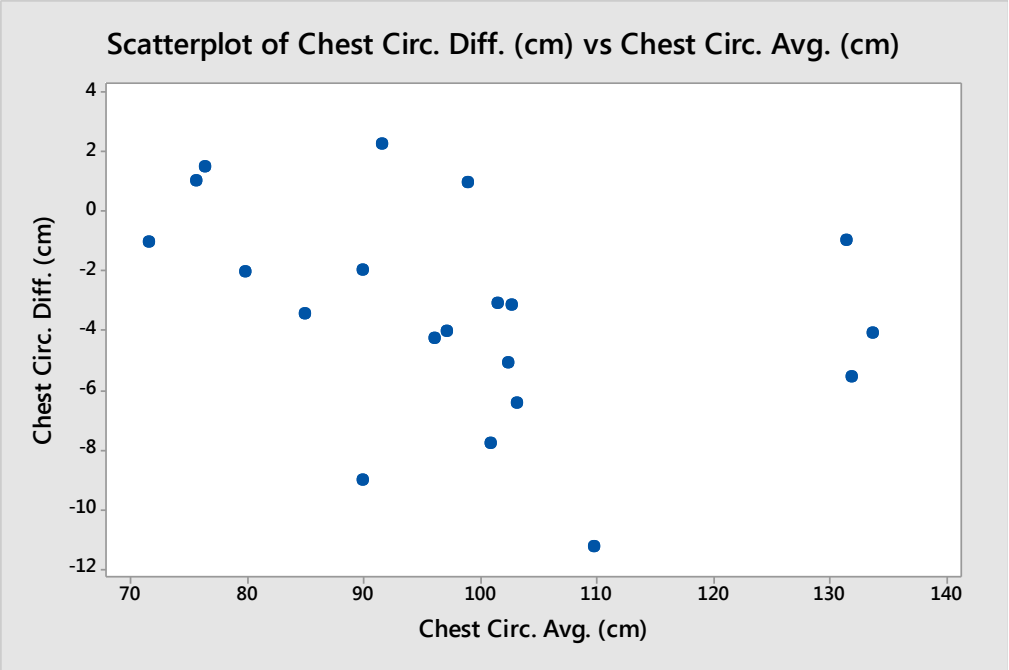

Figure 58: Bland-Altman figure for chest circumference - CI: (-10.4, 3.6) cm

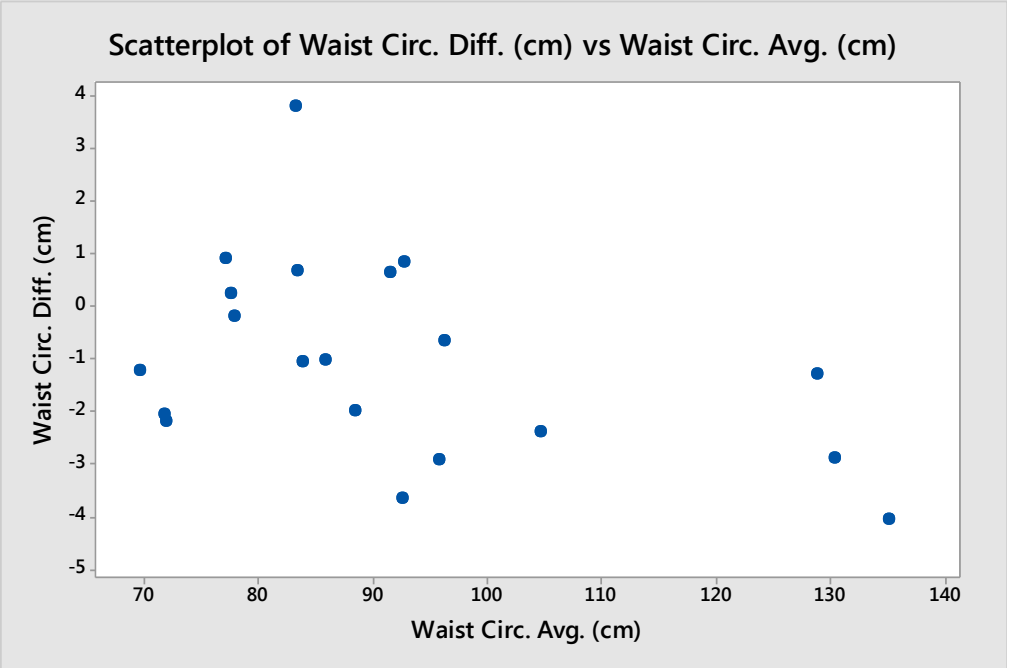

Figure 59: Bland-Altman figure for waist ircumference - CI: (-4.7, 2.6) cm

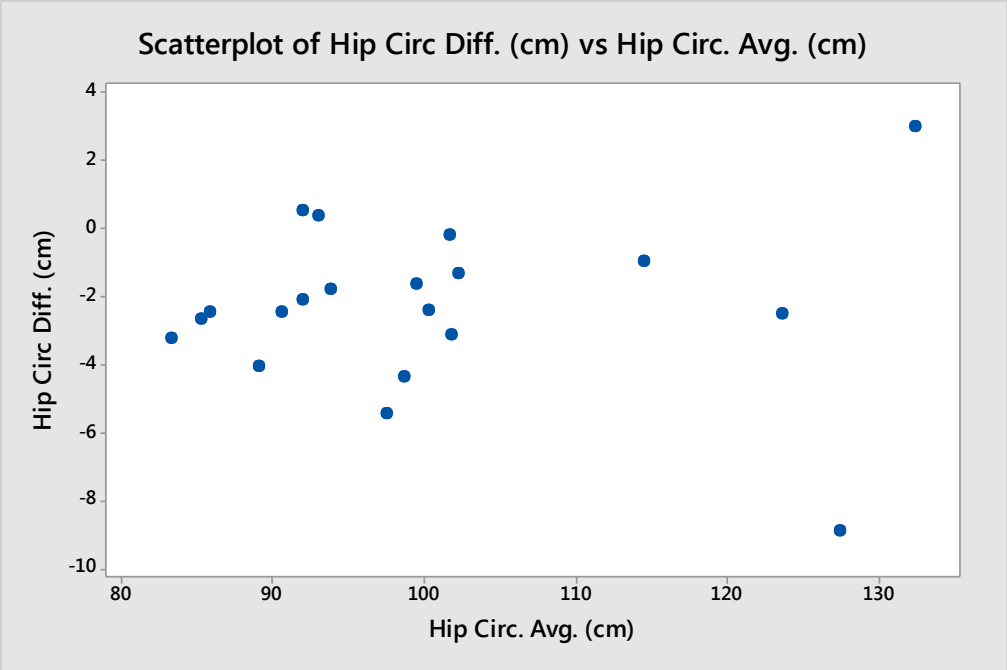

Figure 60: Bland-Altman figure for hip circumference - CI: (-7.1, 2.5) cm

Appendix C Data Cleansing Methodology

The following is an extension of the abstract accepted to the World Congress of Biomechanics: Quality considerations for the use of laser scanner dimensions for anthropometric measures in biomechanics and ergonomics, (Westhaver, Ladouceur, Grandy, and Kozey, 2014)

Introduction

After the scans were processed using ScanAnalysis, the scan-extracted output dimensions were compared for consistency, across linear and segmental volume measurements. As this was a pilot validation of the scan process, there was little training of software users prior to its use. Furthermore, several areas (such as crotch or scye crease) were very difficult to identify consistently. As a result, it was important that a procedure be developed that would allow for the identification and removal of inconsistent measurements upon retrospective analysis. This process was applied to the data prior to any analysis of accuracy, and only compared subsequent scans of a single participant

The three values for each measurement (P_1, P_2, P_3) were ordered according to magnitude, an example of which can be seen in Figure 61.

Figure 61: Example figure of three ordered data points

Minitab was used to calculate simple statistics on the successive measurements. The range of the three ordered measures was normalized to the mean value. While standard deviation or standard error is normally used to determine variation about the mean of a measurement, the low number of samples, and the irregular (non-normal) variation about the mean precluded the use of normal descriptive statistics.

When the normalized range value exceeded a threshold (as a percent of the mean, summarized in Table 31, usually 10%), outlier elimination was performed. The absolute differences between the two pairs of ordered data ($D_1 = |P_2 - P_1|$ and $D_2 = |P_2 - P_3|$) were calculated and the value that caused the greatest difference was rejected. Effectively, this was the value that was furthest from P_2.

Table 31: Thresholds for outlier elimination

Measurement	Threshold
Stature	1.1 %
Chest Breadth	9 %
Hip Breadth	4 %
Chest Depth	7 %
Waist Depth	9 %
Neck Circumference	15.5 %
Chest Circumference	10 %
Waist Circumference	7 %
Hip Circumference	10 %
Head and Neck Volume	8 %
Left Upper Arm	10 %
Left Lower Arm	10 %
Left Hand	20 %
Right Upper Arm	10 %
Right Lower Arm	10 %
Right Hand	20 %
Left Thigh	10 %
Left Leg	10 %
Left Foot	10 %
Right Thigh	10 %
Right Leg	10 %
Right Foot	10 %
Torso	10 %

Results:

Prior to data evaluation, the average variation of mean normalized range values (%) ranged from 0.43% for to 6.13% for stature values, 2.85% to 34.74% for circumference values, and 5.80% to 33.61% for segmental volume values. After the procedure outlined in the analysis was performed, mean normalized range values (%) ranged from 0.30% to 4.18% for linear measurements, 1.92% to 8.86% for

circumferential measurements, and 3.63% to 13.84% for segmental volume measurements.

Discussion

The publication landscape has highlighted the need for quality checks of the scanned images; however, descriptions of systematic methods to identify possible problems in scanned measurements have been limited. The present method greatly improves the intra-subject consistency in the measures which will provide for improvements in applications of the data. Following this data cleaning operation, the output data was used in an accuracy comparison, validating scan-extracted measurements against manual measurement methodologies.

Appendix D Investigations Related to Image Quality

Introduction

In three-dimensional imaging with stereophotogrammetry, the digitization of three-dimensional space with two-dimensional imaging devices requires calibration of two types: intrinsic and extrinsic. Extrinsic calibration deals with developing a relationship between pixel locations and 3D space. Intrinsic calibration involves the determination of physical characteristics specific to each camera and lens. Intrinsic parameters are summarized below in Table 32 (Zhang, 1998).

Table 32: Intrinsic parameters in photogrammetry

Intrinsic Parameter	Description
u_0, v_0	Principal point, in pixels; centre of projection through lens
α	x-direction scale factor
β	y-direction scale factor
γ	Skew factor between x and y axes
k_n	Radial distortion factor $\{k_1, k_2, \ldots, k_n\}$; usually 2 distortion factors is sufficient

In a prior document it was presented that systematic distortion was evident in three-dimensional images output by the Unique Solutions full-body laser scanner, and that this distortion was a function of height in the superior-inferior axis of the scanner, at the limits of the field of view of the scan heads. The software used to calculate scan images utilized a pinhole model for each imaging device, which provides a robust method for the extraction of extrinsic camera information – transformation of real-world coordinates to image coordinates – assuming a rectilinear projection but does not account for radial distortions produced by light passing through the lens.

Originally, the systematic error was modelled by distance measurements in the medial-lateral (M-L) and anterior-posterior (A-P) planes orthogonal to the superior-inferior (S-I) axis, at regular intervals in the S-I axis, which yielded in a parabolic error correction in each orthogonal plane. This demonstrated the systematic nature of the distortion, but did not provide a comprehensive correction for the entire scan volume. Given that one application of the scanner in the OEAB Lab is health

research on human participants, it is critical that the errors be corrected for all scans.

Methods

A set of ten to fifteen photos of the calibration target was captured using each of the scanner's 16 imaging units. The calibration target was positioned at a variety of positions in order to maximize the calibration volume within each imager's field of view (FOV). An example of the images used can be seen in Figure 62 below.

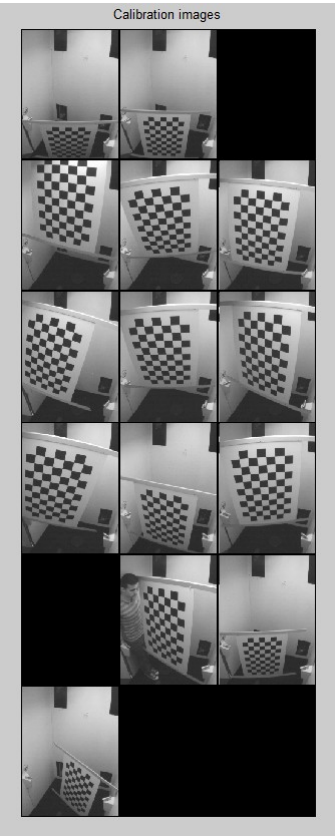

Figure 62: Example intrinsic calibration images

A Matlab toolbox developed at the California Institute of Technology was used to determine the intrinsic parameters of each imaging apparatus separately. Based on *A Four-step Camera Calibration Procedure with Implicit Image Correction* (Heikkilä and Silvén, 1997) this calibration scheme extracted the parameters of each imaging unit by analysing captured photos and comparing expected grid corner location to actual grid corner location in the images. A least mean squares algorithm minimized

the errors, and provided the intrinsic factors needed to correct the images. The magnitude of correction can be seen in Figure 63.

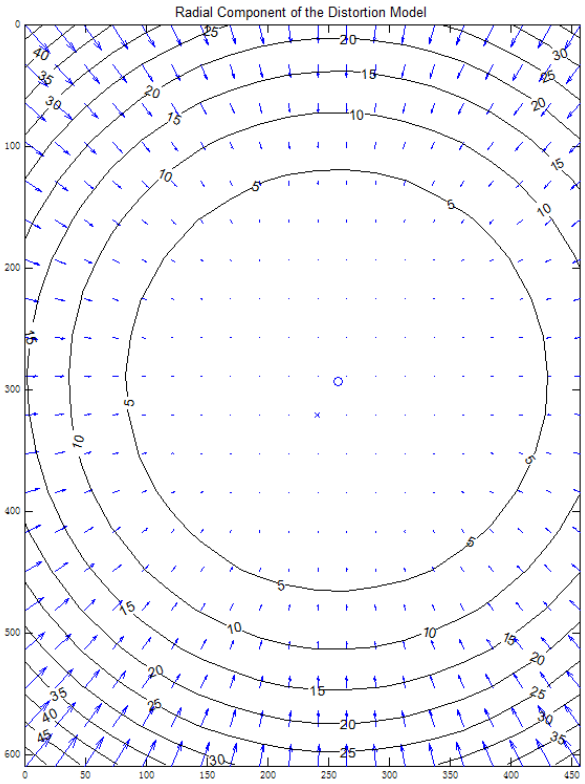

Figure 63: Radial component of the distortion model, output vector map

This example output file that shows the vector of displacement between the ideal (by rectilinear projection) and post-corrected pixel locations of calibration images, it can be seen that the greatest radial distortion can be found at the outermost limits of each imaging device. With the intervention of the industrial partner, Unique Solutions, custom software (*CloudCreator*) was developed that was designed to use the resultant intrinsic factors to correct the scan data. As this software was incorporated into the scanner operating system and is intellectual property of Unique Solutions, the nature of the software will not be discussed here.

On the day of the testing, the scanner underwent extrinsic calibration in order to develop a relationship between the two dimensional image coordinates and the real-world three-dimensional coordinate system. Subsequently, one participant who was asked to wear light coloured undergarments and a white scan cap was

marked with an *X* in washable marker at landmarks listed in the methods. 1 cm diameter white landmark markers were placed at the intersection of each *X.* The participant was provided with a barcode that was used to initiate the scan process, and was asked to assume a standard posture, with feet slightly parted, and outstretched hands resting on scanner handles. The participant then initiated the scan by allowing the barcode reader at the front of the scanner to read the personalized UPC-A barcode.

Results and Discussion

The scan image was extracted prior to post-processing by radial distortion correction software *CloudCreator* and is shown in Figure 64.

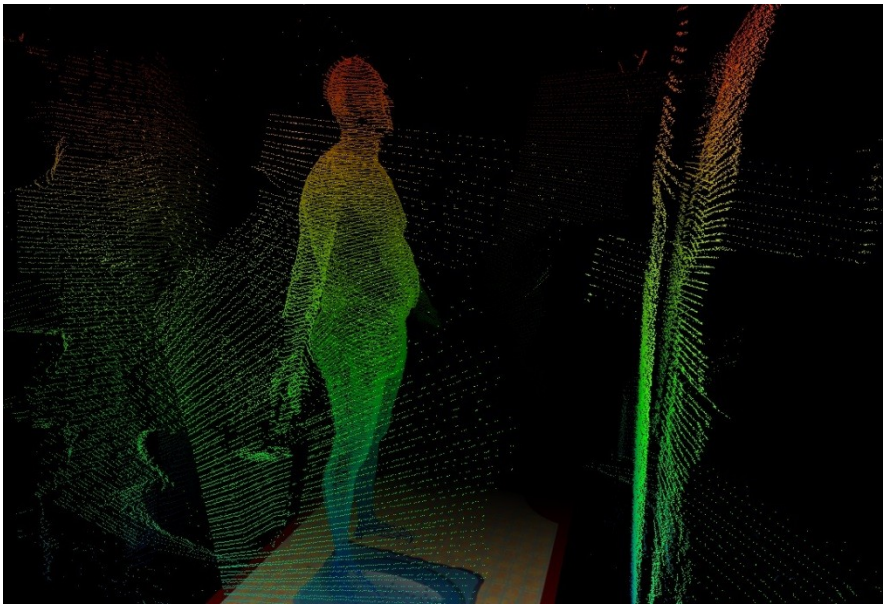

Figure 64: Raw cloud prior to intrinsic parameter correction

As was described in a prior section, the image is visibly distorted in the sagittal plane at the upper and lower regions of the scan. In order to correct for these distortions the intrinsic factors extracted using the CalTech Matlab toolbox were entered into *CloudCreator* and the recalibration process was initiated. The output of the post-processing can be seen in Figure 65.

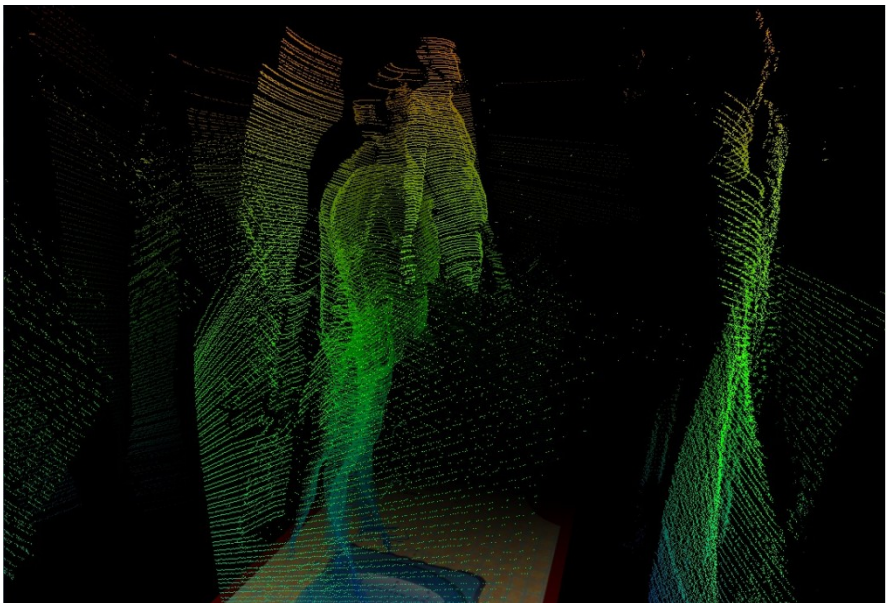

Figure 65: Raw cloud after intrinsic parameter correction

As can be seen in the above image, greater distortion can be seen than had been observed in the prior uncompensated data. Furthermore, as each scan head was compensated separately, the distortion introduced by the radial correction is different for each head, and a cohesive image of the participant is no longer present.

Several methods were employed to improve the intrinsic measures of each imaging apparatus, including collecting a greater number of calibration images, reducing the apparent size of the calibration target in the field of view, and utilizing a feedback routine embedded in the calibration software that re-extracts grid corners and re-calculates the intrinsic measures however the quantifiable errors could not be substantially improved. Furthermore, the intrinsic factor extraction software provided an output scatter plot of pixel errors associated with each image from which grid corners were extracted. Images with the largest deviations were removed from the set of calibration images and the calibration was re-initiated.

Again, this provided minimal reduction in pixel error values. Despite these seemingly ineffective error-reduction strategies, pixel error was frequently reported to be below one pixel. Given that the imaging devices are relatively low-resolution on modern imaging standards (640 x 480 pixels) this error may be due to limited

image acquisition within scanner hardware. Because of restrictions in the intellectual property licensing agreement between the Occupational Ergonomics and Biomechanics Laboratory and Unique Solutions, an evaluation of the *CloudCreator* software beyond identification of errors in the aforementioned output is not possible. Therefore a root-cause analysis of the scans corrected for intrinsic errors cannot be comprehensive.

Conclusion and Recommendations

The original objective of this pilot study on a single participant was a comparison of measurements extracted from scans that had been corrected for intrinsic parameters within each imaging apparatus to measurements collected from the previously uncorrected scans. Unfortunately, the output files of the *CloudCreator* software gave point clouds that did not allow for anthropometric landmarks to be digitized, and did not provide a realistic or acceptable representation of human features. Therefore, the output of this report will list recommendations for further study.

Based on the results presented, improvements to image acquisition should be implemented such that radial distortion can be corrected. The first solution would be a direct replacement of optical equipment with cameras of higher resolution and better lens quality. Furthermore intrinsic parameters should automatically be extracted as part of the initial calibration procedure prior to each scan. Both changes would require that the OEAB lab have access to the on-board software.